Mechanism and Application of a Heterogeneous Catalytic Hydrogen-deuterium Exchange Reaction for Polyolefins

A DISSERTATION
SUBMITTED TO THE FACULTY OF THE GRADUATE SCHOOL
OF THE UNIVERSITY OF MINNESOTA
BY

Yiming Zeng

IN PARTIAL FULFILLMENT OF THE REQUIREMENTS
FOR THE DEGREE OF
DOCTOR OF PHILOSOPHY

Timothy P. Lodge and Frank S. Bates, Advisors

April 2018

© Yiming Zeng 2018

Acknowledgements

My years spent at Minnesota during my graduate study have been a most rewarding experience to me. At the end of this journey, I wish to offer my thanks to many people whom I had the honor to meet. Your support deeply shaped this thesis work.

I am gratefully in debt to my great advisors, Prof. Tim Lodge and Prof. Frank Bates. As educators they extend beyond being only my academic advisors for my research project – for which they have provided more than abundant guidance and resources, but also conveying the altitude of respecting our knowledge, equally for knowing and not knowing. I have also been honored to be able to sit in classes from them, Physical Polymer Chemistry from Frank, and Scattering and Rheology from Tim. Outside of the academic world, Frank and Tim also showed their art in bridging with people of different background and even generations. I still recall being welcomed at Frank's home for the first Thanksgiving that I ever celebrated, and the numerous warm visit to Tim and Susanna's home, plus the great foods. I enjoyed every toast to the newly awarded doctors in Lodge group. All these enlightening moments and memories define a part of me and will go far with me.

I am also deeply thankful to my collaborator and mentor, Dr. Carlos López-Barrón. As a scientist and engineer in the industrial side, he has been remarkably productive and resourceful, which eventually motivates me to pursue a similar track as I first consider my career path. He taught me the first lessons of the power of collaboration, that how we could bring out the best of each contributing individual and unite them towards an advanced target. He has also proven himself to be a good friend, always sincere, and caring in every aspect. I have always felt that he cares not only the science that we are excited about, but also the growth and well being of me as a young professional. These will continue to motivate me and shall not stop with me. I will feel fulfilled and honored if I will ever be able to, in one point of my career, deliver the same tremendous care and help I have received to someone else.

Bates group and Lodge group members, you are incredible! I am appreciated to be welcomed when I first join the group, along with the countless help I have been fortunate to receive. I would like to thank Brian, Matt, Jie and Tuoqi for helping me ramp up fast when I first joined the group. I would also like to thank Aaron, Akash, Boxin, En, John, Jun, Kyungtae, Lucas, Mihee, Qile, Ralm, Ron, Seyoung, Wenjia, Yuanchi, Ziang and many others for the support and discussions. I will not be where I am without all of you.

Special thanks go to my dearest friends, for the support, the unforgettable time spent together, or simply for a good laugh. Yan, these days it is almost impossible to find someone with whom you can share all your life stories. Thank you for being such a great friend, thus I know there is someone I can always go to without being worried for judgement. En, thank you for the support in and outside of the academic world, and all the errands I have had you ran. Han, I owe many thanks to you for all the extra mileage I have had you go. Ziang, thank you for all the joy you have created in the game. Many thanks go to a lot of people, Hongyun, Wenjia, Yuyang, Motao, Tuoqi, Lian, Boxin, Tianqi, and many others. You made the past five years occupy a special place in my memory.

Many thanks to Miss Wubing Ji and Mr. Wushuang Lu. You are the best. Though I never truly understand what you say, you are the best companion ever, who iron all the wrinkles in my emotion. Please continue to eat well, drink well, sleep well, and meow well.

A lot of thanks, and love, to my dear family. Dad and mom, you have been always wonderful, and provide me with the strength to go far, knowing I will always have a home that I am attached to. Xiangjing, it is a blessing to have you showing up in my life. Please stay close with me. Together we will explore many cherished places and moments, and there is no other companion I will ever want to be with.

And finally, a special note to you, Yiming. Well done. And sincerely, thank you.

To My Family And Friends

Abstract

The mechanism of a heterogeneous catalytic H/D exchange reaction with polyolefins is investigated in this thesis. The model polymers used in this study were hydrogenated polybutadienes (hPBDs), and a metallocene linear low density polyethylene (LLDPE). When mixed at 170 ºC with isooctane, Pt/Re-SiO_2 catalyst, and gaseous deuterium, the polyolefins dissolve and undergo H/D exchange reaction at the surface of the catalyst, producing partially deuterium labelled polyolefins. Polymers with varying molecular weight, varying ethyl branch density and narrow molecular weight distribution were synthesized by anionic polymerization of 1,3-butadiene followed by saturation with gaseous hydrogen. The LLDPE polymer with relatively broader molecular weight distribution is a commercial product and was supplied by ExxonMobil Chemical Company. The extent of deuterium labelling is analyzed with density measurement, proton nuclear magnetic resonance spectroscopy (^{1}H-NMR) and Fourier transform infrared (FTIR) spectroscopy. A size exclusion chromatography (SEC) instrument equipped with an IR detector was used to analyze the deuterium concentration within the LLDPE polymer as a function of molecular weight. Small angle neutron scattering (SANS) was conducted for both the pure labelled polyolefins and their blends. The partially labelled LLDPE sample was fractionated according to the molecular weight. The partially labelled fractions were blended with the normal LLDPE to create samples with different molecular weight portions labelled. These labelled blends were uniaxially stretched at room temperature while simultaneously monitored with SANS, providing a method to characterize the single chain alignment process at different stages of polyethylene deformation, as a function of time.

In this thesis, several aspects of the isotope exchange reaction were investigated. We first examined the dependence of the isotope exchange on the molecular weight and branch content of the substrate polyolefins. The extent of isotope exchange was found to strongly favor the high molecular weight molecules. High branch concentration hinders the

exchange reaction, but has a less impact at low branch content. These observations are best explained by viewing the exchange reaction as an absorption controlled process. The deuterium distribution was found to be inhomogeneous evidenced by both the SEC-IR and SANS results. From SANS results modeling, it was confirmed that mathematical accommodation of the inhomogeneous deuterium distribution is necessary to extract chain statistics. Finally, the in situ tensile-SANS experiments revealed that the single chains develop a high degree of alignment along the stretching direction during the elastic and plastic deformation processes of the LLDPE, and maintain that alignment during the strain hardening regime. A remarkable higher degree of chain alignment was found for the high molecular weight chains, a result of longer chains being able to form more tie chains between lamellae. The results of this work provided a scheme of analyzing commercial polyolefins on the single molecular scale, without the necessity to access the synthesis route of the materials.

Table of Contents

List of Tables

List of Figures

Chapter 1

Introduction and background

1.1 Introduction

Polyolefins, such as polyethylene (PE) and polypropylene (PP), are by far the most produced polymers. They are used in multiple applications, such as packaging, containers, tubing, and adhesives. These materials have been extensively studied for decades, yet the field is still gaining new knowledge regarding the material microstructures, phase behavior, and new engineering approaches. Polyethylene is now produced at a scale exceeding 80 million tons each year, which is approximately 60% of the total polyolefin production.[1] It is used in products such as films (agricultural films, bags, food wraps) and containers (pharmaceutical packaging, bottles, oil tanks). Different grades of polyethylene are generally categorized based on the density. At room temperature, low density polyethylene (LDPE) has a density between 0.915 and 0.94 g/cm^3, while the high density polyethylene (HDPE) has a density from 0.94 to about 0.96 g/cm^3.[1] Manufacture of LDPE originated in the 1930s through a high pressure polymerization process,[2] producing chains with long and uncontrolled branches. HDPE resins have been produced since the 1950s following the discovery of the Ziegler catalysts.[3,4] They are produced through a low pressure process and have few branches. Aside from these two families of polyethylenes, later came the linear low density polyethylene (LLDPE) form, which has a density similar to the LDPE. These

are copolymers of ethylene with α-olefins such as 1-butene, 1-hexene and 1-octene. The copolymerization generates linear chains with controlled amount and length of short chain branches. The most important forms of LLDPEs are produced with metallocene catalysts,[5,6] which generate polymers with relative narrow molecular weight distribution.

Modification of polyethylene materials is largely conducted through tuning the chain structure. Researchers can create chains with complex microstructure, such as short chain branching, long chain branching, combs, and bottle brushes.[7–11] Integration of the monomers within a single chain can also be tuned, generating polymers varying from statistical copolymers to block copolymers. Although a wealth of knowledge has been generated by analyzing correlations between their chain architecture and the material properties, such analysis is often based on empirical relationships established from existing systems. The investigation of material properties from engineered materials is still largely a case-by-case task. Once an existing chain structure is modified or integrated with another system, the previous knowledge may no longer be useful. To reduce the time and labor cost in the current trial and error practice for resin development, it is necessary to establish a direct correlation between the molecular structure and the bulk material properties.

1.2 Polyethylene

1.2.1 Semi-crystalline nature of polyethylene

At room temperature polyethylene has both amorphous and crystalline domains. These semi-crystalline materials generally have melting points ranging between 90 – 130 ºC depending on the chain structure, providing robust bulk mechanical properties at ambient temperature, and high processability above the melting point. Due to the semi-crystalline nature of polyethylene, any attempt to establish the chain structure-property relationship has to be based on understanding of the crystal structure. The stable form of

molecular packing for the CH_2 units in the crystalline domain reflects all-trans sequences that chain fold into lamellae. The arrangements of chains in a unit cell is illustrated in Figure 1.1.[12] The thickness of the lamellae is typically ~100 Å, while the contour length of a polyethylene chain with molecular weight of 100 kDa is about 9,000 Å. This means that each polyethylene chain passes through the lamellar crystallites many times, either folding back to enter the same crystallite it emerges from, or extending to enter an adjacent crystallite. A model proposed by Spells and others indicates that in a single crystal sheet (which can be formed by cooling a dilute polyethylene solution) approximately 75% of the chain strands emerging from a crystal sheet fold back and re-enter the same sheet at an adjacent position.[13,14] In the melt, on the other hand, Schelten et al. demonstrated using small angle neutron scattering that the average radius-of-gyration of the polyethylene chains remain approximately the same upon cooling from the melt.[15,16] This indicates that chains cooled from the melt maintain a configuration that interconnects the crystallites.

The most common crystalline structures found in a cooled polyethylene melt are spherulites, which consist of an assembly of lamellar crystallites separated by amorphous domains, where irregularly packed chain segments reside. A scheme of such an assembly is shown in Figure 1.2.[17] Note that the tie molecules traverse the amorphous regions, thus connecting crystal lamellae.

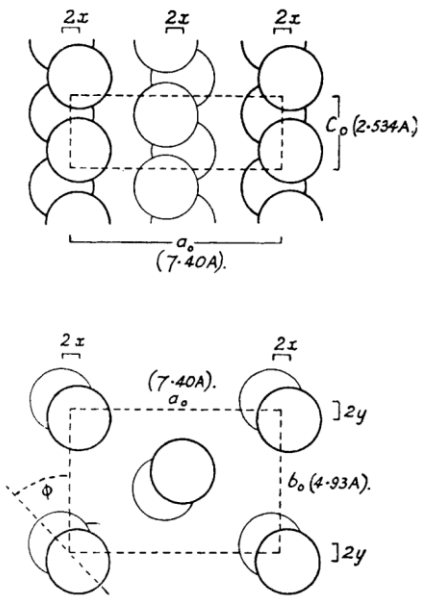

Figure 1. 1 Repeat unit arrangement in the unit cell of polyethylene a crystal. Each sphere corresponds to a CH_2 unit. (Above) Seen along the *b* axis. (Below) Seen along the *c* axis. Reprinted with permission from Bunn, 1939.[12]

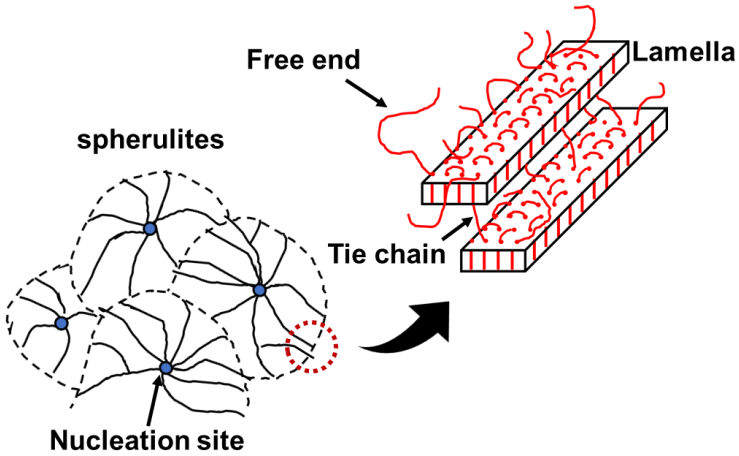

Figure 1. 2 Scheme of spherulites and lamellae within semi-crystalline polyethylene.

1.2.2 Solid deformation of polyethylene

Polyethylene undergoes profound deformation during processing and appreciable stress is applied to the material. Polymers respond to the applied stress across all length scales, rooted in the single chain response. Ethylene-based polymers and copolymers are engineered in forms such as linear chains, chains with short chain branching, chains with long chain branching, and olefin block copolymers, to deliver properties varying between soft rubbers and hard plastics. These days the mechanical properties and processability of these hydrocarbons are tuned by engineering the structure of individual molecules, with most of the modifications on monomer and single chain levels. Understanding the response of these modified chains to external stress is crucial for the formulation of advanced plastic materials.

Due to the semi-crystalline nature of polyethylenes, efforts to interpret the chain behavior during material deformation always center on interpreting the interconnection between chain strands and crystals, and their motion at different stages of deformation. Figure 1.3 illustrates an idealized engineering stress versus Hencky strain relationship of a polyethylene during uniaxial stretching in the semi-crystalline form. The engineering stress is the force normalized by the initial sample cross-section area. The Hencky strain is the natural log of the ratio between the stretched gauge length and the initial gauge length of the specimen. An initial regime where the stress increases with strain while obeying Hooke's law is identified as the elastic deformation stage for the material. Here chains respond to the stress by rearrangement to accommodate the bulk elongation, translating from the low energy state to an entropically less favored elongated state. Macromolecular rearrangement in the linear elastic limit occurs primarily by chain stretching in the amorphous inter-lamellae domains, as these domains have a lower modulus compared to the crystals, and the segments in the crystallites are constrained by the crystalline unit cells. This elastic deformation does not disrupt the long-range configuration of the chains, but

only varies the trans- and gauche- fractions of chain sequences, therefore the strain is recoverable upon unloading of the applied force. At the yield point associated with peak stress, the material enters a regime of plastic deformation, accompanied by a drop in the engineering stress followed by extension at relatively constant stress, possibly accompanied by the formation of a "neck" with reduced cross section. The neck propagates along the gauge section, eventually occupying the entire gauge length. Microfibril structure develops during plastic deformation resulting in stretched and aligned chain bundles,[18,19] with alternating crystalline domains and amorphous regions along the bundles (Figure 1.4). The next stage of stretching results in an abrupt increase in the stress, which is referred to as the strain hardening regime. The extended fibers slide past each other during the final stage of deformation, ultimately ending in fracture of the specimen.

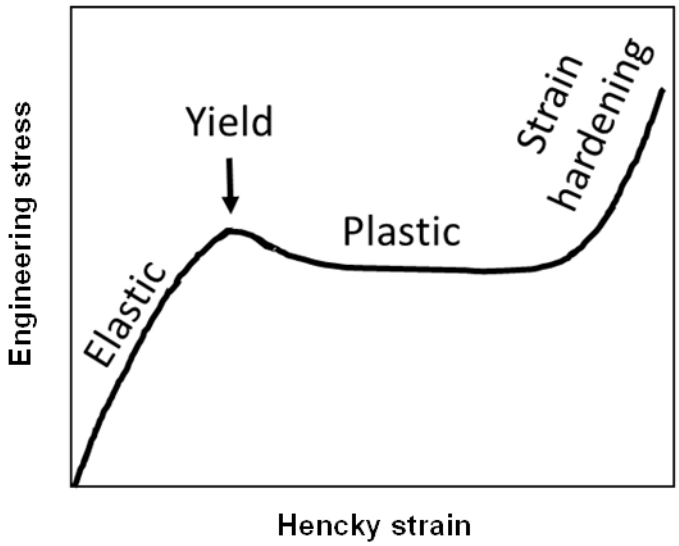

Figure 1. 3 Idealized stress-strain curve of a cold-drawn polyethylene sample.

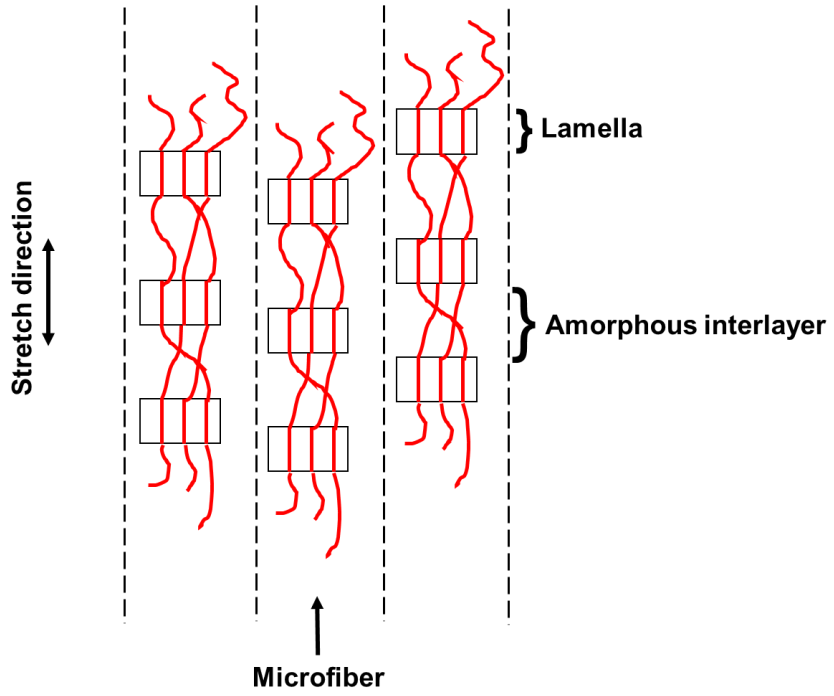

Figure 1. 4 Scheme of the microfibril structure formation of a stretched polyethylene during the plastic deformation regime.

The plastic deformation regime, where the most dramatic chain structure transformation occurs, is at the core of understanding the deformation mechanics of polyethylenes. From the isotropic spherulites (prior to stretching) to the fibril bundles (beyond strain hardening), profound structural changes take place at the molecular level. Any successful modelling has to be able to address both the single chain behavior and the collective movements of the crystals. Peterlin proposed that for uniaxially deformed polyethylene and polypropylene the structural transformation involve three primary processes:[20]

(1) *The continuous plastic deformation of the spherulitic structure before the neck* where crystalline lamellae reorganize by shear, slip, and rotation of crystal stacks, twinning of crystals, chain segment tilt and slip within lamellae. By this means

the spherulites are softened and ready to accommodate later reorganization. At this stage chains remain in their folded state.

(2) *The discontinuous transformation in the neck from the spherulitic to the fibril structure*, during which the lamellae crack and form micro-fibrils (bundles of chains). Chain bundles within the cracks unfold from the lamellae and take the role of tie chains. The transformation from spherulitic domains to fibril-like structure calls for substantial rearrangements of chains. Peterlin hinted that local crystal melting due to heat generated from crystal fragmentation is a potential source of chain flexibility.

(3) *Plastic deformation of the fibril structure after the neck*, which closely aligns with step (2). At this stage the microfibrils slip past each other, while unfolding and stretching the tie molecules.

The above scheme has to be examined carefully due to the complexity of the process it aims to resolve. Specially, investigation over the single molecular level is a fundamentally vital component. As shown in the discussions above, chains tying crystals, either the ones pre-existing in the bulk prior to deformation connecting the lamellae, or the newly formed ones through unfolding of segments within the lamellae cracks, are critical in defining the response of the bulk material.

1.2.3 Tie chains

The mechanical properties of semi-crystalline polyethylene have been studied intensely since its discovery. It has been apparent that the consideration of the amorphous region, especially the portion of chains in that region that connect adjacent crystalline lamellae, the tie chains, has to be incorporated to establish a satisfactory picture of the material structural change during deformation. In 1966 Keith et al. reported an experiment

that successfully visualized the tie chains binding together crystals in spherulites formed by cooling a blend of polyethylene and dotriacontane (n-$C_{32}H_{66}$).[21] They dispersed polyethylenes of various molar mass together with dotriacontane in a decalin mixture, and prepared thin films of the blend by vaporizing the decalin from droplets of the mixture on a hot plate followed by cooling. They then removed the wax content by washing the films with xylene to expose crystalline spherulites. Imaging of the thin films clearly shows bundles tying together crystalline domains, both within single spherulites, and at boundaries of spherulites (Figure 1.5). Note that the long spacing of the crystalline domains observed in that research is approximately 800 nm, a value much higher than values obtained through small angle X-ray scattering (SAXS) of cooled polyethylene melts (20-30 nm), which is most likely a result of the dilution from the wax content.

There have been appreciable efforts in quantifying the tie chain statistics. Lustiger and Ishikawa demonstrated that infrared dichroism is a viable method for estimating the relative concentration of the tie molecules,[22] although the technique does not directly generate the counts of individual tie chains. Qualitatively the number of tie chains increases with polymer molecular weight. They also found that increasing the butene comonomer content in the high molecular weight chains results in higher tie molecule concentration, presumably due to the branched part of the chains being excluded from the crystals, therefore these chains have higher amorphous portion and form longer bridges. The result is in line with the observed crack resistance of the more branched materials. Huang and Brown calculated the probability of tie chain formation by assuming chains will form ties if the end-to-end distance of the coil exceeds the lamellae long spacing.[23] They also conclude that increasing molecular weight has a positive impact on tie chain formation. They reported that the long spacing of the lamellae decreases with increasing branch fraction, mainly as a result of the thinner lamellar plates. The tie chain fraction will therefore be higher in more branched materials. Prasad and Grubb utilized Raman

spectroscopy to identify the taut tie-molecules content in cold-drawn polyethylenes.[24] They reported that 20% of the all-trans configuration sequences are within the tie chains, yet they carry more than half of the stress load on the fiber.

With these efforts in characterizing the concentration and localization of tie molecules, there remains an important question to be answered: by what means can we connect the molecular behavior to the bulk material deformation?

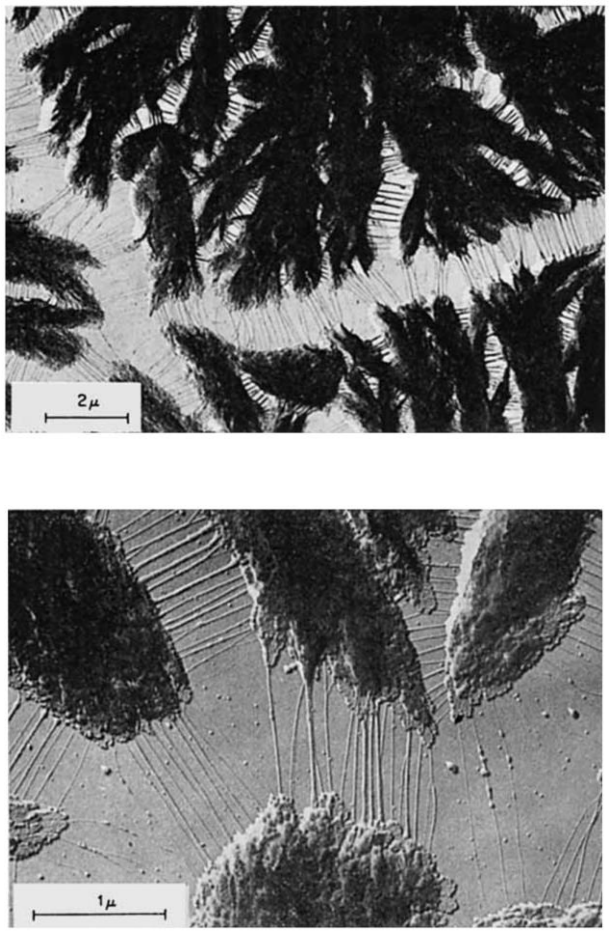

Figure 1. 5 TEM images of polyethylene spherulites and the tie chain bundles. (Upper) Boundary region between spherulites grown at 95 ºC in a polyethylene fraction (M_w = 726,000). (Below) View at higher magnification of the specimen shown in the upper image. Reprinted with permission from Keith et al., 1966.[21]

1.2.4 Molecular characterization of polymer deformation

Through research conducted over recent years there have been a few options developed to characterize structural changes during the deformation of polyethylene. Birefringence and spectroscopy have long been utilized to reveal molecular evolution of deformed polymers. Crawford and Kolsky,[25] as well as Raumann and Saunders,[26] examined experimentally the birefringence of drawn polyethylene and related it to molecular orientation. In a modeling effort, Ward developed an expression that predicts the birefringence evolution of stretched polyethylene that qualitatively aligns with experimental results.[27] Stein and Norris used birefringence and infrared dichroism to characterize the chain orientation within a deformed polyethylene film.[28] Coutry performed small angle neutron scattering and Fourier-transform infrared spectroscopy (FTIR) on a set of drawn polyethylenes with deuterium labeled probe molecules.[29] The experiments were done in a stepwise manner, where the samples were drawn to a desired ratio and held for measurement. The results show that the individual chains become anisotropic upon drawing, evidenced by the distinct radii of gyration parallel and perpendicular to the drawing direction. Relaxation appears to be slow and limited after unloading. A potential problem with the above scheme is that the sample was held static during characterization, therefore it is difficult to establish a direct correlation between the observed chain orientation and the measured mechanical response, especially for amorphous materials that can undergo non-negligible relaxation during the hold time.

To actually pin down the structural response of materials with the observed mechanical strength, rheological techniques have been combined with scattering or spectroscopy methods to reveal information of material flow or deformation *in-situ*. Challenges in successful application of rheo-scattering techniques are mainly 1) obtaining the right contrast, 2) designing the proper sample environment, and 3) matching the

deformation time scale to the instrumental time scale.

To date, in situ characterization of single chain behavior during material deformation remains a challenge. Onogi and Asada showed that FTIR can be applied to track the average orientation of chains within a deforming polyethylene via a rheo-optical steup.[30] Luap et al. designed experiments where the birefringence of an elongating polystyrene melt can be monitored, again generating the average chain orientation.[31] In situ X-ray experiments are well suited for probing the structural evolution of crystals within the material. Butler et al. investigated the solid deformation of different grades of polyethylenes,[32–34] using small angle X-ray scattering (SAXS) to monitor the crystal organization, and wide angle X-ray scattering (WAXS) to probe the local chain segmental arrangement. Notwithstanding the ease of the in-situ X-ray in probing the structural evolutions of polymers, it is not a proper tool for single chain characterization as there is no contrast for distinguishing two chemically similar hydrocarbons. Small angle neutron scattering has the ability to provide direct quantification of chain dimensions. However, due to the considerably lower accessible flux compared to other types of radiation sources, the typical time scale for a successful experiment is often too long (~5 min per measurement) to track rapid molecular motions. Therefore, most efforts on tracking molecules under deformation are either under steady state conditions (for example, a steady shear deformation),[35–38] or performed in a stepwise mode where the sample is held in the deformed state for the measurement.[39–42] An obvious concern with this scheme is that deformed chains could be relaxing during the measurement, resulting in an averaged outcome, unless some quenching steps are performed to freeze chain movements.

A potential solution for the dilemma discussed above lies within the time dimension of the scattering experiments that has attracted less attention in the history of small angle neutron scattering. This involves keeping track of the moment when each neutron hits the detector. In prior research this dimension of information has been mainly used in time-of-

flight SANS experiments associated with pulsed sources, where the time when neutrons arrive at the detector are correlated with the neutron wavelength. This dimension has been of less interest for neutron research facilities that use reactor generated continuous neutron beams, such as the facility at National Institute of Standard and Technology (NIST). NIST first introduced an event mode data processing algorithm to their data processing software in 2013, which opened access to time-based neutron scattering data analysis. Now the software has been iterated through a few generations and is much more stable. Taking this time dimension of information, the neutron counting statistics on the detector of a fast process (thus a short time period) can be enhanced, by repeating the experiment in an identical manner and accumulating the scattering data from a specific stage of experiment that is being investigated, through picking only the SANS patterns from the time window corresponding to that stage and combining the patterns obtained from separate experiment runs. Recently, Calabrese et al. showed an example where a wormlike micellar solution under oscillatory shear was monitored continuously with SANS,[43] while through post data processing, different stages of micellar deformation were successfully resolved. The time binning scheme is illustrated in Figure 1.6.

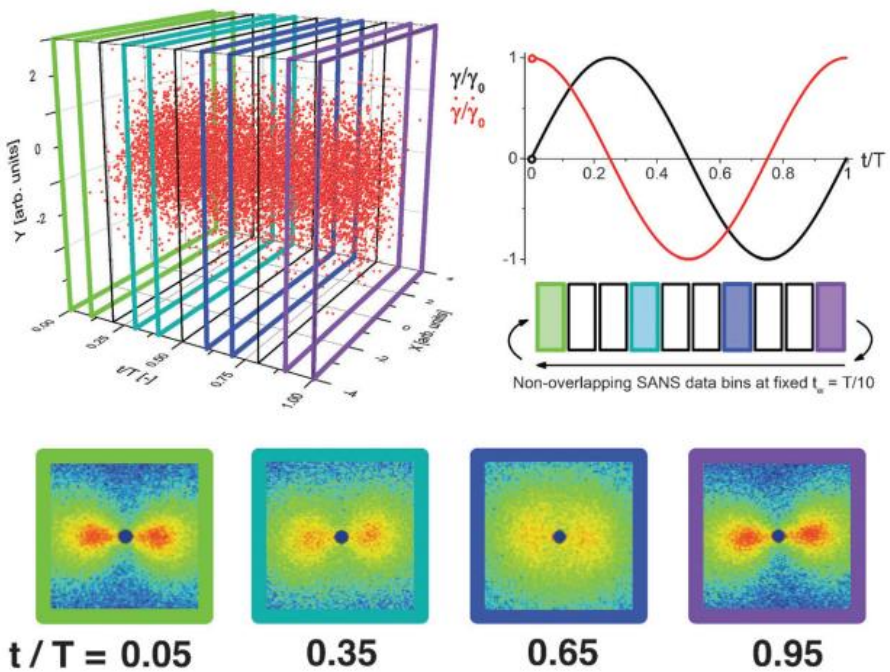

Figure 1. 6 Example time-resolved neutron scattering experiment of period T, where the detector records the spatial X and Y positions, and time of detection, for each scattered neutron. Each red dot represents an individual scattering event. The standard binning method for an oscillatory shear experiment groups neutrons registered within an interval of time, t_w, together (indicated by colored and black lines), forming a single scattering pattern with temporal resolution t_w. Here, $t_w = T/10$. Note the two temporal ends of the figure are joined, such that $t/T = 0 = 1$. Reprinted with permission from Calabrese et al., 2016.[43]

1.3 Small angle neutron scattering (SANS) enabled by the isotope exchange reaction

1.3.1 Introduction

To resolve the correlation between the single chain structures with the material properties, SANS is the most direct technique. SANS is a unique method for probing

information such as single chain conformation,[44] blend phase behavior,[45–47] ordering of block copolymers,[48–50] micellization, and thermodynamics of micelle structures.[51–54] There are many other systems that can potentially be analyzed with the assistance of SANS.[55–58] Like any other type of scattering technique, contrast between the scatterers and matrix has to be present to extract useful information from SANS experiments. Indeed, the application of SANS to polymers is enabled by the ability to tune the scattering length density of individual molecules by isotope substitution. Such isotopic substitution leaves the chemical and physical properties of the labelled material largely unaffected. The most frequently performed isotope labelling is by replacing hydrogen with deuterium, as these isotopes exhibit a considerable difference in the coherent scattering length (Table 1.1). A few examples of coherent scattering length and coherent scattering length densities of materials (calculated based on the material density) are listed in Table 1.1. An important observation is that large differences in coherent scattering length densities between protonated polyolefins and their deuterated counterparts are present. Contrast for SANS experiments can therefore be acquired and tuned by deuterating polyolefins to various degrees. Incorporation of the heavier isotope, deuterium, into polymers, therefore has been a topic being discussed for decades.[59–62]

Conventionally, deuterium is introduced by synthesizing polymers from isotopically labeled monomers.[59,60] However, there exist two drawbacks that limit the application of this method: (i) deuterated monomers are usually quite expensive, with a few examples listed in Table 1.2, and (ii) it is difficult to prepare deuterated products that match protonated materials exactly in aspects such as molecular weight and distribution. Another option of isotopic labeling is addition of deuterium to unsaturated polymers such as polybutadiene (PB),[63] polyisoprene (PI),[64] and polystyrene (PS).[65] Labeled molecules of polyethylene (PE), polyethylenepropylene (PEP), and polycyclohexylethylene (PCHE) can thus be prepared. This method produces matched hydrogenous and partially deuterium

labelled pairs of polymers. However, the limitation is also obvious: this method can only be applied to polymers that contain unsaturated bonds.

A third option involves substitution of existing hydrogen atoms with deuterium atoms, a method that avoids the above shortcomings, especially for saturated polyolefins. Considering the size of the synthetic polymer market in which over 50 wt% of polymers produced are polyolefins such as polyethylene and polypropylene,[66] it is beneficial to develop this H/D exchange as the labeling technique for commercial polyolefins, as it can be applied regardless of the synthetic history of these products.

Table 1. 1 Scattering length densities of hydrogenous and deuterium labelled materials

Material	Formula	Molar mass of repeat unit (g/mol)	Material density (g/cm^3)	Volume per repeat unit (v, 10^{-22} cm^3)	Coherent scattering length per unit (b, 10^{-12} cm)	Coherent scattering length density ($\rho = b/v$, 10^{10} cm^{-2})	Incoherent scattering length per unit (b_{inc}, 10^{-12} cm)
Carbon-12	^{12}C				0.665		0
Hydrogen	H				-0.374		2.527
Deuterium	D				0.667		0.404
h-PE	$(CH_2)_n$	14	0.779[a]	0.299	-0.0830	-0.278	
d-PE	$(CD_2)_n$	16	0.890[b]	0.299	2.00	6.69[c]	

[a] Density was calculated for melt at T = 150 ℃.

[b] Density of deuterated material was calculated by assuming that the volume per repeat unit is the same as that of protonated material.

[c] For partially deuterated polyolefins with formula of $(CH_xD_{2-x})_n$, the coherent scattering length density will take intermediate values between those of h-polymer and d-polymer.

Table 1. 2 Commercially available deuterated materials and their cost

Material	Price per gram ($/g)	Price per mole D ($/mol D)
Styrene-d8	107[a]	1498
Butadiene-d6	134[a]	1342
Cyclohexane-d12	39[a]	312
Deuterium	1.4[b]	2.9

[a] From Sigma-Aldrich

[b] From Cambridge Isotope Laboratories, Inc

1.3.2 Hydrogen-deuterium exchange in small molecules: evidence of C–H activation with transition metal catalyst

As early as the 1960s, there was great interest in studying methods for C–H bond activation, with the intention to synthesize functionalized compounds from industrially abundant hydrocarbon sources, including saturated, aromatic and olefinic molecules. At first the activation was mainly conducted with C–H bonds associated with aromatic and unsaturated structure due to their higher reactivity. Garnett and Hodges showed that deuterium can be introduced into aromatic compounds by exchanging hydrogen with deuterium from D_2O when using a platinum salt catalyst.[67] Fujiwara et al. managed to add olefin units directly to aromatic substrates using a palladium salt catalyst,[68] showing that the C–H bonds in unsaturated compounds can also be activated. Chatt and Davidson reported the activation of alkyl hydrogen and formation of metal-alkyl complex with a ruthenium catalyst.[69] These pioneering work showed that C–H bonds can be readily activated and dissociated, forming metal-carbon and metal-hydrogen/deuterium bonds.

Both heterogeneous and homogeneous catalytic examples exist. Researchers found that such bond activation could be exploited to swap hydrogen and deuterium between protonated compounds and deuterated materials, such as heavy water or other deuterated species.[70–75]

Subsequently researchers found that similar reactions can be applied to alkanes.[71,72,76] A few other transition metals, such as Zr, Mo, Re, and Th, are also capable of activating C–H bonds. Many of these examples uses homogeneous catalysts, such as platinum salts.[67,71] It is generally accepted that the C–H dissociation/association process randomizes the isotope content in a mixture of normal and deuterium labelled species therefore mixing a substrate compound with a highly deuterated material essentially generates a deuterium labelled substrate. An example scheme of labelling alkane with assistance of a homogenous Re catalyst and benzene-d6 is illustrated in Figure 1.7.[70] The structure of the substrate alkanes was found to be a key factor that affects the exchange process. Hodges et al. found that among the protons within a few n-alkanes and their isomers, the rate of exchange follows: primary C–H > secondary C–H > tertiary C–H.[72] A similar observation was reported by Jones and Maguire using several n-alkanes and cycloalkanes,[70] with an interesting example that tetrahydrofuran can also participate in the exchange reaction, and at a high rate. These results suggest it may be possible to replace hydrogen with deuterium in polyolefins using similar bond activation processes.

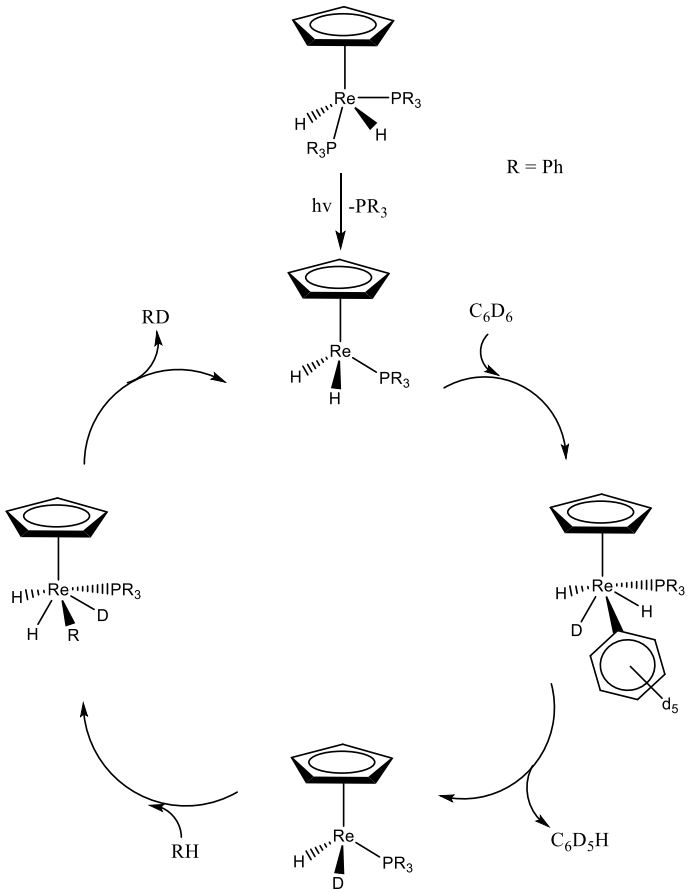

Figure 1. 7 Example of a hydrogen/deuterium exchange scheme. Reprinted with permission from Jones and Maguire, 1986.[66] Copyright (1986) American Chemical Society.

1.3.3 Hydrogen-deuterium exchange in polymers

When researchers realized that the H/D exchange reaction performed with small molecule hydrocarbons can potentially be translated to large hydrocarbons, they started to investigate whether the same mechanism can be translated to polymers.[61,62,77,78] A desired protocol should provide deuterium labelled products with adjustable deuterium content and statistically random substitution of deuterium for hydrogen atoms, while maintaining the structure and properties of the original material. Such deuterium labelled polymers will make ideal probe materials, as that they mimic the parent hydrogenous material in every

way, with only differences in isotope content, automatically providing "matched" pairs of protonated and deuterated materials. This is especially important in the application of SANS to commercially relevant polyolefins. Preparation of commercially relevant polyolefin from deuterated monomers is impractical. These polymers are produced on a large scale of 10^5 - 10^6 kg per line, per year, and an exact reproduction of the material made at the large scale in the laboratory is difficult or impossible. Moreover, the cost of deuterated monomer is high. Saturation of polydienes with hydrogen and deuterium separately does serve the task of generating matched pairs, however, as discussed above, it is limited to polyolefins that have unsaturated precursors, which is not usually true for commercial polyolefins. Another advantage of the isotope exchange reaction is the potential to adjust the deuterium amount of the molecules, by adjusting the source and concentration of deuterium, reaction time, reaction temperature, and catalyst type and amount. Controlling the deuterium content is especially important with high molecular weight polymers, which can phase separate due to isotope effect.[79,80] Reducing the deuterium content reduces the driving force for such phase separation. However, partial deuterium labelling can introduce inhomogeneous placement of the isotope along a polymer chain, which can complicate the application of the SANS technique.

Despite the advantages described above, early efforts to perform H/D exchange with polyolefins proved to be difficult. In an attempt to test a theory that the isotacticity of semi-crystalline polypropylene is merely a consequence of stereoregular arrangement of repeat units, Case and Atlas performed H/D exchange with several isotactic propylene samples, hoping to generate atactic material through racemization.[61] They used cyclohexane as the solvent, and a nickel-kieselguhr catalyst. In the end most of the deuterium (from D_2 gas) entered the solvent, with maximum degree of exchange being only 3%. Tanzer and Crist exchanged 6.5% of the hydrogen from a hydrogenated polybutadiene sample with deuterium,[81] using a rhodium-charcoal catalyst, and again cyclohexane as the solvent. They

later tried to push the degree of exchange to a more feasible level. They prepared cyclohexane-d6 through catalytic saturation of benzene with deuterium, which was then used as the deuterium source. The degree of deuterium labelling increased to 60% for a polyethylene sample.[82] In another example, Willenberg demonstrated a method capable of exchanging up to 90% of the aromatic hydrogens in polystyrenes with deuterium,[78] using perdeuterated benzene as both the deuterium source and the solvent, and a homogenous aluminum based catalyst. However, degradation of chains occurred during the reaction.

Recently, Habersberger and co-workers demonstrated a new isotope exchange technique for saturated polyolefins,[62] where the degree of exchange for the first time becomes attractive for application to commercial polyolefins. Gaseous deuterium was used as the isotope source. The catalyst, Pt/Re-SiO_2, which was previously used for hydrogenation of unsaturated polymers,[65] showed unexpected activity in exchanging hydrogen with deuterium. A set of polyolefins including high density polyethylene (HDPE), polyethylenepropylene (PEP), and isotactic PP (iPP) were used for labeling; several alkane solvents including isooctane, heptane, decane, decalin and cyclohexane were used as the reaction medium. Several important observations are summarized below:

(1) Deuterium content ranging from less than 1% to 68% was observed in the polymer products, depending on experimental conditions.

(2) The most extensive deuterium exchange occurred with isooctane, while products in heptane and decane were not exchanged as much. Products from reaction in decalin showed no detectable amount of deuteration.

(3) With isooctane solvent, the deuterium content of d-HDPE products varied from as high as 68% with HDPE after a single cycle, to modest exchange (20% - 40%) with PEP, and eventually no exchange with iPP, although a recent progress suggests that varying the solvent is potentially a viable route for iPP labelling.[83]

(4) Molecular weight average and distribution are largely maintained after the exchange cycle, though a slight decrease in molar mass was noticed for HDPE, a result related to fractionation during sample recovery procedures rather than chain scission.

It is worth noting that the exchange reaction utilizes a heterogeneous system through incorporation of the Pt/Re-SiO_2 catalyst. The micron sized catalyst particles have ultra-wide pores sized at a few hundreds of nanometers, allowing polymers to freely diffuse through pores and probe the surface, as the typical radii of gyration of polymers used in this research are below 20 nm (for polyethylenes with molecular weight around 100 kDa). Transition metal particles with sizes around 10 nm are supported by the porous substrate.[84] The schematic diagram of the heterogeneous reaction system is illustrated in Figure 1.8.

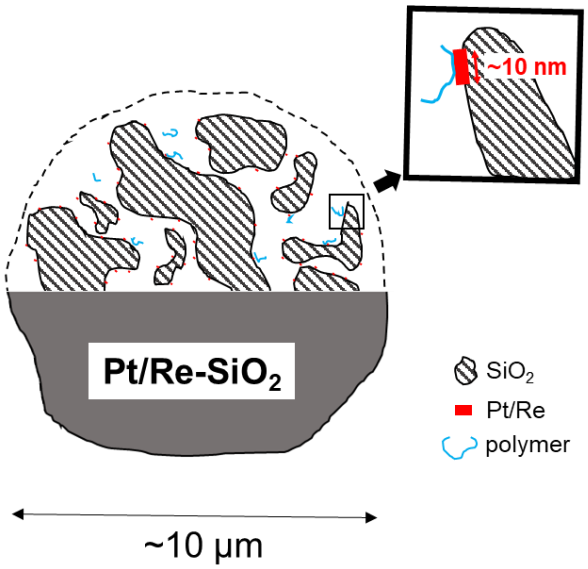

Figure 1. 8 Schematic diagram of the Pt/Re-SiO_2 catalyst used for isotope exchange. The upper hemisphere is shown as an intersection cut of the porous catalyst.

1.3.4 Emerging challenges in understanding the isotope exchange reaction

The method discovered by Habersberger and co-workers for the first time introduced a route to add deuterium to existing polyolefins, without synthetic complexity and

essentially no side reactions. There are, however, several interesting questions that need to be addressed prior to translating the approach to routine application.

Whether the exchange generates statistically random deuterium labelling remains unclear. The pure labelled polyethylene samples in Habersbersger's work showed significant coherent scattering when investigated with SANS,[62] even though the sample was not blended with hydrogenous polymer to introduce contrast. This presents a clue that the distribution of deuterons within the material is neither uniform nor statistically random. Indeed, they reported that the concentration of $(CH_2)_{n>5}$ sequences is higher than there should be in a randomly labelled polyethylene. It is not clear, at this point, whether the inhomogeneity in deuteron distribution is limited to the local segment scale, or extends to the whole molecule level. It is also not clear what is the source of the inhomogeneity.

Whether the materials can be used to extract correct chain statistical information should be analyzed. Researchers have been utilizing deuterium labelled polymers, either through synthetic approach or saturation approach, to analyze chain conformation with SANS. In most of these studies the labelled polymers have controlled and uniform deuteron distribution. We need to, however, understand whether the same information can be obtained while using the polymers with inhomogeneous deuterium distribution. Balsara et al. analyzed a series of deuterated polybutadienes,[63] and found that the total deuterium quantity in the polymers is higher than that calculated from the stoichemistry of polybutadiene deuteration, possibly due to isotope exchange during catalytic saturation. The exchange must lead to an inhomogeneous deuterium distribution, as the SANS results showed considerable coherent scattering. They proposed a model capable of describing the SANS results obtained from the labelled polymers while considering the inhomogeneity in deuterium labelling, and successfully extracted the chain statistics accordingly. It is worth investigating whether the same approach can be applied to the isotope exchanged polymers. Additionally, since we are targeting commercial polyolefins which often have wide

distributions of molecular weights and branch content, proper models capable of describing such non-uniform materials must be developed.

1.4 Summary and scope

This thesis work aims to provide insight into the solid deformation mechanisms of polyethylene, by extrapolating in situ characterization capabilities on the single molecular level. A clearer picture of how single chains evolves during the polymer deformation is essential in resolving the current models describing the solid deformation of semi-crystalline polyolefins.

Three interrelated pieces of work were performed in order to achieve the proposed goals. First, in Chapter 3, the isotope exchange reaction is described and applied to several polyolefins to produce deuterium labelled polyolefins. The factors affecting the exchange are investigated and discussed, mainly concerning the molecular weight distribution and branch structure of the substrate molecules. In Chapter 4 these deuterium labelled polyolefins are investigated with SANS, primarily to resolve the concern of the inhomogeneous deuterium labelling, by mathematically accommodating these inhomogeneities in modeling efforts, to prove that the labelled materials are capable of revealing single chain conformation of polyethylenes. In Chapter 5, a labelled polyethylene material is used as the model material to build an in situ rheo-SANS platform, while simultaneously providing the single chain evolution information of a cold-drawn polyethylene. This platform is now ready to be extended to other type of polyolefin materials, as well as polyolefins in the melt state. Lastly, in Chapter 6, we summarize the thesis work, and suggest possible future directions worth investigating.

Chapter 2

Materials preparation and characterization

The objective of this chapter is to summarize and describe the techniques and instruments for preparing and characterizing the polyolefin materials, prior to sending these materials to the next stage of the research: the isotope exchange unit. The materials investigated in this research are derived, in general, from two sources, and have unique characteristics related to their origin. The first category of polymers came from lab scale synthesis by anionic polymerization. Polymers prepared via this route are free from ambiguities from molecular weight and microstructure, and therefore hold the potential of serving as an ideal model molecule database, although they are synthetically demanding in terms of reaction conditions and purity. On the other hand, the industrial polyolefins, as the motivation and the primary target of the techniques developed through the course of this study to be applied on, are the product of industrial plants that are produced in the order of 10^{11} kg each year. These polymers are complex mixtures of chains with varying length and microstructure, which are all interacting in a complex manner. To effectively engineer these complex materials, a good understanding of the chain structure - material property relationship has to be established. Fortunately, a bridge between the lab scale model

materials and the industry scale commercial materials can be constructed. By analyzing the behavior of the model molecules with carefully controlled molecular characteristics, we can mimic the behavior of the different molecular components of the commercial materials. The leverage here, as it becomes clear, is a good understanding of the molecular architecture of both the model materials and the commercial materials.

2.1 Material preparation: anionic polymerization

2.1.1 Overview

Living polymerization, a key synthesis technique used in this research, is defined as "a chain polymerization from which irreversible chain transfer and chain termination are absent".[85] Like other polymerization techniques, living polymerization provides a route to unite monomer molecules and make long chain molecules. It also shares features of other polymerization routes such as initiation and chain propagation steps although, as a note which we will come back to, the initiation step is usually much faster than the propagation step. The unique aspect of this polymerization technique, as the definition suggested, is the lack of chain transfer and "automatic" chain termination, which are essentially the cause of the wide molecular weight and microstructure distribution often observed in other types of polymerization schemes. Indeed, the word "living" suggests that the macromolecules in the reaction will retain their active chain ends and remain ready for addition of new monomers, either of their same type or a completely different family of molecules. This allows the researchers to design a series of chain structure that are impossible or hard to synthesis before, especially block copolymers. A manual termination step is performed when the desired chain architecture is achieved, marking the retirement of the molecules from addition and delivering terminated, non-reactive polymers.

Living anionic polymerization is one of the various types of living polymerization.

The active chain ends, as the name suggests, are anions paired with metal cations from the initiator. Ziegler first suggested the possibility of polymerizing styrene and butadiene via consecutive addition of monomer molecules to the alkyl lithium initiator molecules.[86] In 1956, Szwarc et. al. first proved the viability of anionic polymerization experimentally using styrene monomer.[87] After that, the types of monomers that can be polymerized has expanded considerably, including several types of dienes, styrenes, epoxides, acrylates, and many other examples. A key feature to look for in the monomer molecules is substitute groups that are able to stabilize the negative charge of the anionic propagation center, which can often be achieved by delocalization of electrons.

The key aspects that make anionic polymerization attractive are the absence of chain transfer and self termination, and that the initiation step is usually much faster than the chain propagation. This leaves two major consequences regarding the polymer product of living anionic polymerization: first, the number average degree of polymerization, $\overline{\mathrm{DP}}_\mathrm{n}$, can be determined solely from the ratio between the molarity of the monomer and the initiator. Second, the dispersity of the product will be increasingly narrow as the chain propagates, in the following form

$$\text{Dispersity } (Đ) = \frac{\overline{M}_\mathrm{w}}{\overline{M}_\mathrm{n}} = 1 + \frac{1}{\overline{\mathrm{DP}}_\mathrm{n}} \qquad (2.1)$$

Flory first proposed this relation for polymerization of ethylene oxide as early as 1940.[88] Experimentally, this means living anionic polymerization has the potential of generating polymers essentially approaching the monodisperse limit of polymer synthesis, and that the degree of polymerization of the product is highly predictable and controllable. Indeed, living anionic polymerization has proved to be one of the most assessible routes of preparing model molecules without ambiguities in terms of molecular weight and

microstructure distribution. However, as suggested previously, it is not the panacea for all model polymer building tasks. The main limitations are: (1) the reaction has to be conducted in a highly controlled environment free of impurities such as air or moisture, as the highly reactive living chain ends will react with them; (2) there are only a finite number of monomer species that can be polymerized successfully, although the selection of monomers has been quite expanded since the method was first discovered; (3) and unfortunately in some instances, the microstructure of synthesized polymers is not always that we targeted (such as the inevitable side chain incorporation when polymerizing butadiene). We will discuss these limitations in later sections.

Polymers synthesized in this research are polybutadienes, or PBD, which are polymers derived from the butadiene monomer. The reaction scheme consists of three major procedures: reaction initiation, chain propagation, and a final termination step. These procedures are illustrated in Figure 2.1. The addition of the ion pairs to the unsaturated monomer has two forms: 1,2 addition and 1,4 addition, as illustrated in Figure 2.1. Addition via the 1,2 form leaves a vinyl side group in the C4 repeat unit, which can be transformed to an ethyl side group through hydrogenation. The relative fraction of 1,2 and 1,4 addition can be tuned by adjusting experiment parameters such as the solvent, polarity adjustment from modifiers, and reaction temperature.

Due to the high reactivity of the anionic propagation centers, the polymerization reaction has to be conducted under strictly controlled conditions. Considerable attention has to be paid to purify the monomer and solvent, as well as maintaining an air and moisture free environment throughout the polymerization. In the following section, procedures for purifying each component of the reaction are introduced, followed by an example protocol for preparing a polybutadiene homopolymer.

2.1.2 Polymerization procedures

Glassware. All glassware was rinsed with tetrahydrofuran and deionized water followed by drying at 400 °C prior to use. The reactor is a 2 L round bottom flask with five threaded ports. The solvent flask is a 1 L one port round bottom flask sealed with a Teflon stopcock. The sample burette is a one port glass column sealed with a Teflon stopcock. Manifold connectors provide connection between the reactor and the Schlenk line, the monomer burette, and the pressure gauge, with one manifold bearing a rubber septa sealed port allowing injection of materials with a syringe. The assembled reactor was evacuated using rotary pump and refilled with argon for at least five times before use.

Solvent purification. For a typical anionic polymerization reaction, over 90% of the materials used are the solvents, therefore obtaining dry and impurity free solvents is a procedure that needs extra attention. The solvents used for living anionic polymerization in this research are cyclohexane and tetrahydrofuran, with quite different polarity and therefore different impact on the microstructure of the polymer product. Butadiene has a higher tendency to be polymerized following the 1,4 addition route when reacting in cyclohexane, a non-polar solvent, producing polybutadienes with fewer side groups. The maximum fraction of 1,4 addition in the material series generated in this research is 92%. The polymerized molecules, therefore, contain at least 2 side groups per 100 backbone carbons, making the hydrogenated polymers similar to linear low density polyethylenes (LLDPE), a material with relatively high crystallinity. Tetrahydrofuran, on the other hand, favors 1,2-addition, producing amorphous materials even after hydrogenation. The solvents serve three main purposes during the polymerization process: (1) disperse the reaction materials so the reaction proceeds in a controlled manner; (2) dissolve and dilute the butadiene monomer that boils below room temperature (boiling point of butadiene: -4.4 °C), so the reaction can take place safely at ambient temperature; and (3) by combination of the two solvents and modifier molecules, the polarity of the reaction

medium can be tuned to generate polybutadienes with different microstructures.

The solvents were purified by purging with argon and passing through activated alumina and/or copper redox catalyst (CU-0226S, Engelhard) columns under inert atmosphere, thereby removing both residual moisture and polar impurities. For polymerization targeting high molecular weights (> 200 kDa), extra purification procedures were performed as any residual impurity will affect the eventual product molecular weight at a non-negligible level. In these experiments, the solvents collected from the purification columns were first mixed with sec-butyl lithium (1.4 M in cyclohexane, Sigma-Aldrich) at a ratio of 1 mL sec-butyl lithium / 500 mL solvent, stirred at room temperature overnight, and then distilled at 40 °C into a flask vacuumed and cooled with liquid nitrogen before entering the polymerization reactor.

Monomer purification. The monomer, 1,3-butadiene, was purchased from Sigma-Aldrich containing p-tert-butylcatechol as the inhibitor. As the monomer has a boiling point below room temperature (-4.4 °C) and is highly flammable, extra care has to be taken to handle the material. Cooling baths have to be used to retain the stability of the monomer at all times. Generally, a liquid nitrogen bath (-196 °C) can be used for material condensation, and an ice / salt bath (-10 °C) can be used for thawing and short-time storage of the monomer in liquid form.

n-butyl lithium (1.6 M in hexanes, Sigma-Aldrich) is used as the purification agent that reacts with residual air and reactive impurities in the butadiene monomer. The purification agent is used at ratio of 1 mL n-butyl lithium / 5 g monomer, and is evacuated to remove the hexane solvent. To purify the monomer, butadiene is first distilled into flasks containing the purification agent and cooled with a liquid nitrogen bath. The frozen mass is then thawed in an ice / salt bath and stirred with a magnetic stirring plate for an hour while submerged in the ice / salt bath. The procedure is repeated using another fresh batch of n-butyl lithium. The purified monomer is distilled into a glass burette cooled with liquid

nitrogen, and subsequently thawed for introduction into the poly merization reactor.

Microstructure tuning. The branching structure of the polymers made in this research can be tuned by varying the polarity of the medium, which is achieved by introducing polar molecules, tetrahydrofuran (THF) and bispiperidinoethane (DIPIP), into the non-polar solvent, cyclohexane (CHX). Modifying the [modifier]:[initiator] ratio is the most effective method for controlling the vinyl branch content in the resulting polybutadiene.[89] The reaction temperature is varied as well. Conditions for preparing the polymers used in this research are listed in Table 2.1. The range of 1,2 addition or vinyl fraction of the products in this research is between 10% and 100%, corresponding to 2.6% to 50% of ethylene branches per 100 backbone carbon atoms.

Reaction initiation. The reaction is initiated by mixing the initiator, sec-butyl lithium or n-butyl lithium, and the monomer in the solvent. Both initiators are capable of generating polymers with $Đ < 1.1$. The quantity of initiator necessary was calculated using the monomer mass m_{BD} and initiator concentration c_{ini}:

$$V_{\mathrm{ini}} = \frac{m_{\mathrm{BD}}}{M_{\mathrm{n}} c_{\mathrm{ini}}} \qquad (2.2)$$

where V_{ini} is the initiator volume required for making a batch of polybutadiene with number average molecular weight M_{n}.

To initiate the reaction, the purified solvent is first introduced into the reaction flask and stabilized in a bath at the target reaction temperature for 30 min. A calculated amount of initiator is drawn from the container with a gas tight glass syringe inside a glovebox. The syringe tip is protected by puncturing into a rubber septum to isolate the reactive initiator from air. The syringe is then removed from the glovebox and used to inject the initiator into the reaction flask through a rubber septum that seals the reactor. Polar modifier

is subsequently injected into the reactor where necessary. The purified monomer is then slowly added into the reactor from a glass burette cooled with ice / salt bath, through a stainless-steel flex tubing. Pressure is closely monitored during the material addition, and the monomer buret is returned to the cooling bath when the system pressure is above 8 psi. Dissolution of the monomer is evidenced by a monotonic decrease in pressure readings. The reaction is allowed to react for at least 12 h prior to termination.

Reaction termination. Polymerization reactions are terminated by addition of degassed methanol. For each reaction, 10 mL of methanol is first frozen in a liquid nitrogen trap and evacuated, followed by thawing at room temperature. The procedure is performed for five times to produce degassed methanol liquid. Purified methanol is then poured into the reaction flask through a manifold, and allowed to react with the living species for 30 min. The solution inside the reactor is then poured into cold methanol for precipitation of polymer products. The polybutadienes recovered was dried under vacuum at room temperature for at least 12 h, and immediately passed to the hydrogenation unit for saturation, which will be discussed in the next section.

Table 2. 1 Polybutadiene (PBD) polymerization conditions and products

Polymer	Modifier	[Modifier]:[Initiator]	Temperature (ºC)	M_w[b] (kDa)	$Đ$[b]	Vinyl fraction[c] (%)
PBD22-3	-	-	40	22	1.04	10
PBD25-9	THF	5	30	25	1.03	30
PBD23-10	THF	5	20	23	1.06	34
PBD22-12	THF	12	25	23	1.04	39
PBD25-15	THF	40	40	25	1.05	45
PBD27-19	THF	90	40	27	1.04	56
PBD26-24	THF	90	30	26	1.05	65
PBD34-33	THF	90	20	34	1.06	79
PBD22-41[a]	-	-	-77	22	1.04	90
PBD31-50	DIPIP	10	25	31	1.09	100
PBD4-3	-	-	40	4	1.06	11
PBD7-3	-	-	40	7	1.09	11
PBD100-3	-	-	40	100	1.08	10
PBD210-3	-	-	40	210	1.08	10
PBD610-3	-	-	40	610	1.06	10

[a] Tetrahydrofuran as the solvent; all others cyclohexane.

[b] Determined by SEC with THF as the mobile phase and universal calibration with PS standards.

[c] Determined with ^{1}H-NMR spectroscopy.

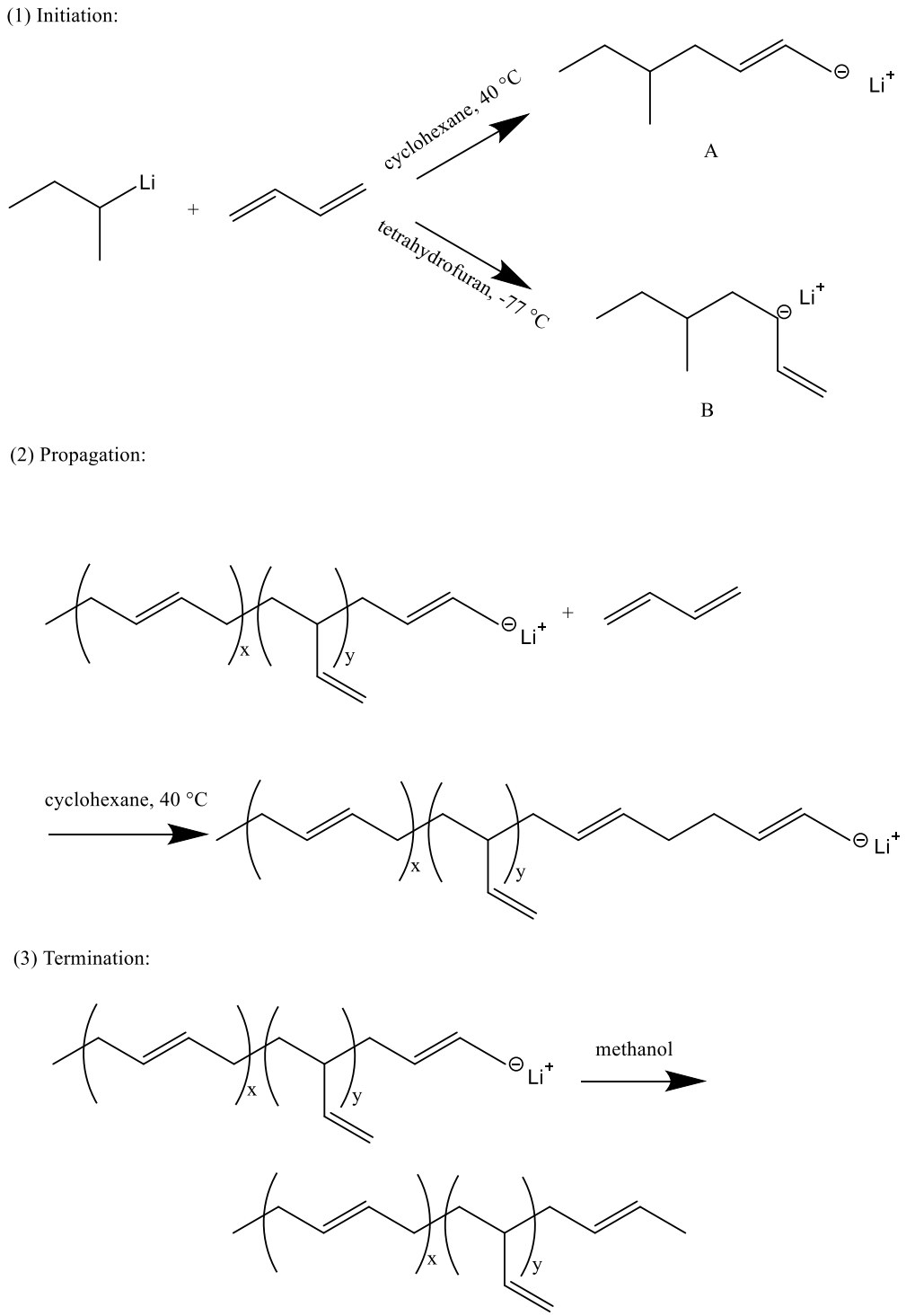

Figure 2. 1 Synthesis scheme of polybutadiene (PBD). (1) Initiation: the 1,4 addition product (A) and 1,2 addition product (B) are both illustrated. (2) Propagation: only the 1,4 addition product is illustrated. (3) Termination: only showing chain ends from 1,4 addition.

2.2 Materials preparation: catalytic hydrogenation.

Polybutadiene, the product of the anionic polymerization reaction in this research, has unsaturated bonds and by nature has a tendency to crosslink when contacted with air. The polymers are passed to a hydrogenation unit for addition of hydrogen to the double bonds following the anionic polymerization, generating polyolefins with relatively higher chemical stability. The hydrogenation follows the scheme as illustrated in Figure 2.2. The vinyl branches in the polybutadienes are converted to ethyl branches in the saturated polymers.

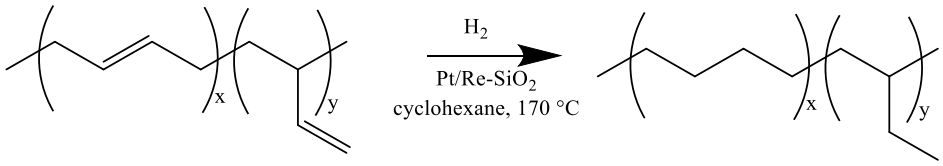

Figure 2. 2 Scheme for catalytic hydrogenation of polybutadienes.

Hydrogenated polybutadiene (hPBD) samples were prepared by addition of hydrogen to the unsaturated polymer samples in a 1 L stainless steel vessel. Polymers were dissolved in cyclohexane at a loading between 5 and 20 g per 500 mL solvent. Pt/Re-SiO_2 catalyst was used at a loading of 1 g catalyst per 5 g polymer. Polymer solution and catalyst were mixed in the vessel, which was then sealed and purged with argon for 15 min. The vessel was then pressurized with 500 psi H_2, followed by heating to 170 ºC for 17 h under magnetic stirring, during which the pressure in the reactor typically dropped by 50 – 150 psi. Hydrogenated polybutadiene with less than 3% branching is insoluble at room temperature in cyclohexane due to crystallinity. For these samples with M_w < 100 kDa, solvent was removed by filtration at room temperature followed by dissolution in 1,2,4-trichlorobenzene at 150 ºC, filtration through a 0.22 μm filter (Millipore) at 130 ºC (thus

removing residual catalyst), and precipitation in methanol. Filtration of the high molecular weight hPBD samples with this procedure, however, resulted in clogging of the filter membrane. Separation of catalyst from these samples was therefore performed by dissolving the polymers in 1,2,4-trichlorobenzene (TCB) at 150 ºC without stirring and recovering the polymers in the clear solution layer above the precipitated catalyst (removing most, but not all of the catalyst). Hydrogenated polybutadienes with more than 3% branching were soluble at room temperature in cyclohexane, and could be filtered through a 0.22 μm filter (Millipore) followed by polymer precipitation in cold methanol. Recovered polymers were dried under dynamic vacuum for at least 24 h prior to use.

2.3 Materials preparation: catalytic isotope exchange

The polyolefin materials, including the commercial ones and the lab synthesized hydrogenated polybutadienes, are labelled with deuterium through a heterogeneous isotope exchange reaction, which directly replaces the hydrogen atoms with deuterium atoms in the polymers. Generally, the polymer is dissolved in a hydrocarbon solvent at a temperature well beyond the melting point of the semicrystalline polyolefins, with the presence of a transition metal catalyst (Pt/Re on SiO_2) and gaseous deuterium for reaction. Habersberger et. al. previously discovered the exchange efficiency to be dependent on solvent type.[62] In this thesis work, the solvent applied is isooctane, the one found to deliver the highest amount of deuterium to the labelled products.

Isotope exchange reactions were performed in a 1 L pressurized stainless steel vessel. For each reaction cycle, weighed amounts of polymer and Pt/Re-SiO_2 catalyst were mixed with 500 mL of isooctane at loading ratios of 5 g polymer/1 g catalyst for a commercial linear low density polyethylene (LLDPE1), and 1 g polymer/1 g catalyst for hPBDs. The sealed vessel was purged with argon for 15 min then pressurized to 500 psi with deuterium gas. The reactions were conducted at 170 ºC for 17 h, after which the solutions were cooled

to room temperature and filtered through a 0.22 μm filter. Filtrate from samples with more than 3% branching was poured into cold methanol for precipitation. For samples with less than 3% branching, the solid polymer was dissolved in 1,2,4-trichlorobenzene at 150 ºC prior to filtration at 130 ºC. The filtered solutions were subsequently poured into 2 L of cold methanol for precipitation. The precipitates were recovered and dried at 150 ºC under vacuum for 12 h prior to any further characterization.

2.4 Materials characterization: size exclusion chromatography (SEC)

2.4.1 Overview

Size exclusion chromatography (SEC), or gel permeation chromatography (GPC), is a chromatography technique that separates and analyzes the analytes based on their size (hydrodynamic volume). For polymers, the hydrodynamic volume varies with chain structure, chain length, and solvent conditions; for a polymer with a specific microstructure in a controlled solvent condition, the molecular weight becomes the sole parameter controlling the hydrodynamic volume of the polymer. SEC uses a non-interacting column to separate polymers dissolved in the solvent on the basis of hydrodynamic volume, essentially probing the molecular weight distribution of the polymer sample. An SEC column has a core packed with porous gel particles, creating a porous space with wide pore size distribution across the chain sizes to be analyzed. The volume that is accessible to chains with different sizes thereby is different; larger chains are able to probe less volume when travelling through the column. For a typical experiment, a polymer sample is dissolved in the solvent and passes through the column with the mobile phase (the solvent) pumped at a steady flow rate. Time of chains exiting the column spreads out due to the different column availability for chains, with larger chains exiting earlier. The elution is analyzed with a refractive index (RI) detector or a multi-angle light scattering detector.

2.4.2 Molecular weight calibration

The data directly generated by the SEC unit is the detected intensity, corresponding to the concentration of the polymer (RI detector) in that elution volume, as a function of elution time. Calibration has to be performed to identify the molecular weight of the polymer within each elution volume, thus converting the intensity-elution time signal to a concentration-molecular weight result. According to the detector type used, there are generally two calibration methods, through universal calibration, or through calculating the absolute molecular weight from the light scattering data.

Universal calibration. Universal calibration is applied for the data collected by the refractive index detector. From the empirical Mark-Houwink equation, the intrinsic viscosity $[\eta]$ of a polymer solution follows

$$[\eta] = KM^{\alpha} \qquad (2.2)$$

where M is the polymer molecular weight, and K and α are the Mark-Houwink parameters specific to the polymer type, solvent and temperature conditions. According to Grubisic et. al.,[90] the quantity $\ln([\eta]M)$ of all polymer species falls on a single curve when plotted against their hydrodynamic radii in the same solvent and temperature, making it possible to calculate the molecular weight of a polymer by comparing to the known molecular weight of a polymer with identical hydrodynamic radius. In this thesis work, 10 polystyrene (PS) standards are used to establish the M_{PS} - t calibration curve, where M_{PS} represents the molecular weight of polystyrene and t is the retention time. The conversion of PS molecular weight and PBD molecular weight is performed by the following

$$\ln M_{PBD} = \frac{1+\alpha_{PS}}{1+\alpha_{PBD}} \ln M_{PS} + \frac{1}{1+\alpha_{PBD}} \ln \frac{K_{PS}}{K_{PBD}} \qquad (2.3)$$

thereby establishing an M_{PBD} - t relationship.

Light scattering detector calculation. In a dilute polymer solution (below the overlapping concentration, c^*), the measured angle dependent light scattering intensity follows[91]

$$\frac{Kc}{R_\theta} = \frac{1}{M_w} + 2Bc + \ldots \quad (2.4)$$

$$K = \frac{4\pi^2}{\lambda_0{}^4 N_A}\left(n_0 \frac{dn}{dc}\right)^2 \quad (2.5)$$

$$R_\theta = \frac{r^2 I_\theta}{I_0} \quad (2.6)$$

$$\lim_{c\to 0}\frac{Kc}{R_\theta} = \frac{1}{M_w} \quad (2.7)$$

where c is the polymer concentration, M_w is the weight average molecular weight, B is the second virial coefficient, λ_0 is the laser wavelength in vacuum, N_A is the Avogadro's parameter, n_0 is the solvent refractive index, n is the refractive index of the solution, r is the distance from the sample to the detector, I_θ is the measured scattering intensity at scattering angle θ, I_0 is the incident laser intensity, R_g is the radius of gyration of the polymer. By plotting $\frac{Kc}{R_\theta}$ against $\sin^2\left(\frac{\theta}{2}\right)$ and extrapolating to c = 0 and θ = 0, the intercept value corresponds to $\frac{1}{M_w}$. The multi angle light scattering (MALS) detector used in this research detects R_θ of the elution content at multiple angles and converts the measured values to the molecular weight of the polymer following the extrapolating manner outlined above.

2.4.3 Calibration results

Molecular weight averages and dispersities of PBD samples were measured using a SEC instrument operated at 30 ºC with THF flowing at a rate of 1 mL/min, and calibrated against 10 polystyrene standards with peak molecular weight between 1000 kDa and 400,000 kDa via universal calibration. Mark-Houwink parameters for branched polybutadienes were calculated by extrapolating published values according to the vinyl fraction of polymers; α = 0.670 and K ranges from 4.600×10^{-4} dL/g (10% vinyl) to 3.595×10^{-4} dL/g (100% vinyl).[92] For polystyrene α = 0.717 and K = 1.251×10^{-4} dL/g. Several polybutadiene samples were also measured using a multi-angle light scattering detector (Wyatt DAWN), with dn/dc = 0.130 mL/g, operated with SEC separation in THF.[93] The results are summarized in Table 2.1 and Table 2.2. The molecular weight of the hydrogenated PBD samples were calculated based on full saturation of unsaturated bonds of the PBDs, which is verified by NMR discussed in the next section:

$$M_{\mathrm{hPBD}} = \frac{M_{0,\mathrm{hPBD}}}{M_{0,\mathrm{PBD}}} M_{\mathrm{PBD}} \qquad (2.8)$$

where the $M_{0,\mathrm{hPBD}}$ and $M_{0,\mathrm{PBD}}$ are the repeating unit molar mass of hPBD and PBD respectively. The calculated results are listed in Table 2.3.

The SEC traces of the hPBD and d-hPBD are presented in Figure 2.3 and Figure 2.4. The chain architecture remains unaltered after the isotope exchange reaction, which is an essential benefit of applying the isotope exchange reaction.

Table 2. 2 Comparison of molecular weight measured with RI detector and LS detector

Polymer	Refractive index (RI) detector		Light scattering (LS) detector	
	M_w[a] (kDa)	$Đ$[a]	M_w[b] (kDa)	$Đ$[b]
PBD4–3	4	1.06	5	1.05
PBD610–3	610	1.06	620	1.05

[a] THF mobile phase, 30 ºC. Via universal calibration. α_{PBD} = 0.670, K_{PBD} = 4.600×10^{-4} dL/g; α_{PS} = 0.717 and K_{PS} = 1.251×10^{-4} dL/g.

[b] THF mobile phase, 30 ºC. dn/dc = 0.130 mL/g.

Table 2. 3 Polymers used for H-D exchange

Polymer	M_w[a] (kDa)	$Đ$[b]	Branch fraction (%)[c]	DL for deuterated specimens, %		
				FTIR	density	^{1}H-NMR
hPBD23-3[f]	23	1.06	2.6	78	79.1	-
hPBD26-9	26	1.03	8.8	65	66.9	67
hPBD24-10	24	1.05	10.1	60	65.3	60
hPBD23-12	23	1.05	12.1	59	67.4	57
hPBD26-15	26	1.04	14.5	76	77.2	73
hPBD28-19	28	1.05	19.4	62	66.2	62
hPBD27-24	27	1.06	24.1	67	70.4	68
hPBD35-33	35	1.06	32.9	69	68.1	64
hPBD23-41	23	1.04	41.0	55	52.2	54
hPBD32-50	32	1.09	50.0	34	32.4	35
hPBD4-3[g]	4	1.08	2.9	65	68.3	-
hPBD7-3	7	1.09	2.8	66	65.6	-
hPBD23-3	23	1.06	2.6	69	73.2	-
hPBD103-3	103	1.09	2.6	72	-	-
hPBD216-3	216	1.08	2.7	84	-	-
hPBD635-3	635	1.09	2.6	< 1	-	-
LLDPE1a[d]	113[e]	2.46	2.1	51	58.4	-
LLDPE1b[d]	113[e]	2.46	2.1	61	65.3	-

[a] Calculated from PBD molecular weight and assuming complete saturation.

[b] Determined with SEC at 30 ºC with THF mobile phase for polymers with more than 8% branches, or at 135 ºC with TCB mobile phase for polymers with fewer than 3% branches.

[c] Number of branches per 100 backbone carbons. Calculated from vinyl fraction of PBD samples.

[d] Has C4 branches. Reaction loading: 5 g polymer/ 1 g catalyst/ 0.5 L solvent

[e] Determined with SEC at 145 ºC with TCB mobile phase. Calibrated via universal calibration with PS standards.

[f] Reaction loading for this sample and the nine that follow: 1 g polymer/1 g catalyst/0.5 L solvent

[g] Reaction loading for this sample and the five that follow: 0.2 g polymer/0.2 g catalyst/0.1 L solvent

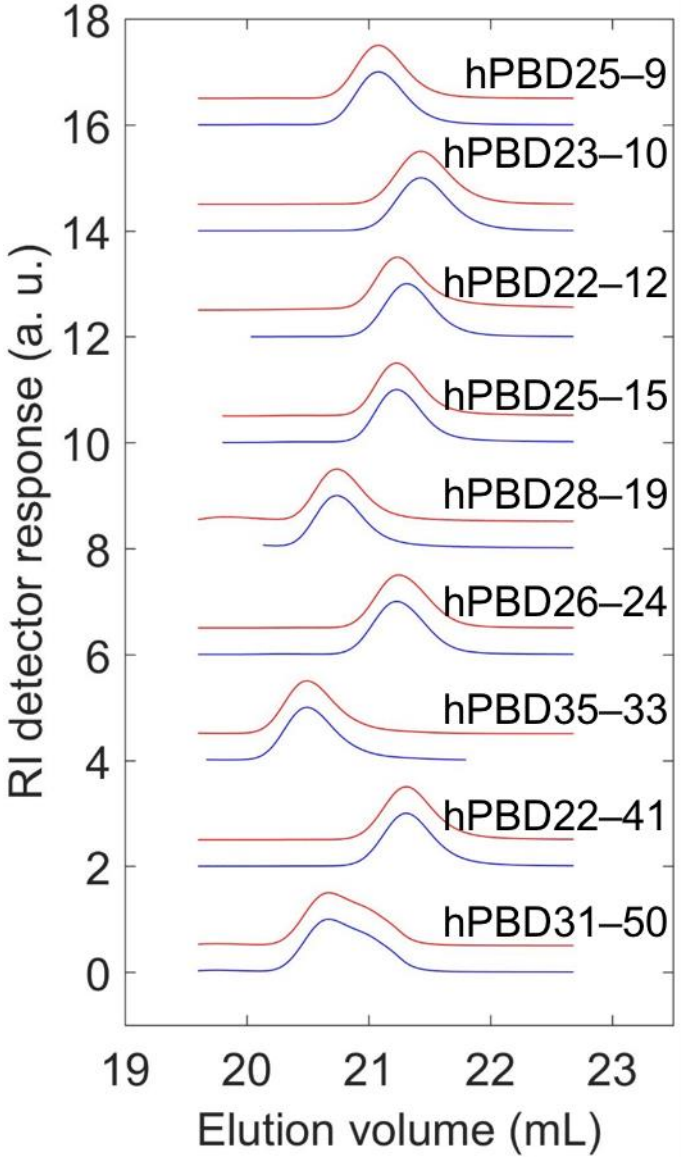

Figure 2. 3 SEC traces of deuterium labelled (red) and hydrogenated (blue) hPBDs. The overlapping traces confirms the chain architecture is not altered after deuteration.

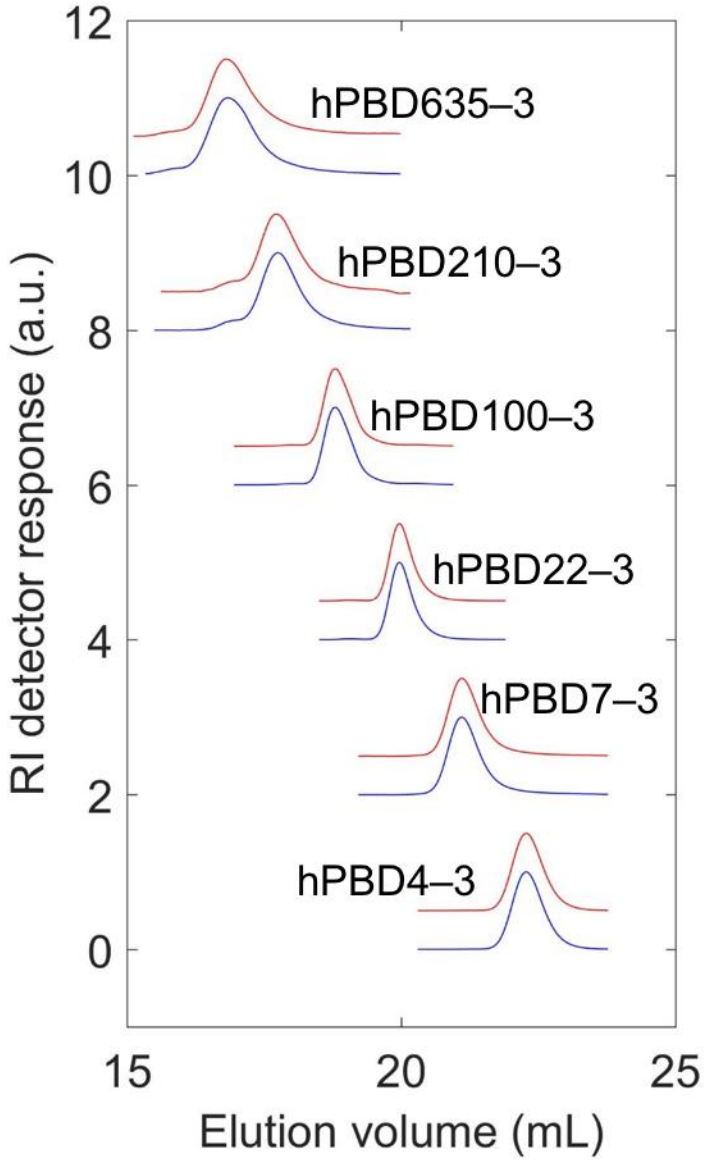

Figure 2. 4 SEC traces of deuterated (red) and hydrogenated (blue) hPBDs, series 2. The overlapping traces confirms the chain architecture is not altered after isotope exchange.

2.5 Material characterization: proton nuclear magnetic resonance (^{1}H-NMR)

Proton NMR is a technique that detects the interaction between applied magnetic field

and hydrogen nuclei inside the measured substance. It is essentially a method for determining the type and quantity of protons within the material. In this thesis work, it was used to (1) determine the relative ratio of 1,2 and 1,4 addition of the PBD samples; (2) verify the fully saturation of the unsaturated bonds; (3) determine the amount of deuterium in the labelled samples; and (4) identify potential preferential labelling on the side groups. NMR spectra are taken for all PBD samples, as well as hPBD and d-hPBD samples with more than 8% branches; the hPBD with the lowest amount of branches is not soluble at room temperature. The experiments were performed by dissolving the polymer in chloroform-d1 and measure the resonance signal by ^{1}H-NMR spectroscopy (Varian UNITY 300, Varian INOVA 500). The results from a PBD sample is illustrated in Figure 2.5. The corresponding hPBD and d-hPBD signal are presented in Figure 2.6. For the synthesized polybutadienes the integrated peak area of protons in vinyl (1,2) groups between and backbone (1,4) units between 4.8 ppm and 5.8 ppm were used to calculate the fraction of vinyl side groups, as well as for verification of saturation. For the deuterium amount determination, pyridine was used as an internal reference as the pyridine signal (7.2 ppm to 8.8 ppm) is well separated from the polyolefin signal (0.6 ppm to 1.5 ppm). The polyolefin signal between 0.6 ppm and 1.5 ppm was used to determine potential labelling preference. Deuterium content results are listed in Table 2.3. An example of PBD, hPBD and d-hPBD characterization with proton NMR is elaborated in the next section.

Example of characterizing PBD, hPBD and d-hPBD with ^{1}H-NMR spectroscopy

PBD microstructure and hPBD branch fraction. The ^{1}H-NMR spectra of PBD34-33 is illustrated in Figure 2.5. The integrated peak area of signal between 5.2 ppm and 5.8 ppm ($A_{b,f}$) and the signal between 4.8 ppm and 5.1 ppm (A_a) are used for microstructure determination. The fraction of 1,2 addition is

$$f_{1,2} = \frac{A_a}{A_{b,f} + \frac{1}{2}A_a} \qquad (2.9)$$

The branch fraction of the corresponding hPBD is

$$f_b = \frac{f_{1,2}}{4 - 2f_{1,2}} \qquad (2.10)$$

The 1,2 addition content for this sample is determined to be 79%, correspondingly the hPBD sample has 33% ethyl branches.

Deuterium content of d-hPBD. Two samples are prepared to determine the deuterium content of each d-hPBD sample and the mass of each component within the samples are recorded: (1) reference: hPBD (m_h) + pyridine (m_{p1}); (2) sample to be evaluated: d-hPBD (m_d) + pyridine (m_{p2}). The ^{1}H-NMR profiles of these two samples are illustrated in Figure 2.6. The integrated peak area of two protons from pyridine (peak 1, area A_{p1} and A_{p2} for the two samples) and the peak area of the polyolefin proton signal (peak group 2, area A_h and A_d) are calculated for deuterium content calibration. The calculation is performed by simultaneously solving Equations 2.11 and 2.12, which generates Equation 2.13. Note that though the densities of the hPBD35-33 (ρ_H) and d-hPBD35-33 (ρ_D) are incorporated in Equations 2.11 and 2.12, measurements for both quantities are not necessary. They are not contained in Equation 2.13.

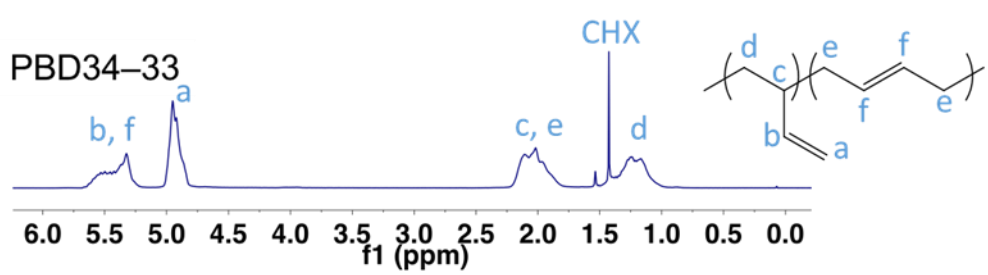

Figure 2. 5 ^{1}H–NMR traces of a polybutadiene (PBD34-33). The proton signal associated with unsaturated bonds (4.8 ppm to 5.8 ppm) is used for microstructure determination.

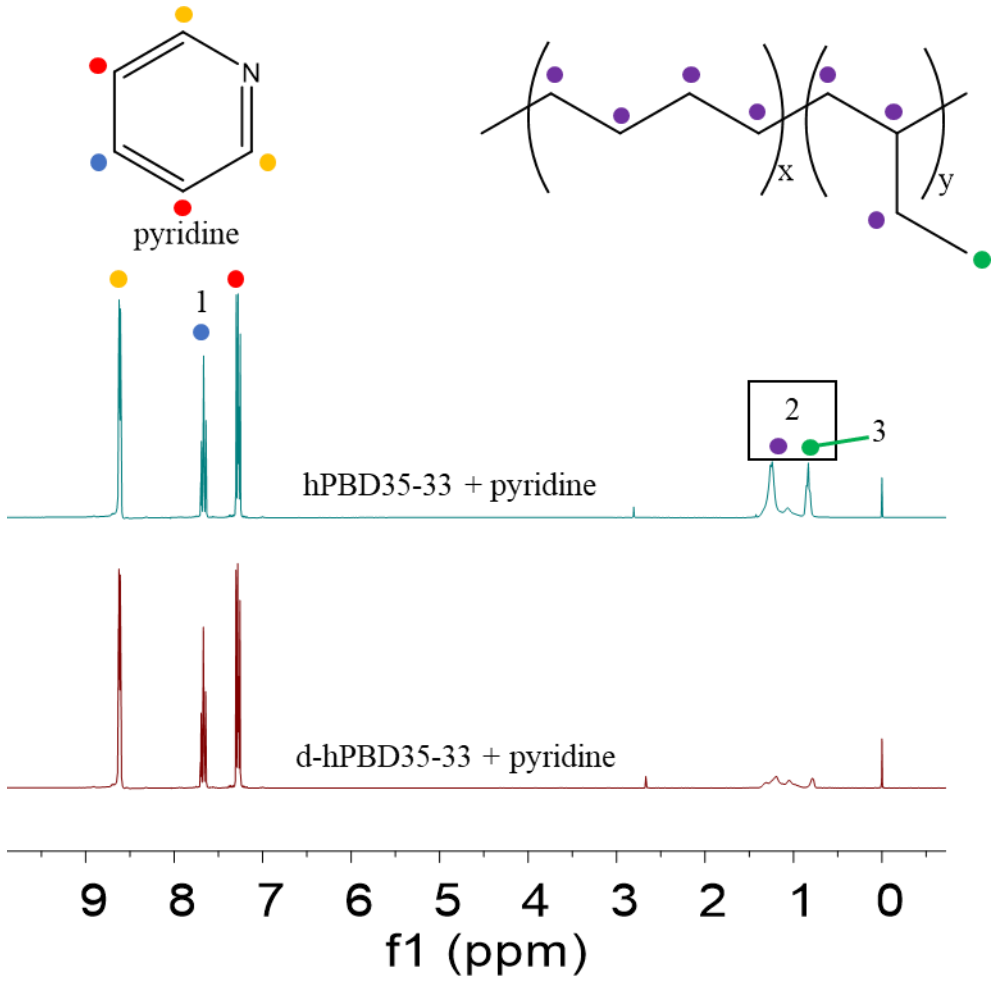

Figure 2. 6 ^{1}H-NMR traces of an hPBD35-33 and corresponding d-hPBD35-33. The proton signals associated with two of the pyridine protons (peak 1) and the polyolefin protons (peak group 2) were used for deuterium content determination. The relative ratio of the proton signal associated with the methyl side groups (peak 3) and all the polyolefin protons (peak group 2) was used for labelling preference identification. The peak at 2.65 ppm is from a contaminated d-chloroform solvent.

$$\mathrm{DL} = 1 - \frac{m_{\mathrm{p2}} m_{\mathrm{h}} A_{\mathrm{d}} A_{\mathrm{p1}}}{m_{\mathrm{p1}} m_{\mathrm{d}} A_{\mathrm{h}} A_{\mathrm{p2}}} \times \frac{\rho_{\mathrm{D}}}{\rho_{\mathrm{H}}} \qquad (2.11)$$

$$\mathrm{DL} = \frac{M_{\mathrm{o}}}{8(M_{\mathrm{D}} - M_{\mathrm{H}})} \left(\frac{\rho_{\mathrm{D}}}{\rho_{\mathrm{H}}} - 1\right) \qquad (2.12)$$

where M_o = 56 g/mol represents the molecular weight of a four-carbon repeating unit, and M_D = 2 g/mol and M_H = 1 g/mol are the atomic mass of D and H. Solving the two equations simultaneously yields the following relationship

$$\mathrm{DL} = (1 - \frac{m_{p2} m_h A_d A_{p1}}{m_{p1} m_d A_h A_{p2}})/[1 + \frac{8(M_D - M_H)}{M_o} \times \frac{m_{p2} m_h A_d A_{p1}}{m_{p1} m_d A_h A_{p2}}] \qquad (2.13)$$

DL of d-hPBD35-33 is determined to be 64%.

Preference ratio. Potential preferential labelling on the methyl end group of the ethyl branches in the d-hPBD samples is examined by calculating the fraction of protons residing in the methyl groups before and after the isotope exchange, and by taking their ratio. The methyl proton fraction (f_{me}) before the exchange reaction can be calculated from the branch fraction (f_b), as well as by taking the ratio of the NMR peak area of peak 3 ($A_{me,h}$) over all hPBD proton signal (peak group 2, A_h). For hPBD35-33, the calculations are

$$f_{me,h} = \frac{3f_b}{2 + 4f_b} = 0.30 \qquad (2.14)$$

$$f_{me,h} = \frac{A_{me,h}}{A_h} = 0.28 \qquad (2.15)$$

from branch fraction calculation and NMR measurement respectively. The difference between the two values is within instrument error. For the rest of the discussion, the methyl proton value from actual NMR measurement (following Equation 2.15) is adopted.

The fraction of methyl protons remaining in the methyl groups in d-hPBD35-33 are calculated following an analogous route as that of Equation 2.15:

$$f_{\mathrm{me,d}} = \frac{A_{\mathrm{me,d}}}{A_{\mathrm{d}}} = 0.16 \qquad (2.16)$$

The ratio of the two values is defined as the preference ratio:

$$P = \frac{f_{\mathrm{me,d}}}{f_{\mathrm{me,h}}} = 0.57 \qquad (2.17)$$

2.6 Materials characterization: density measurements

Due to the replacement of hydrogen by the heavier isotope, deuterium, the density of the polyolefins will increase upon isotope labelling. Measurement of density values after the exchange reaction can therefore be adopted as a method for deuterium content determination. Under the assumption that each labelled repeat unit occupies the same volume as its unlabeled peers, the amount of deuterium in the polymer can be expressed by Equation 2.12. The measurement of density requires a density gradient column, where density gradient is established along a vertical graduated glass cylinder. The building scheme for the density gradient column is illustrated in Figure 2.7.

To build a density gradient column, two liquids with different densities that are miscible with each other but not with the target polymer should be used. The density values of the two liquids define the lower limit and upper limit of the accessible density range of the column. In this research, 800 mL of isopropanol (IPA, ρ = 0.786 g/mL) and 800 mL of ethylene glycol (EG, ρ = 1.11 g/mL) are used. The platform is installed as illustrated in Figure 2.7, with two valves controlling the flow of liquids contained in the Erlenmeyer flasks (A and B). The valves are adjusted such that a gentle and stable flow driven by gravity is established through the glass tubing. The liquid entering the bottom of the graduated cylinder most immediately upon opening of valves is IPA, the lighter liquid. As EG enters flask A and mixes with IPA, the density of the liquid flowing out shifts towards

the higher EG value. The heavier liquid reaches the bottom of the graduated cylinder and pushes the less dense liquid upwards. In the end a density gradient is created in the column with heavier liquids residing at the bottom.

The flasks and tubing are removed from the column after filling. Thirteen glass floats with densities between 0.8492 g/cm^3 and 1.0410 g/cm^3 are dropped into the column and allowed to stabilize for three days. The positions of the floats are read from the cylinder. The densities of the floats are plotted against their positions, and either a linear fitting or a polynomial fitting is performed to generate a smooth calibration curve. An example calibration curve is illustrated in Figure 2.8.

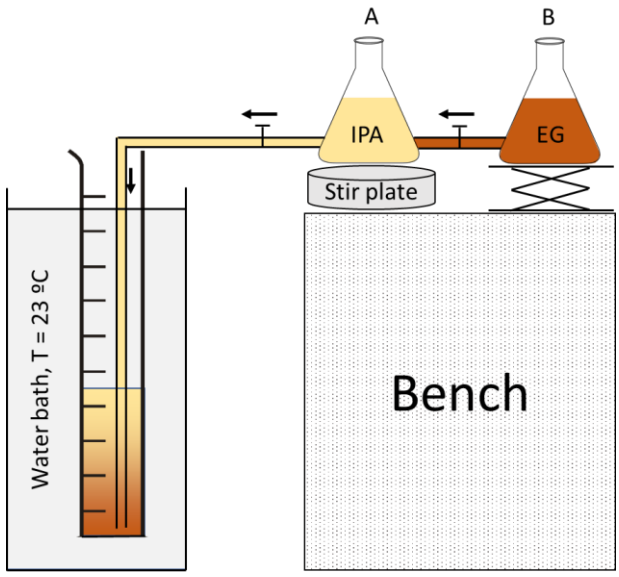

Figure 2. 7 Scheme for building a density gradient column. The liquid used are isopropanol (IPA, ρ = 0.786 g/mL) and ethylene glycol (EG, ρ = 1.11 g/mL).

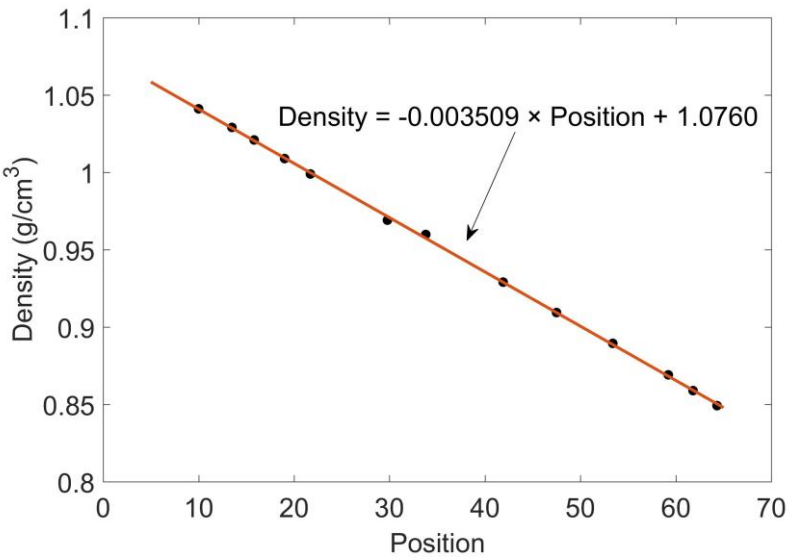

Figure 2. 8 Calibration curve established from the positions of 13 glass floats stabilized at 23 ºC. The floats have densities ranging from 0.8492 g/cm^3 and 1.0410 g/cm^3.

Table 2. 4 Deuterium content calibrations of d-polyolefins

	Density (g/cm^3)		Deuteration level (%)		
Polymer	h–polymer	d–polymer	density	^{1}H–NMR	FTIR
LLDPE1a	0.9182 ± 0.0003	0.9947 ± 0.0003	58.3 ± 0.2	-	51 ± 5
LLDPE1b	0.9182 ± 0.0003	1.0035 ± 0.0002	65.1 ± 0.2	-	61 ± 3
hPBD22-3	0.8830 ± 0.0003	0.9828 ± 0.0002	79.1 ± 0.2	-	78 ± 2
hPBD25-9	0.8495 ± 0.0004	0.9307 ± 0.0003	66.9 ± 0.3	67 ± 3	65 ± 6
hPBD23–10	0.8460 ± 0.0002	0.9249 ± 0.0003	65.3 ± 0.2	60 ± 5	60 ± 3
hPBD22-12	0.8458 ± 0.0002	0.9635 ± 0.0005	67.4 ± 0.4	57 ± 3	59 ± 7
hPBD25-15	0.8465 ± 0.0005	0.9399 ± 0.0002	77.2 ± 0.4	73 ± 3	76 ± 6
hPBD28-19	0.8491 ± 0.0003	0.9294 ± 0.0003	66.2 ± 0.3	62 ± 2	62 ± 5
hPBD26–24	0.8489 ± 0.0001	0.9343 ± 0.0002	70.4 ± 0.2	68 ± 1	67 ± 4
hPBD35-33	0.8497 ± 0.0006	0.9324 ± 0.0002	68.1 ± 0.4	64 ± 2	69 ± 5
hPBD22-41	0.8515 ± 0.0003	0.9150 ± 0.0002	52.2 ± 0.3	54 ± 3	55 ± 5
hPBD31-50	0.8528 ± 0.0002	0.8823 ± 0.0005	32.4 ± 0.4	35 ± 3	34 ± 2

* Errors are the standard deviation from three repeats.

To measure the densities of the polyolefins before and after labelling, the samples are first degassed by annealing at 150 ºC under dynamic vacuum for 12 h, and allowed to cool at ambient temperature. At least three sample pieces are cut from each sample and placed in the density gradient column. The samples are allowed to stabilize for three days before reading their positions. The positions values of the sample pieces are compared with the most recent calibration curve to calculate the corresponding density values. The results are

listed in Table 2.4.

2.7 Material characterization: Fourier-transform infrared spectroscopy (FTIR)

Infrared spectroscopy is a technique that detects the interaction between external infrared radiation with chemical bonds within the material. It is useful in identifying and quantifying multiple types of bonds. In this research, FTIR is performed for the labelled polyolefins to determine the amount of C–D bonds in the material, essentially revealing the deuterium content in the material.

Measurements were performed using a Bruker Alpha ATR-FTIR instrument with a room temperature detector. Samples were degassed at 150 ºC under vacuum for 2 h and pressed into thin films. The films were pressed against the diamond crystal window of the instrument and held in place with a clamp. Thirty-two scans with resolution of 4 cm^{-1} were acquired over the spectral range of 400 cm^{-1} to 4000 cm^{-1}. An example of the measured FTIR absorbance obtained from d-LLDPE1 and d-hPBDs are shown in Figure 2.9 and Figure 2.10. When hydrogen is replaced by deuterium the associated infrared active C–H bond stretching vibration shifts to lower wavenumber. The area of the C–D stretching bands between 1900 cm^{-1} and 2400 cm^{-1}, A_{CD}, and the C–H stretching bands between 2700 cm^{-1} and 3100 cm^{-1}, A_{CH}, were integrated from the spectrum for deuterium content determination, which is discussed in the next chapter.

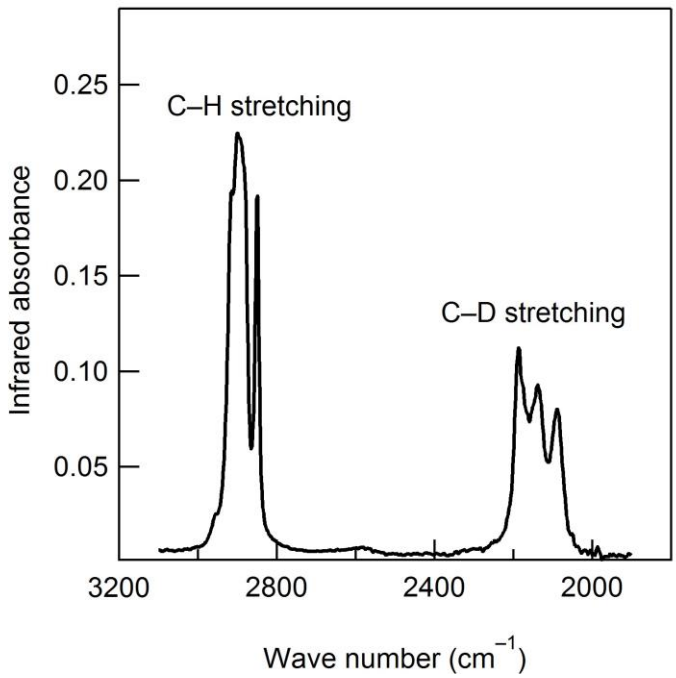

Figure 2. 9 Example of FTIR measurement from d-LLDPE1 at room temperature. Characteristic C–D stretching peaks and C–H stretching peaks are labeled.

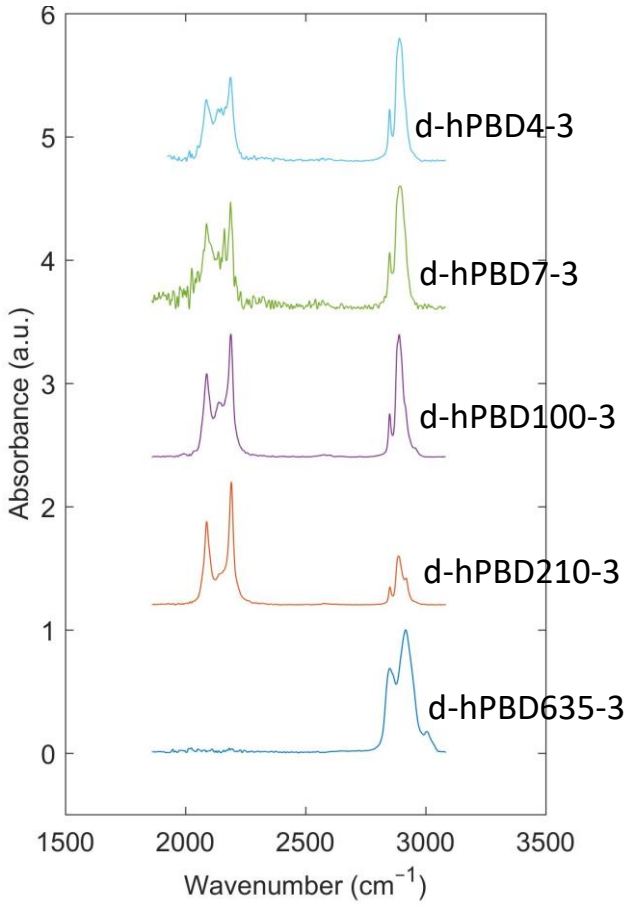

Figure 2. 10 FTIR profiles of deuterated hPBDs between 1700 cm^{-1} and 3200 cm^{-1}.

Chapter 3

Impact of molecular weight and short chain branching on the isotope labelling of polyolefins

* Reproduced in part from Zeng, Y.; López-Barrón, C. R.; Eberle, A. P. R.; Lodge, T. P.; Bates, F. S. *Macromolecules* **2017**, 50, 6849-6860. Copyright 2017 American Chemical Society.

3.1 Introduction

In Chapter 1, we briefly summarized the previous efforts devoted to understanding the isotope exchange mechanism associated with small hydrocarbon molecules, usually catalyzed by transition metal catalysts. For large hydrocarbon materials, especially polyolefins, Habersberger et al. demonstrated in 2012 that a presumably similar route exists to effectively label the polyolefin with deuterium through direct replacements of hydrogen by deuterium.[62] However, what is mysterious about the exchange mechanism is the mismatch between the relative amount of materials in the system and the eventual

deuterium distribution among the substances. In a typical reaction cycle, the solvent occupies over 97% of the total mass of interacting materials, yet roughly only 40% of the heavier isotope enter the solvent molecules. Besides, deuterium takes up only 2 mol% of the total H/D species inside the hydrogenator, yet it ends up concentrated in the polymers and pushes the deuterium exchange level (DL) of polymers up to as high as 80%. This implies the polymer species have an unusual ability of taking up deuterium from the reservoir of isotopes, especially when considering the assumptions that (1) both the solvent and the polymer have the ability to exchange isotopes on the catalyst surface, and (2) the isotope exchange process is reversible.

Other than satisfying the curiosity to understand the nature of the polymer labelling mechanism, studying possible factors that shape the exchange reaction has very practical considerations. Commercial polyolefins, which are currently the most obvious application targets of the exchange reaction, are often a complex combination of molecules with different chain lengths, different branch types and lengths, and different amounts of branching, which can all end up affecting the labelling outcome. In this chapter, a series of lab generated model polyolefins with well defined molecular weight and branch structure are adopted as substrates for the isotope exchange reaction, and their behavior in the exchange reaction is analyzed. A few commercial polyolefins with different branch structure and less defined molecular weight distribution are also analyzed in a similar manner, in an effort to provide clues in understanding the deuterium distribution behavior in these polymers.

3.2 Experiment

Cyclohexane (CHX) and tetrahydrofuran (THF) were purified by purging with argon and passing through alumina and/or copper redox catalyst columns as described elsewhere.[94] n-butyllithium (Sigma-Aldrich) and bispiperidinoethane (Sigma-Aldrich)

were used as received. 1,3-butadiene (Sigma-Aldrich) was purified by distillation from n-butyllithium twice before use. Ultra wide-pore Pt/Re-SiO_2 catalyst was provided by the Dow Chemical Company. Hydrogen gas, deuterium gas, methanol, ethylene glycol, isopropanol and isooctane were used as received.

Two series of low dispersity hPBD samples are prepared per the procedures outlined in Chapter 2. The series 1 contains 10 samples with molecular weight constrained between 20 kDa and 35 kDa, and branch content between 2% and 50%. The series 2 contains 6 samples (one duplicate with series 1) with low branching (2%-3%) and a wide span of molecular weight averages between 4 kDa and 635 kDa.

Six commercial polyethylene samples including one high density polyethylene (HDPE) and 5 LLDPE samples (LLDPE1 through LLDPE5) were provided by ExxonMobil Chemical Company and used without modification. The molecular weight distribution was determined by size exclusion chromatography (SEC) at 145 ºC with 1,2,4-trichlorobenzene (TCB) (Sigma-Aldrich) as the mobile phase. The molecular weight values were calibrated against polystyrene standards whose Mark-Houwink parameters are α = 0.670 and K = 1.75×10^{-4} dL/g using universal calibration reference. The Mark-Houwink parameters for homopolymer polyethylene were obtained from literature values (α = 0.695 and K = 5.79×10^{-4} dL/g) while for LLDPE the parameters are calculated from empirical equations according to their comonomer content.[95] The molecular identities of these polymers are tabulated in Table 3.1. The LLDPE polymers have varying amount of branching according to the supplier (2% to 13%), and have rather homogeneous branch distributions across all molecular weights.[95]

All polyolefin materials were isotope labelled through the H/D exchange reaction. The amount of isotope incorporated was characterized with ^{1}H-NMR spectroscopy, density measurements and FTIR for the amorphous samples, while for the semi-crystalline samples only density measurements and FTIR were performed.

Additionally, a series of five tetracosane samples were adopted as part of the isotope content calibration standards. The samples were prepared by solvent blending a hydrogenous tetracosane sample with a 98% deuterated tetracosane sample at different volume ratios, followed by vacuum removal of the solvent. The amount of deuterium within each sample is calculated from the volume fraction of the two blending components.

Table 3. 1 Commercial polyethylenes for isotope exchange

Polymer	M_w (kDa)	Đ	Branch fraction (%)[a]
HDPE	110	6.5	-
LLDPE1[b]	113	2.5	2.6
LLDPE2[b]	80	3.2	2.9
LLDPE3[b]	110	3.2	8.8
LLDPE4[c]	130	2.1	10.1
LLDPE5[c]	90	2.4	12.1

[a] Number of branches per 100 backbone carbons.

[b] Has C4 branches.

[c] Has C2 branches.

3.3 Results and discussion

3.3.1 FTIR calibration of deuterium content

Although it has long been known that C–D bonds and C–H bonds have quite different IR absorbances, a direct quantification of deuterium content of an isotope labelled hydrocarbon from FTIR spectra is lacking. In this research, benefiting from the series of deuterium labelled polyolefins generated, a DL quantification method specific to

polyolefins with FTIR is established. The area of the C–D stretching bands between 1900 cm^{-1} and 2400 cm^{-1}, A_{CD}, and the C–H stretching bands between 2700 cm^{-1} and 3100 cm^{-1}, A_{CH}, were integrated from the spectra for deuterium content determination. Under the assumption that the concentration of deuterium atoms and hydrogen atoms within the material contributes linearly to the measured C–D and C–H signal strength respectively, the following relationship can be established

$$\mathrm{DL} = \frac{A_{CD}}{A_{CD} + \varepsilon A_{CH}} \qquad (3.1)$$

where the parameter ε is an adjustable parameter that normalizes the relative absorptivity of C–D and C–H bonds. To find an appropriate value of ε, least squares regression is performed to minimize the sum of the squares of residuals between the FTIR predicted deuterium content, DL_{IR}, and the deuterium content characterized by other techniques such as ^{1}H-NMR and density measurements, DL_{other}. The quantity to be minimized is

$$R = \sum(\mathrm{DL}_{IR} - \mathrm{DL}_{other})^2 \qquad (3.2)$$

where the sum is over all labelled polyolefins available and the tetracosane blends. The value of ε that was found to minimize the sum of residual squares is 0.63. Correspondingly, plotting the DL calculated with FTIR profiles against DL calibrated with ^{1}H-NMR and density measurements generates Figure 3.1, where the data points all reside close to the $y = x$ line, confirming the validity of the FTIR based DL quantification method.

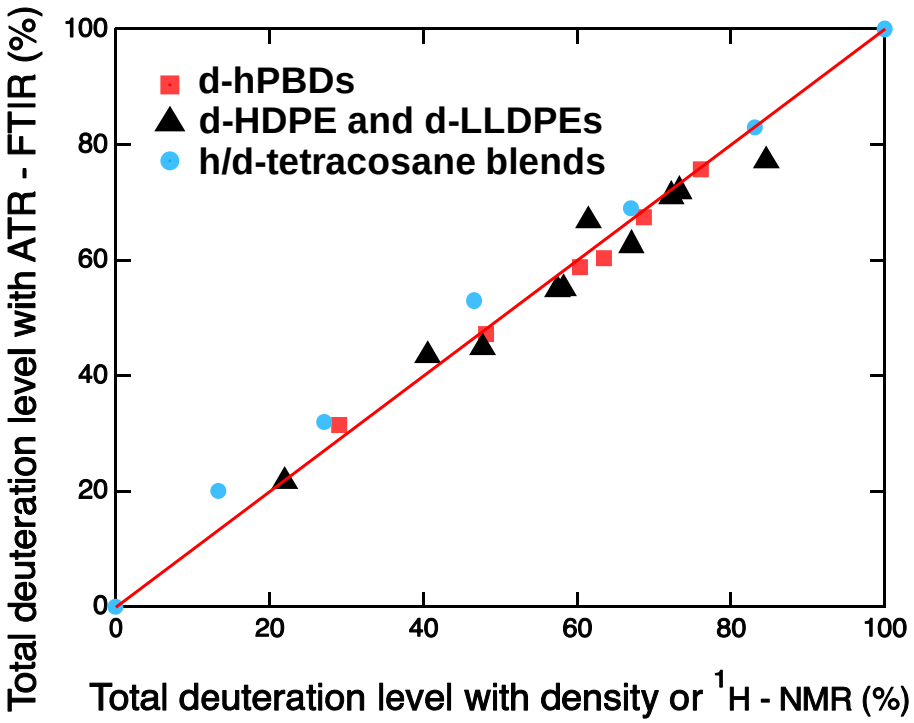

Figure 3. 1 Comparison of DL measured with FTIR by taking $\varepsilon = 0.63$ and the values measured with NMR and density increment. The solid line is the line generated from $y = x$ function.

3.3.2 Impact of molecular weight and branch content on isotope exchange: commercial polyolefins

The deuterium content of the non-uniform, commercial polyolefins are characterized with FTIR and plotted against their weight average molecular weight and branch fractions respectively. The results are illustrated in Figure 3.2. All materials have DL between 35% and 70%. Although the dispersity values and branch type vary across these materials, still

a trend appears that the materials with higher molecular weight tend to pick up more deuterium during exchange. Branching extent, on the other hand, has a less obvious impact on the result of exchange. The observed outcome is further examined in the next sections, with the model hPBD materials, which have a narrow distribution of molecular weights and uniform branch structure.

3.3.3 Impact of molecular weight on isotope exchange: model hPBDs

Figure 3.3 illustrates the extent of deuterium exchange determined for the d-hPBD samples with the lowest branch fraction (2.6-2.8%) as a function of molecular weight, based on both FTIR and density techniques. Increasing the molecular weight from Mw = 4 kDa to 210 kDa leads to an increase in deuterium content from 65% to 84%, with the most dramatic rise occurring at the higher molecular weight increment. Increasing Mw further to 635 kDa produced a surprising result. This polymer failed to exchange any deuterium (< 1%) when subjected to the same treatment as the lower molecular weight specimens in isooctane (see FTIR results in Figure 3.4). Here we note that inspection of the contents of the reactor following the reaction protocol suggested that this polymer had limited solubility at the reaction conditions; the sample specimen was only slightly swollen and catalyst was not dispersed in the mass of polymer. However, a labeling experiment performed in n-octane resulted in a modest amount of exchange (about 11%) as shown by the FTIR trace of this sample in Figure 3.4.

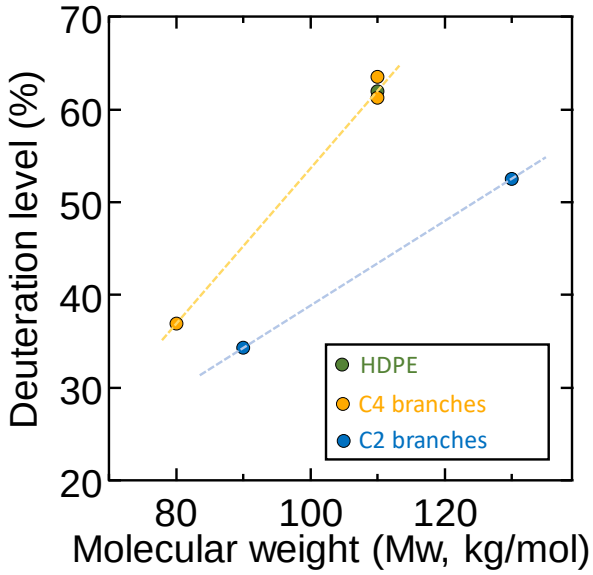

(a)

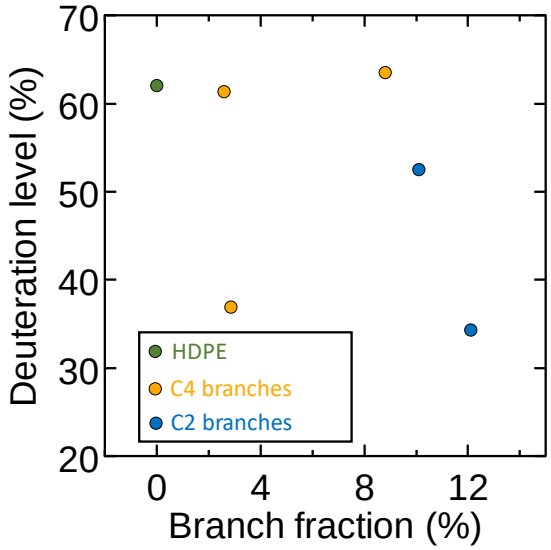

(b)

Figure 3. 2 DL of commercial polyolefins as a function of weight average molecular weight (M_w, **(a)**) and branch fraction **(b)**. The dashed lines are guides of eyes for the trend.

The observed increase in DL with molecular weight can be explained by the difference in absorption of low molar mass chains and high molar mass chains on the heterogeneous catalyst. We speculate that chains adsorbed on the catalyst surface have a residence time that is much greater than the timescale associated with segment scale exchange of deuterium for hydrogen. High molecular weight polymers will adsorb more strongly than low molecular weight ones, and presumably for longer times, due to the combined effects of more sites of contact per molecule and a less favorable entropy of mixing in solution. This would lead to greater extents of exchange, as observed experimentally. Moreover, this argument also rationalizes why solvent quality influences the overall extent of deuterium exchange as reported by Habersberger, et al.[62] Furthermore, this may be consistent with the finding that hPBD635-3, the highest molecular weight specimen, exchanged no deuterium in isooctane. Polyolefins are known to exhibit LCST behavior in saturated hydrocarbon solvents due to equation of state (compressibility) effects.[96,97] Increasing molecular weight lowers the LCST temperature, which can lead to macroscopic phase separation. We speculate that isooctane is a marginal solvent at elevated temperatures and that hPBD635-3 failed to dissolve at the reaction condition of 170 ºC, possibly also impacted by the elevated pressure.[98] Switching to n-octane apparently alleviates this problem. However, solvent quality is a double-edged sword. Decreasing solvent quality probably enhances adsorption of the polymer on the catalyst surface, thereby increasing the level of deuterium exchange, yet this can only be pushed to the point that phase separation is avoided. This balance will become most delicate at the highest molecular weights. This solvent effect may also explain the dramatic drop in deuterium content at the highest molecular weights in SEC-IR results reported by Habersberger, et al. for a non-uniform polyethylene sample.[99]

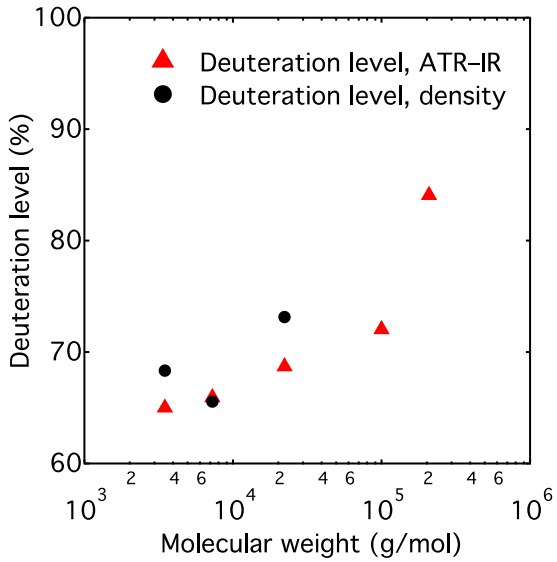

Figure 3. 4 Deuterium exchange level as a function of hPBD molecular weight with relatively low branch content (2-3%), characterized by FTIR and density gradient column at room temperature. Two replicate measurements were performed for each sample, and the averages are presented. Polymer loading is 0.2 g polymer/0.2 g catalyst/0.1 L solvent.

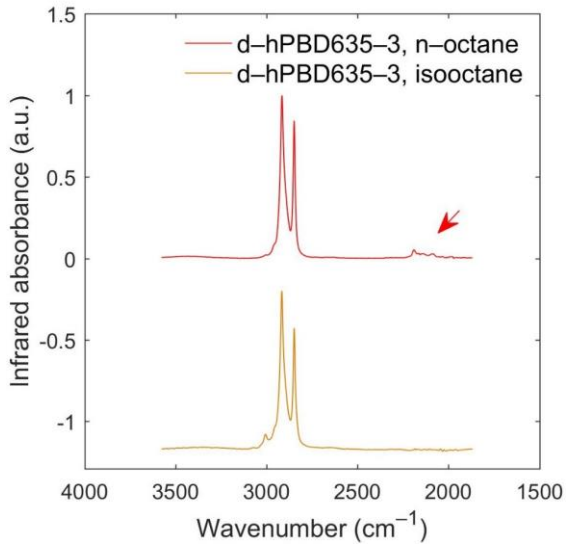

Figure 3. 3 FTIR profiles of d-hPBD635-3 prepared by isotope exchange in n-octane and isooctane at 170 ºC. Arrow indicates the C–D stretching band region. Calculated deuterium labeling level is 11% for the polymer exchanged in n-octane, and less than 1% for the polymer exchanged in isooctane.

3.3.4 Impact of branch content on isotope exchange: model hPBDs

Commercial polyolefins are produced with various levels of short side branches. We examined the role of such comonomers using the model hydrogenated polybutadiene samples, with branch content ranging from 2.6 to 50 per 100 backbone carbon atoms at relatively constant molecular weight (ca. 30 kDa, Table 2.3). Figure 3.5 presents the extent of labeling obtained from three different characterization methods (density gradient column, ^{1}H-NMR and FTIR) as a function of ethyl branch content. The three techniques give consistent results, and indicate essentially no effect of ethyl branches up to at least 30 per 100 backbone carbons. Above that, the extent of exchange drops significantly, from ca. 70% at low branching down to 35% at the highest branch level considered (50 per 100 backbone carbons).

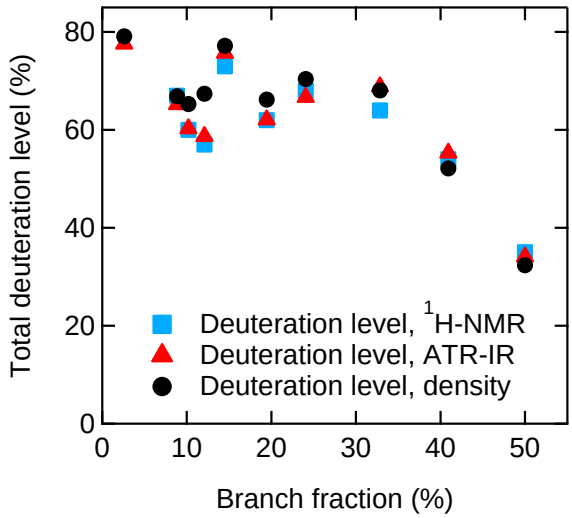

Figure 3. 5 Overall deuterium exchange level determined by ^{1}H-NMR, FTIR and density measurements as a function of ethyl branch content for hPBD samples. Polymer loading was 1 g polymer/1 g catalyst/0.5 L solvent.

We also analyzed by ^{1}H-NMR spectroscopy the distribution of deuterons on the methyl groups versus methylene carbons. Representative ^{1}H-NMR spectra obtained from a matched pair of hPBD and d-hPBD specimens are shown in Figure 3.6. The methyl group signal, which is separated from the resonances of the other protons, can be used to quantify the fraction of protons remaining in the methyl groups after deuterium exchange. As shown in the scheme in Figure 3.6, the fraction of methyl protons before isotope exchange can be calculated from the branch fraction determined for the polybutadiene precursor. We define the ratio of methyl proton fraction after isotope exchange to that before exchange as the preference ratio. Since deuterons are invisible in the ^{1}H-NMR profiles, this ratio can be used to reveal any position preference of isotope exchange; the fraction of methyl protons should remain the same after isotope exchange if all protons have equal probability of being replaced. On the other hand, this ratio will change if there is a preference for a specific site. In the case presented in Figure 3.6, the relative fraction of protons in the methyl groups decreases with deuterium labeling, resulting in a preference ratio less than unity. A preference ratio higher than unity would indicate a preference for replacing methylene protons in the backbone and ethyl branches. Characterization of the d-hPBD series is included in Figure 3.7. No preference is found at branch fractions less than 14%, while a relatively strong methyl side group preference occurs at high branching content, coincident with a reduction in the overall extent of isotope exchange.

We attribute the cause of the decrease in DL within the highly branched material to the steric repulsion from crowded side groups. As in the scheme in Figure 3.8, side groups at high branch content can essentially act as contact points between the polymer and the catalyst surface, as evidenced by the preferential side group labelling detected. Consequently, the backbone units are screened from the catalyst, essentially reducing the contacting area between the catalyst and the hydrocarbon molecules. Additionally, polymer molecules with low branching retain the adsorption capability through the linear,

unbranched backbone units. Side groups also limit available configuration placements of the backbone units, presumably limiting the labelling as the chains must move and expose the less labelled segments to the catalyst through altering chain conformation to accommodate further segment labelling. This also explains the observation that DL of the commercial polyethylenes show less dependence on the branch content, as all the polyethylenes inspected have relatively low branch content.

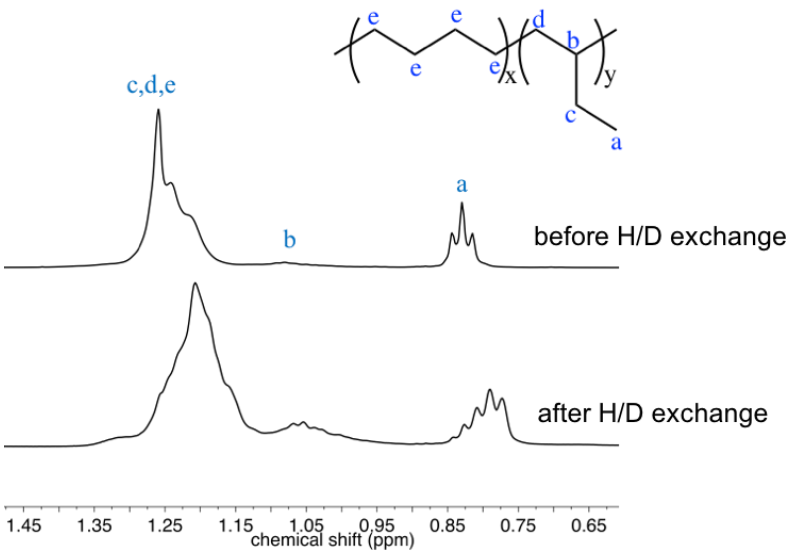

(a)

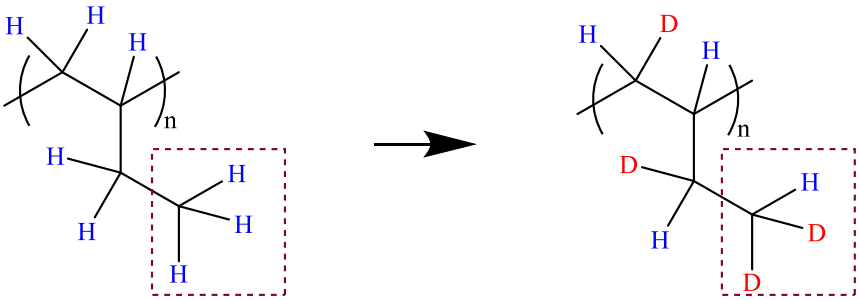

(b)

Figure 3. 6 (a) ^{1}H-NMR spectra from hPBD26-15 and d-hPBD26-15, before and after the isotope exchange reaction, respectively. **(b)** Preferential isotope exchange on methyl side groups (dashed square) during isotope exchange for hPBD. Ratio of H atoms in the methyl groups over total proton content will decrease if such preference over methyl groups is present (37.5% to 25% in this specific scheme). The preference ratio is 25%/37.5% = 0.67.

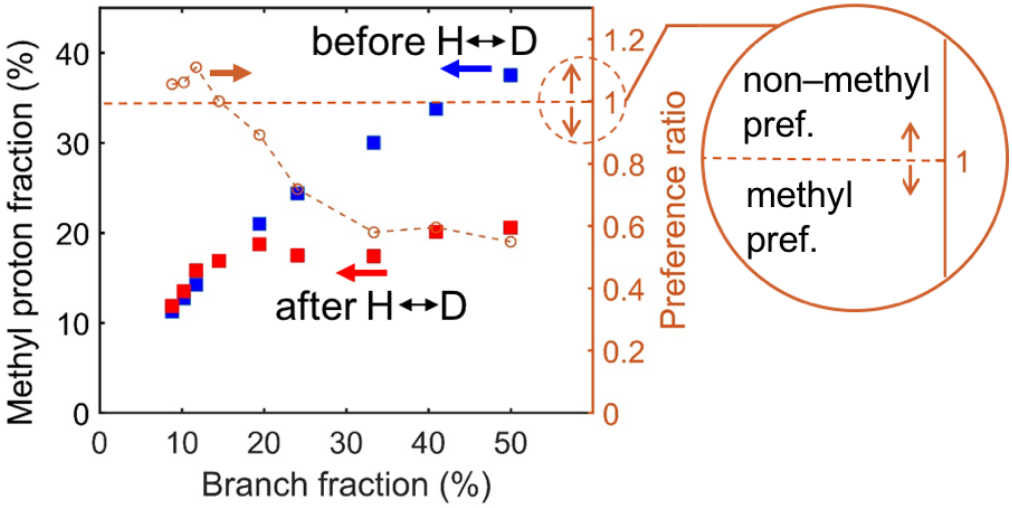

Figure 3. 7 Methyl proton fractions before and after isotope exchange reaction for hPBD samples, determined with ^{1}H-NMR spectroscopy. Blue squares): methyl proton fraction before isotope exchange. Red squares: methyl proton fraction after isotope exchange. Brown circles: preference ratio.

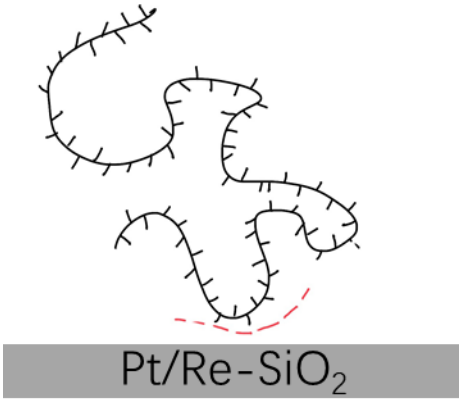

Figure 3. 8 Steric repulsion from polymer side groups at high branching.

3.3.5 Additional remarks on the isotope labelling scheme

We finally comment on the deuterium distribution across all reacting materials. A material mass balance sheet is tabulated in Table 3.2 for one of the many LLDPE1 labelling batches produced in the 1 L vessel. Correspondingly, the DL of the hydrocarbons, including both the polymer ($y_{polymer}$) and the solvent ($y_{solvent}$), were calibrated with FTIR for the polymer, and with ^{1}H-NMR for the solvent following the manner similar to that used for measuring the DL of polymers with NMR (Section 2.5). We then calculate the fraction of total deuterium that enters the polymer ($f_{polymer}$) and the solvent ($f_{solvent}$), respectively, based on the DL of the polymer and the solvent. The results are listed in Table 3.3.

Table 3. 2 List of materials during the isotope exchange reaction

Material	Mass (g)	Weight fraction
Isooctane	345[a]	0.975
LLDPE1	5.0	0.014
Pt/Re-SiO_2	1.5	0.004
D_2	2.4[b]	0.007

[a] Calculated for 500 mL solvent with ρ = 0.69 g/mL

[b] Calculated for 500 cm^3 gas volume with ideal gas assumption

Table 3. 3 DL of components after labelling and fraction of D consumed by each component

$y_{polymer}$[a]	$y_{solvent}$[a]	$f_{polymer}$[b]	$f_{solvent}$[b]
0.59	0.012	0.35	0.54

[a] DL of the component characterized with FTIR

[b] Fraction of D consumed by the component

A quick examination of relative fraction of the materials in the system highlights an obvious fact, that the system is mostly made of hydrogenous species, i.e., the solvent, which constitutes over 97% of the total mass of the reacting materials, while the polymer accounts for only weighs roughly 1%. If we restrict our attention to the H/D isotopes, the recipe leads to only 2.1% of the total isotope species being deuterium, thus the eventual equilibrium DL of all H/D related components should be 2.1%. However, the polymer managed to consume more than 30% of the total D reservoir, reaching a 59% average deuterium content, as illustrated in Figure 3.9. This implies that the polymer has an unusual capability for taking in deuterium. With the observation that the DL in the polymer increases quickly with increasing molecular weight, we can now attribute the high deuterium consumption of the polymer to the much higher absorptivity on the heterogenous catalyst comparing to the small solvent molecules. We now see the reaction system after 17 h as trapped in a non-equilibrium intermediate state, with deuterium chemically bound to the polymer due to isotope exchange driven by preferential adsorption on the metal catalyst relative to the solvent. This also indicates that although many early examples of isotope exchange for small molecules have used homogeneous catalysts, they are less likely favored in polymer labelling due to the lack of such absorptivity difference that tends to

concentrate the deuterium in the polymers.

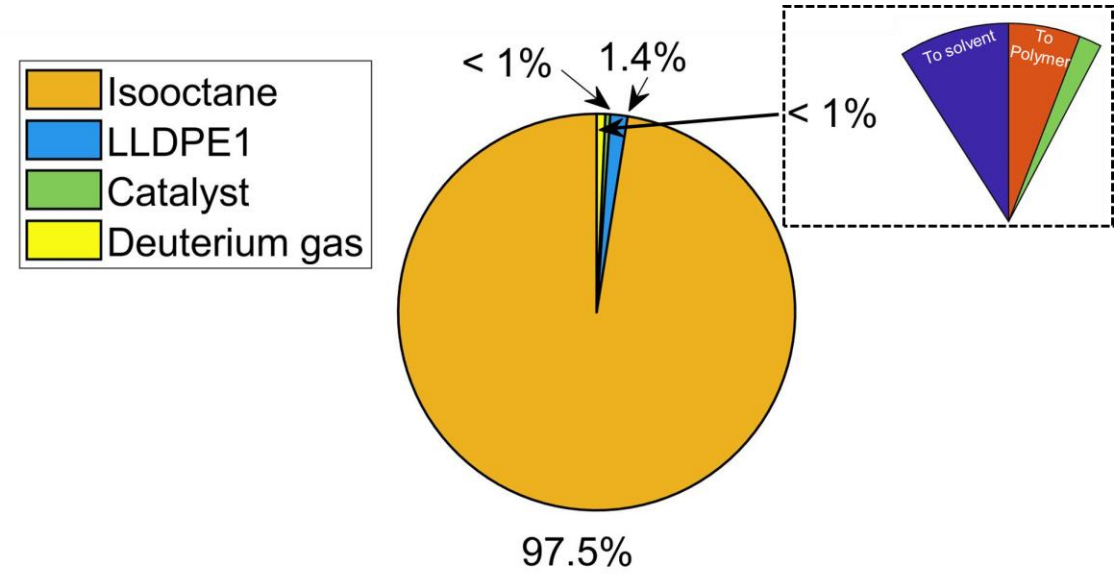

Figure 3. 9 Mass fraction of the components within the isotope exchange system at the beginning of the exchange reaction, and the deuterium split up between different species at the end of the isotope exchange reaction.

Chapter 4

Small angle neutron scattering from isotope labelled polyolefins

* Reproduced in part from Zeng, Y.; López-Barrón, C. R.; Eberle, A. P. R.; Lodge, T. P.; Bates, F. S. *Macromolecules* **2017**, 50, 6849-6860. Copyright 2017 American Chemical Society.

4.1 Introduction

An important goal of performing isotope exchange reactions with the polyolefins is that it opens the possibility of investigating premade polyolefin materials with small angle neutron scattering (SANS). As do other scattering techniques such as X-ray scattering and light scattering, SANS interrogates the target material with an incident radiation beam, and interprets the spatial correlation of the scatterers by analyzing the wavevector dependent intensity of the scattered radiation. Also like other scattering approaches, contrast between the target structure and the matrix has to be present to create scattering intensity. What is unique with SANS is that neutron scattering is sensitive to the isotope content of the

materials, thus contrast can be created by isotopic labeling with limited alteration of other important physical properties of the material. However, until recently, the most accessible methods for creating deuterium labeled polymers were either through addition of deuterium to unsaturated bonds, or through polymerization of deuterated monomers. Both routes require full control over the synthetic path of the materials, which is rarely realistic in the commercial polyolefin world; the latter route is unreasonably expensive at large scales. We considered the isotope labelling technique in Chapter 3. In Chapter 4, we focus on exploiting the catalytic labeling technique for the purpose of extracting the single chain structure of polyolefins.

4.2 Models describing the scattering intensities from isotope labelled polymers

4.2.1 General concepts of SANS

The conceptual scheme of small angle neutron scattering is illustrated in Figure 4.1. An incident beam of neutrons is shined onto the sample specimen with defined exposure area and thickness. The angular dependent intensity of the neutrons is recorded by a 2D detector. The immediate transmitted beam is masked by a beamstop located at the center of the 2D detector, allowing analysis of the scattered component only.

Scattered intensity from the polymer represents the sum of incoherent scattering and coherent scattering. The incoherent scattering is an angular independent scattering that has to do with the element composition of the material. The coherent scattering, on the other hand, is dependent on the angle of the scattered neutrons, and reflects the spatial correlation of the scatterers, which can be used to reveal the dimensions of the individual scatterers. For the scope of this research, only the coherent scattering is analyzed, with the incoherent scattering substracted as a baseline. Note that though not analyzed in this research, the incoherent baseline values can act as an indicator of the amount of deuterium in the

materials where a higher deuterium content results in a lower baseline value as the incoherent scattering length of D is lower than that of H (see Table 1.1).

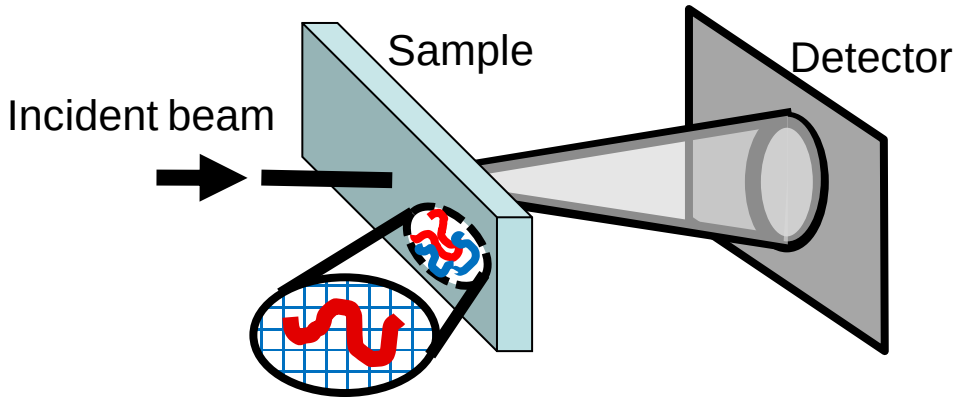

(a)

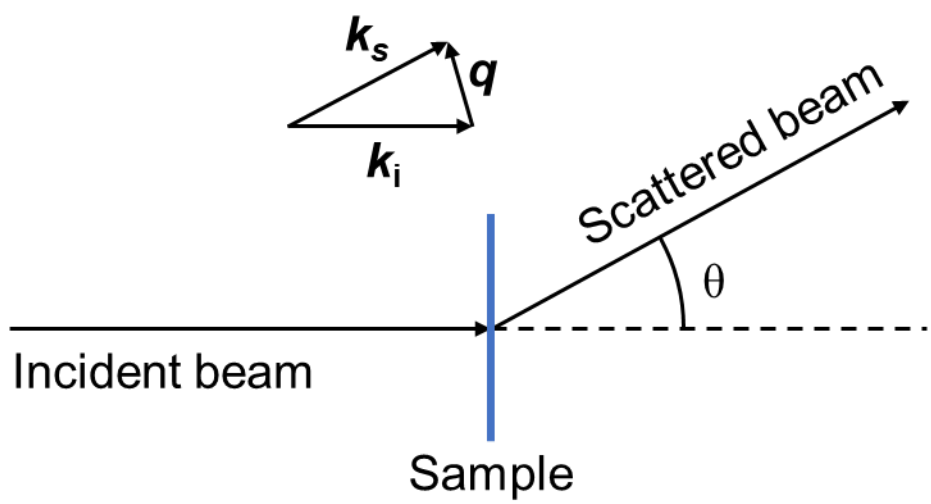

(b)

Figure 4. 1 Illustration of a typical SANS experiment. **(a)** Setup for SANS. **(b)** Incident and scattered beams from a thin sample.

Several quantities are used to describe the scattering experiments: the incident radiation wavelength λ, the incident unit vector $\boldsymbol{k}_i$, the unit vector along the scattered beam

$\boldsymbol{k}_s$, the measured scattering intensity $I(q)$, the scattering angle θ, the scattering vector $\boldsymbol{q}$ and its magnitude q, the coherent scattering length of a repeat unit b, the volume of the repeat unit v, and the form factor of the scatterer $P(q)$. These quantities are related through the following relations:

$$\boldsymbol{q} = \frac{4\pi}{\lambda} \sin\frac{\theta}{2} \frac{\boldsymbol{k}_s - \boldsymbol{k}_i}{|\boldsymbol{k}_s - \boldsymbol{k}_i|} \qquad (4.1)$$

$$q = \frac{4\pi}{\lambda} \sin\frac{\theta}{2} \qquad (4.2)$$

$$I(q) = \left(\frac{b_1}{v_1} - \frac{b_2}{v_2}\right)^2 P(q) \qquad (4.3)$$

Note while 4.1 and 4.2 generally hold, Equation 4.3 only represents a simple case where there are only two components and the labelled component is in the dilute, non-overlapping limit. The subscripts 1 and 2 denote to the two components in a homogeneous blend. For systems with more components or systems that are not dilute, further consideration of the inter-scatterer structure factor, $S(q)$, has to be considered.

4.2.2 Pure labelled, uniform polyolefins: analytical method

Ideally, the pure isotope labelled polyolefin should not generate any coherent scattering, due to lack of contrast. However, the real world is more complicated: impurities such as dust will be present, often generating low q scattering as the sizes of such impurities is usually beyond the single chain dimension; we usually avoid interpreting data that contains scattering from impurities, which can obscure the single chain conformation information we are after. More importantly, the labelling from the isotope exchange is often

incomplete, and the placement of deuterons from chain to chain and within each single chain can vary, thereby creating contrast and generating coherent scattering. Balsara et al. have attributed such coherent scattering to non-uniform isotope labeling within the material, when variation from molecular weight distribution and branching are absent by using a uniform model polymer.[63] After subtraction of the incoherent scattering background, the remaining coherent component can be modeled using the following relation:

$$I(q) = (\overline{B^2} - \overline{B}^2)Nv_0 g_D(x) \qquad (4.4)$$

where B is contrast factor that represents the difference of the coherent scattering length densities between the labeled and unlabeled chains. The average is an ensemble average over all chains within the investigated component. N is the degree of polymerization (assuming $N_w/N_n = 1$), and v_0 is the reference volume defined based on a four-carbon repeat unit. The term $g_D(x)$ is the Debye function,

$$g_D(x) = (2/x^2)(e^{-x} - 1 + x) \qquad (4.5)$$

$$x = q^2 R_g^2 \qquad (4.6)$$

$$R_g^2 = Na^2/6 \qquad (4.7)$$

where a is the statistical segment length of the four-carbon repeat unit.

4.2.3 Pure labelled, uniform polyolefin: numerical method

For incompressible, homogeneous polymer mixtures, the random phase approximation can be applied to predict the structure factor of the blend, essentially predicting the scattering pattern. For this work, the polymer sample can be viewed as a multiple component blend, and each blend has a single molecular weight value and deuterium exchange level. The equations to solve are

$$I(q) = \Delta\boldsymbol{\rho}^{\mathbf{T}}\cdot\boldsymbol{S}(\boldsymbol{q})\cdot\Delta\boldsymbol{\rho} + \text{bkg} \qquad (4.8)$$

$$\boldsymbol{S}^{-1}(\boldsymbol{q}) = \boldsymbol{S}_{\mathbf{0}}^{-1}(\boldsymbol{q}) + \boldsymbol{V}(\boldsymbol{q}) \qquad (4.9)$$

$$S^0_{ii}(q) = \phi_i N v_0 g_D(x) \qquad (4.10)$$

$$V_{ii}(q) = S^{0\ -1}_{nn}(q) - 2\chi_{in}/v_0 \qquad (4.11)$$

$$V_{ij}(q) = S^{0\ -1}_{nn}(q) + \chi_{ij}/v_0 - \chi_{in}/v_0 - \chi_{jn}/v_0 \qquad (4.12)$$

$$\chi_{ij} = \chi_{hd}\left(y_i - y_j\right)^2 \qquad (4.13)$$

where $\Delta\boldsymbol{\rho}$ represents the difference in scattering length density between each fraction and a reference fraction, which is here arbitrarily selected as the component with maximum volume fraction. $\boldsymbol{S_0(q)}$ is the bare system response matrix and has the form $S^0{}_{ii}(q) = \phi_i N_i v_0 P(z)$, where ϕ_i is the volume fraction of the i-th component, N_i is the degree of polymerization of that component, and $g_D(x_i)$ is given by equation 6 with $x_i = q^2a^2N_i/6$.

The term χ_{ij} represents the Flory-Huggins interaction parameter associated with the isotope effect between the *i*-th and *j*-th component, with DL values of y_i and y_j.[100] The bkg term is the incoherent background scattering, estimated from the experimental high *q* asymptote.

4.2.4 Blend of hydrogenous and deuterium labelled polyolefin

The scattering from polymer blends prepared by blending the isotope labelled polymer with the unlabeled polymer can also be interpreted by the RPA method, after subtracting the extra factor from the inhomogeneous labelling, $\phi_d(\overline{B^2} - \overline{B}^2)Nv_0 g_D(x)$. In the limit of a two-component homogeneous blend of uniform polymers, the scattering intensity is

$$I(q) = v_0^{-1}(b_h - b_d)^2 S(q) \tag{4.14}$$

$$S^{-1}(q) = \left[\phi_h N g_D(x_h)\right]^{-1} + \left[\phi_d N g_D(x_d)\right]^{-1} - 2\chi_{hd} \tag{4.15}$$

where *b* is the average coherent scattering length of a four-carbon repeat unit. The subscript h indicates the property of the h-polymer, while the subscript d stands for the d-polymer.

4.3 Experiment

SANS

SANS experiments were performed at the NG-7 30 m SANS instrument at the National Institute of Standards and Technology (NIST), located in Gaithersburg, MD. Samples were dried and degassed under vacuum at 150 ºC prior to use. A blend of hPBD35-33 and d-hPBD35-33 was prepared by dissolving the two polymers in cyclohexane at room

temperature followed by precipitation in cold methanol. The concentrations of the two polymers were controlled at 0.4770 g polymer / 100 mL solvent for hPBD35-33, and 0.5230 g polymer / 100 mL solvent for d-hPBD35-33, producing an equal volume fraction blend after accounting for the densities of these two polymers. d-LLDPE1b and LLDPE1 were dissolved in TCB at 140 ºC for blending and precipitated in methanol. Concentrations were 0.0542 g d-LLDPE1b and 0.9458 g LLDPE1 per 100 mL solvent, which gives a blend with 5% d-LLDPE1b by volume. The blends were dried under vacuum for 24 h. Homopolymers and blend specimens were pressed between two quartz windows with stainless steel spacers to form discs of 1 mm thickness. SANS experiments were performed with radiation wavelength $\lambda = 6$ Å ($\Delta\lambda/\lambda = 0.11$) and sample-to-detector distances of 1, 4, and 13 m. The acquired neutron scattering profiles were corrected for empty cell scattering, background noise, detector sensitivity, and sample transmission, and normalized against direct neutron beam flux to give absolute scattering intensity (in cm^{-1}). Azimuthal averaging of the 2D patterns was performed to generate 1D plots of scattering intensity versus the magnitude of the scattering vector q.

SEC-IR

Motivated by the molecular weight dependence of deuterium exchange shown in Figure 2, we sought to assess the distribution of deuterium across the broad range of molecular weight polymers that make up sample d-LLDPE1a/b. This was accomplished using a technique initially described by Habersberger et al. and subsequently modified by Kang et al.[95,99,] The measurement was accomplished using an SEC instrument equipped with a FTIR detector, which could selectively monitor either C–D or C–H absorption, although not both simultaneously. The commercial LLDPE sample has Đ ≈ 2.5, covering the molecular weight range from 1 kDa to 103 kDa.

4.3 Results

4.3.1 Scattering from d-hPBD35-33

Figure 4.2 includes SANS patterns measured from separate d-hPBD35-33 and hPBD35-33 specimens at 25 ºC, as well as a 50/50 blend. The average deuterium content of d-hPBD35-33 was determined to be 68.1% by density measurements and 69% by FTIR. All scattering patterns display coherent and incoherent scattering intensity at low and high q, respectively. Isotope exchange is reflected in the incoherent intensity of d-hPBD35-33, which is significantly lower than that of hPBD35-33; the incoherent scattering cross-section of deuterium is smaller than that of hydrogen. Forward (coherent) scattering can be observed with both pure samples at low q. The origin of the coherent scattering in hPBD35-33 (< 0.015 $Å^{-1}$) is not known with certainty, but may derive from heterogeneities such as residual catalysts, dust and other impurities. Sample d-hPBD35-33 exhibits significant coherent scattering over the range q < 0.2 $Å^{-1}$. Following Balsara's model, the coherent scattering intensity of d-hPBD35-33 is fit with equations 4.4 to 4.7 with the prefactor, $(\overline{B^2} - \overline{B}^2)Nv_0$, and the statistical segment length, a, as independent variables, as shown by the dashed curve in Figure 4.2. For data fitting, v_0 is calculated to be 109.5 $Å^3$ at room temperature according to the measured density for hPBD35-33. Based on the optimal fit to the d-hPBD35-33 result (and blend data, see below) a = 6.8 ± 0.2 Å. The coefficient of variation for the number of deuterium atoms per repeat unit (n_D) was determined to be:

$$\left((\overline{n_D^2} - \overline{n_D}^2)/\overline{n_D}^2\right)^{\frac{1}{2}} = \left((\overline{B^2} - \overline{B}^2)/\,\overline{B}^2\right)^{\frac{1}{2}} = 0.12 \qquad (4.16)$$

This approach gives an excellent description of the data for d-hPBD35-33.

For comparison, we also performed a numerical calculation of the SANS intensity for d-hPBD35-33 assuming a completely random distribution of deuterons per polymer

molecule. For each non-carbon atom connected to the carbon atoms in the polymer, the probability of finding a deuteron was assumed to be $y = 0.68$, the average deuterium content of the sample. For a polymer chain with N four-carbon repeat units, and N_d deuterons per chain, we assumed a binomial distribution $N_d \sim B(4N, y)$. We generated 50 discrete fractions with homogeneous deuterium content y_i, and volume fraction of

$$\phi_i = P(4N \times (y_{i-1} + y_i)/2 < N_d < 4N \times (y_i + y_{i+1})/2) \qquad (4.17)$$

which is the probability of N_d being between $4N \times (y_{i-1} + y_i)/2$ and $4N \times (y_i + y_{i+1})/2$. Values of y_i were selected so that $\phi_1 = \phi_{50} = 0.001$, with ϕ_{25} as the maximum value of all volume fraction values. The scattering intensity from an arbitrary blend of polymer chains can be calculated based on the n-component RPA model using equations 4.8 through 4.13, where the n components are slices of the material by deuterium exchange level or molecular weight.[99,101–103] At the molecular weight and extents of deuterium content under consideration for d-hPBD35-33, χ_{ij} can be safely assumed to be zero.[45] For this calculation, $N_i = 625$ for all 50 components and $a = 6.8$ Å. The resulting calculated scattering intensity for a random distribution of deuterium is shown by the dash-dot curve in Figure 4.2, and is barely different from the incoherent contribution. Clearly, the coherent scattering from sample d-hPBD35-33 is not accounted for by a random distribution of deuterium labeling within each chain.

The scattering intensity from a 50/50 blend of d-hPBD35-33 and hPBD35-33 is also included in Figure 4.2. The coherent scattering from non-uniform labeling, $\phi_d(\overline{B^2} - \overline{B}^2)Nv_0 g_D(x)$, accounts for less than 3% of the total coherent scattering intensity observed for the blend, indicating that the dominating contrast is between the partially deuterated and the non-deuterated components. The blend scattering intensity was corrected by

subtracting the weighted contribution from pure d-hPBD35-33, and then fit with equations 4.14 and 4.15. Again χ_{hd} is assumed to be 0. Fitting the polymer blend scattering intensity to the RPA model using a least-squares method gives an excellent fit, with the only adjustable parameter a = 6.8 ± 0.1 Å. The important conclusion is that, despite significant inhomogeneity of deuterium distribution during the isotope exchange reaction, SANS can still be performed on blends of native and partly exchanged model polyolefins, and interpreted via the RPA model.

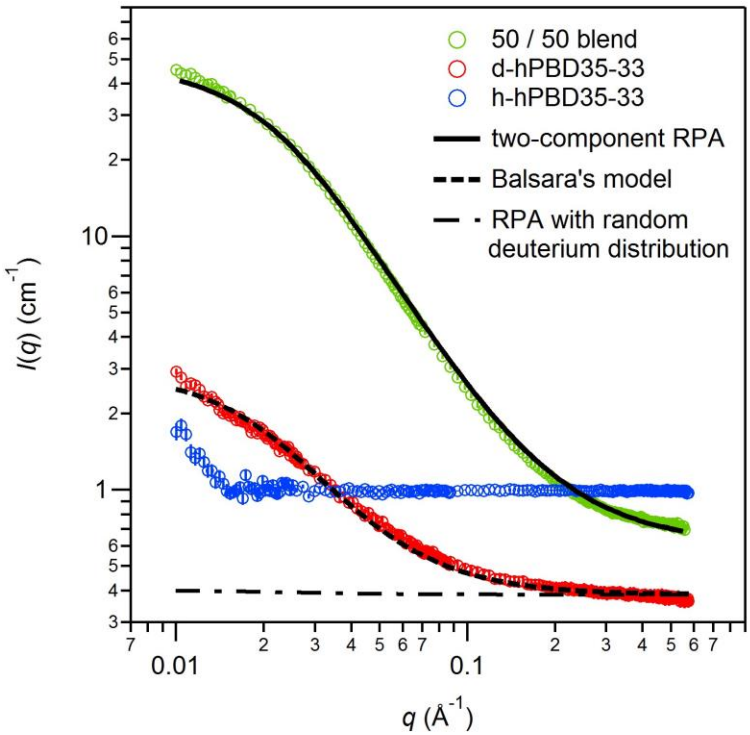

Figure 4. 2 SANS intensity for pure hydrogenous and deuterated hPBD35-33 polymers, and a 50:50 blend ($\phi_d = \phi_h = 0.5$) at 25 ºC. The solid curve is a fit to the two-component RPA model. The dashed curve is a fit with the Debye form factor and inhomogeous deuterium labeling. The dash-dot curve is the predicted SANS intensity for a polymer with a completely random distribution of deuterium and the same overall level of deuterium exchange (68%).

4.3.2 DL of LLDPE1 as a function of molecular weight from SEC-IR

The SEC-IR result shown in Figure 4.3 reveals significant inhomogeneity regarding deuterium content within d-LLDPE1a, ranging from about 25% to 60% substitution from lowest to highest molecular weight. This result reveals the same qualitative trend found in Figure 3.3, although the overall average deuterium content is somewhat lower in d-LLDPE1a than in the d-hPBD specimens with low branch content, presumably due to the higher polymer concentration used in isotope exchange experiments of LLDPE1. We believe that the FTIR result is more accurate than the density measurements for d-LLDPE1. The effects of variable crystallization on density among specimens solidified from the melt state introduces significant variability in DL deduced from the density, which can result from differences in cooling rate and annealing time. Hence we rely on the FTIR-based values in evaluating SANS data in the following sections.

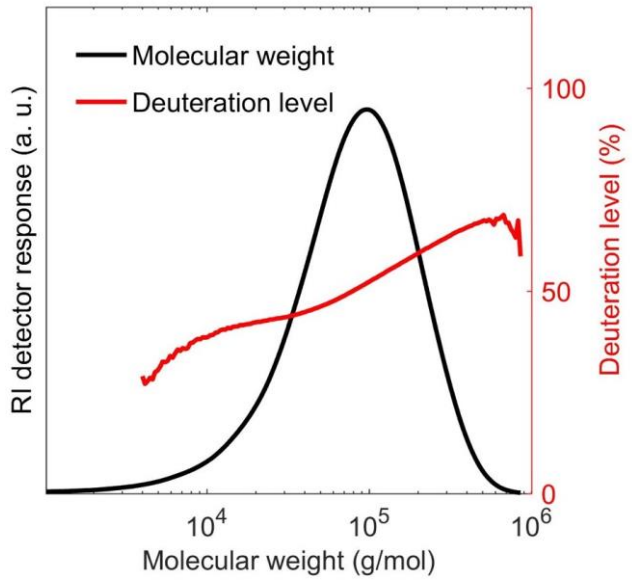

Figure 4. 3 Molecular weight distribution and deuterium content distribution of d-LLDPE1 measured with SEC-IR. Measurement was conducted at 145 ºC in TCB. Molecular weight values were calibrated with PS standards via universal calibration. Infrared detection is limited to wave numbers between 2700 cm^{-1} and 3000 cm^{-1}.

4.3.3 SANS from d-LLDPE1

Figure 4.4 presents the SANS scattering intensities measured for separate d-LLDPE1a and LLDPE1 specimens at 150 ºC. The d-LLDPE1a sample was prepared using the H/D exchange reaction and characterized by FTIR to be 51% deuterated on average. Forward scattering was observed at $q < 0.02$ $Å^{-1}$ for LLDPE1 and at $q < 0.1$ $Å^{-1}$ for d-LLDPE1a. The coherent scattering in LLDPE1, which resembles that found in hPBD35-33 (Figure 4.2), is likely a result of residual impurities. The deuterated sample, on the contrary, exhibits significant coherent scattering over a wider q range in the melt state. This reveals an inhomogeneous distribution of deuterium among the polymer chains, as observed with d-hPBD35-33. However, in contrast to Figure 4.2, this sample is also very broad in terms of molecular weight distribution. We calculated the scattering intensity for uniform PE with M = 113 kDa and 51% deuterium content using the two strategies employed in the previous

section: (a) completely random placement of deuterium atoms, and (b) a non-uniform distribution with $\left((\overline{n_D^2} - \overline{n_D}^2)/\overline{n_D}^2\right)^{\frac{1}{2}}$ the same as that measured for d-hPBD35-33. The statistical segment length was set to be 7.6 Å, a value derived from the collective fitting results discussed below. The calculated results, shown in Figure 4.4, bracket the SANS intensity from sample d-LLDPE1a; specifically, the random labeling assumption yields negligible coherent scattering, while the non-uniform model slightly overestimates the experimental results. We then analyzed the scattering intensity measured from d-LLDPE1a based on two further, more realistic assumptions: (1) the average deuterium content is uniform across all molecular weights, but fluctuates from chain to chain at each molecular weight, and (2) the average deuterium content varies with molecular weight, but is uniform for all chains with the same molecular weight. In both cases, we adjust the statistical segment length to obtain a satisfactory fit to experiment data. In the latter case, it is the only adjustable parameter for fitting.

Analysis with the first assumption follows the procedure of Balsara et al.,[63] with adjustment for the dispersity of the polymer, obtained from the SEC measurement shown in Figure 4.2. Equation 4.4 is modified to

$$I(q) = (\overline{B^2} - \overline{B}^2)v_0 < N g_D(x) >_w \qquad (4.18)$$

where $<\ldots>_w$ stands for an ensemble average by weight fraction. The best fit to the data yields $a = 7.7 \pm 0.3$ Å, and $\left((\overline{n_D^2} - \overline{n_D}^2)/\overline{n_D}^2\right)^{\frac{1}{2}} = \left((\overline{B^2} - \overline{B}^2)/\overline{B}^2\right)^{\frac{1}{2}} = 0.14$. Analysis with the second assumption was performed using equations 11-15, with the deuterium level for each slice of molecular weight as measured by SEC-IR. This procedure gives $a = 7.6 \pm 0.2$ Å. Thus, within experimental uncertainty both methods are consistent with $a = 7.6$ Å. Both methods provide a satisfactory description of the experimental trace, with the only

significant deviation occurring at the lowest q, where the unexplained forward scattering contributes the most.

In order to verify both the reproducibility of the H/D exchange reaction and the reliability of the data analysis method, we analyzed sample d-LLDPE1b, generated from a separate deuterium exchange experiment with the same reaction conditions as those for d-LLDPE1a. The deuterium content of d-LLDPE1b was 65% by density measurements and 61% by FTIR, i.e., somewhat higher than for d-LLDPE1a. Figure 4.5 shows the SANS results from d-LLDPE1b, LLDPE1 and a 5/95 blend containing 5% of the deuterated component. Due to material and instrument availability, SEC-IR was not performed for d-LLDPE1b, but a corrective scaling factor of 0.61/0.51 = 1.20 was applied to the DL(MW) profile of d-LLDPE1a as an estimate of the DL(MW) profile of d-LLDPE1b. This assumes that the trend of DL with MW does not differ significantly between d-LLDPE1a and d-LLDPE1b, and they differ mainly in overall deuterium content. Scattering from the pure polymer, d-LLDPE1b, was first fit successfully to equation 4.4, resulting in a = 7.6 ± 0.1 Å, and $\left((\overline{n_{\mathrm{D}}^2} - \overline{n_{\mathrm{D}}}^2)/\overline{n_{\mathrm{D}}}^2\right)^{\frac{1}{2}} = \left((\overline{B^2} - \overline{B}^2)/\overline{B}^2\right)^{\frac{1}{2}} = 0.091$. A calculation with equations 11-15 using a = 7.6 Å, however, overestimated the scattering intensity as shown in Figure 4.5. This could be due to error associated with scaling of the deuterium level, as the variation of deuterium content is the source of contrast in the pure d-LLDPE1b polymer and the calculated scattering intensity is sensitive to the detailed distribution.

The 5/95 blend scattering in Figure 4.5 was analyzed using two strategies: (1) fit to the RPA model for the blend of d-LLDPE1b/LLDPE1, with molecular weight distribution measured by SEC, and (2) calculate the scattering intensity with statistical segment length derived from the above fitting according to equations 4.8 – 4.13. Strategy (1) requires modification of the model in equations 4.14 and 4.15 as the following

$$I(q) = v_0^{-1}(b_{\mathrm{h}} - \overline{b_{\mathrm{d}}})^2 S(q) \tag{4.19}$$

$$S^{-1}(q) = \left[\phi_h \langle N g_D(x_h)\rangle_w\right]^{-1} + \left[\phi_d \langle N g_D(x_d)\rangle_w\right]^{-1} - 2\chi \qquad (4.20)$$

where $\overline{b_d}$ is the average scattering length of a four-carbon repeat unit in d–LLDPE1b and χ is the Flory-Huggins parameter between d-LLDPE1b and LLDPE1. χ is calculated by adjusting the Flory-Huggins parameter between perdeuterated d-PE and PE at the specified experiment temperature and volume fraction for partial labeling ($\overline{y}$ = 61%), which yields $\chi = 1.8 \times 10^{-3} \times 0.61^2$.[100] Fitting produces a = 7.6 ± 0.3 Å. The calculated intensity following strategy (2) with a = 7.6 Å falls close to the experiment result as shown in Figure 4.5. Since the dominating contrast in the blend is between the deuterated and the non–deuterated species, the scaling of deuterium content is likely a less important source of error. Together, the results and analyses illustrated in Figures 4.3 and 4.4 demonstrate general consistency in the ability to model the SANS data obtained from catalytically deuterated commercial polyethylene and blends of these polymers with the hydrogenated precursor.

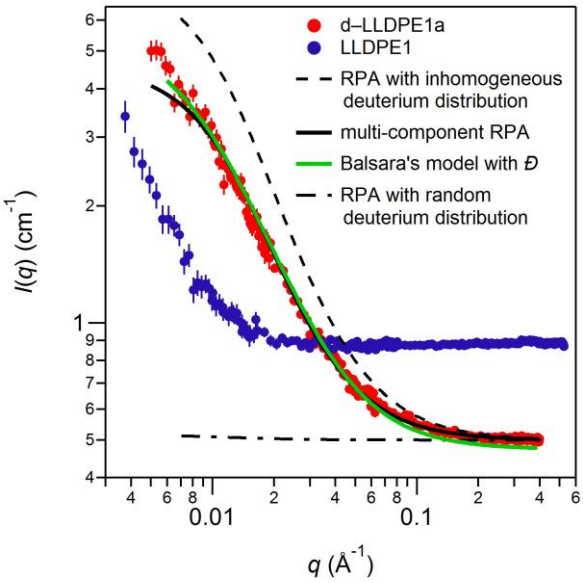

Figure 4. 4 SANS intensity of d-LLDPE1a and LLDPE1 at 150 ºC. The black solid curve is a multicomponent RPA calculation using the deuterium distribution measured with SEC-IR. The green solid curve is a fitting according to equation 18. The dashed curve is the predicted SANS intensity for a uniform polyethylene with M = 113 kDa, and with the same degree of deuterium content variation as that measured from d-hPBD35-33. The overall deuterium content is the same as that of d-LLDPE1. The dash-dot curve is the predicted SANS intensity for the uniform polymer with completely random deuterium distribution and the same overall labeling extent (51%).

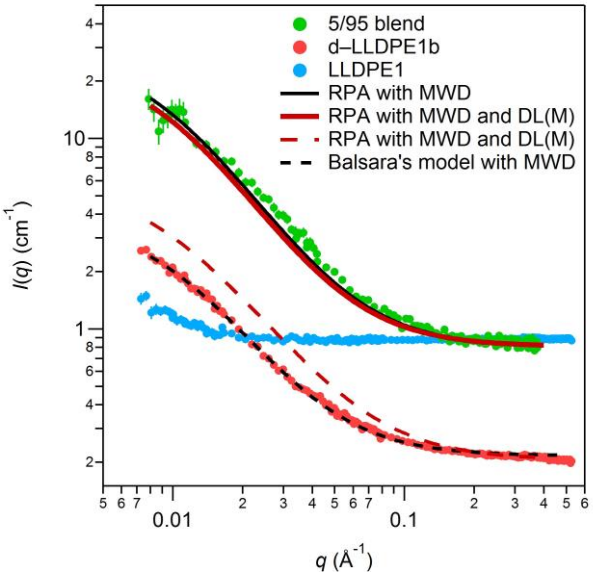

Figure 4. 5 SANS intensity for pure hydrogenous LLDPE1 and deuterated d-LLDPE1b (DL = 61%), and 5/95 blend (ϕ_d =0.05, ϕ_h = 0.95) at 150 ºC. RPA calculations for d-LLDPE1b assuming DL does not vary with molecular weight (MW) (black dashed curve), and with DL(MW) scaled to the overall level of labeling according to the results from Figure 4 (red dashed curve). 5/95 blend data have been modeled with the RPA theory assuming DL is independent of MW (solid red curve) and corrected for DL(MW) (solid black curve). All calculations have been done with *a* = 7.6 Å.

4.4 Discussion

The primary motivation for this research was to address fundamental questions regarding the heterogeneous catalytic isotope exchange mechanism, including (1) how

deuterium is distributed in the polymers, (2) what factors influence the extent of labeling, and (3) whether inhomogeneous deuterium labeling interferes with the ability to apply this technique to SANS with commercial polyolefins. During the course of characterizing the deuterated samples with SANS, we realized that the deuterium distribution in the labelled materials cannot be uniform. Further analysis confirmed that the isotope labeling technique does not produce uniform, i.e. random, isotope labeling. Molecular weight and short chain branching are found to be two factors that affect the labeled product.

Molecular scale heterogeneity. We first address the coherent neutron scattering recorded from the pure deuterated polymers and blends with the hydrogenous analogues. The existence of coherent scattering in d-hPBD35-33 and d-LLDPE1a/b reveals that the deuterium labeling is not uniform; this conclusion is supported by the calculations regarding random placement of the isotopes, as shown in Figures 9 and 10. Analysis of the scattering data from d-hPBD35-33 following the method suggested by Balsara et al. quantitatively accounts for the intensity as a function of q where $\left((\overline{n_{\mathrm{D}}^2} - \overline{n_{\mathrm{D}}}^2)/\overline{n_{\mathrm{D}}}^2\right)^{\frac{1}{2}}$ = 0.12.[63] A statistical segment length of a = 6.8 Å results in excellent fits of the RPA theory to the SANS data from pure d-hPBD35-33 and a 50/50 mixture with the protonated analogue hPBD35-33. This a value is somewhat higher than that reported by Fetters et al., a = 6.1 Å for hPBD with 33% branching at 27 °C.[104,105,]

Interpreting the data from d-LLDPE1 is complicated by the fact that the labeled material has at least two sources of possible contrast factor heterogeneity: (i) variation in the average deuterium content as a function of molecular weight (Figure 4.3), which is qualitatively similar to what we found with the narrow dispersity d-hPBD samples (Figure 3.3), and (ii) possible variation of $\left((\overline{n_{\mathrm{D}}^2} - \overline{n_{\mathrm{D}}}^2)/\overline{n_{\mathrm{D}}}^2\right)^{\frac{1}{2}}$ with molecular weight. Moreover, there is some variability in the overall deuterium content measured by FTIR between specimens of the same sample that were deuterated under nominally the same conditions, DL = 51% and 61% for for d-LLDPE1a and d-LLDPE1b, respectively (Table 2.4). Such

variability is not surprising given the heterogeneous nature of the catalyst and (unknown) sensitivity to fluctuations in temperature, deuterium pressure, and mixing non-idealities. Nevertheless, the values of $\left((\overline{n_D^2} - \overline{n_D}^2)/\overline{n_D}^2\right)^{\frac{1}{2}}$ obtained from the two d-LLDPE1 specimens are qualitatively consistent with the results for d-hPBD35-33, ranging from 0.09 to 0.14, depending on the assumptions used regarding the distribution of deuterium within specific slices of, and across, the molecular weight distribution in modeling the SANS data. Significantly, the value of the statistical segment length associated with all these calculations is consistently a = 7.6 ± 0.2 Å, which is slightly smaller than what is reported by Fetters et al., a = 8.0 Å for hPBD with 2.1% branching at 167 °C.[104,105] Importantly, the SANS results from the 5/95 d-LLDPE1b/LLDPE1 blend are modeled equally well with or without inclusion of an assumed variation in deuterium content with molecular weight (Figure 11).

Overall, these results show general consistency in the heterogeneous placement of deuterium at the macromolecular scale ($q << a^{-1}$) in polyolefins with high (d-hPBD35-33) and low (d-LLDPE) branch contents, and across a wide range of molecular weights. If such heterogeneity were blocky in nature (i.e., long runs of deuterated segments separated by runs of protonated segments within individual molecules) we would not expect to obtain the quality of fits to the RPA theory shown in Figures 9, 10, and 11. For example, in the limit of an ideal diblock the scattering intensity would peak at $q \sim R_g^{-1}$ and fall to zero as $q \rightarrow 0$.[106] The fact that SANS data from both the pure deuterated polymers and corresponding blends can be interpreted self-consistently with a single statistical segment length implies that the chains are individually relatively uniformly labeled.

While there are quantitative differences in the average amount of deuterium exchanged as a function of molecular weight, these results suggest a common mechanism of isotopic exchange. We picture the polymer chains adsorbed to and moving around on the catalyst like a caterpillar walking on a leaf. Multiple points of contact keep the caterpillar from

falling off. Similarly the polymer can dynamically explore the surface of the catalyst while continuously trading hydrogen for deuterium present in and on the metal. Statistically, different chains spend different periods of time on the surface resulting in variability in the amount of deuterium per chain. Due to the chemical similarity of H and D, the isotope exchange is assumed to be reversible and to take place throughout the course of the reaction. The ultimate equilibrium state of the reacting system should be one that has deuterium uniformly distributed among the components of the system, including the gaseous phase, the polymer, and the solvent. Under this scenario, the number of times an individual chain visits the catalyst during the finite reaction time must be limited, otherwise the chains would all end up with the same amount of deuterium, in contradiction with the observed coherent scattering. The limited reaction time leaves the system trapped in an intermediate state, where the deuterium is more concentrated in the polymer species due to their higher adsorption capability. We suspect that most of the labeling occurs in just a few adsorption steps. This mechanism has been shown to be operative during the hydrogenation of 1,2-polybutadiene on a heterogeneous Pd catalyst.[107] However, in that case the coordination of double bonds to metal sites provides a clear mechanism. We do not know whether differences in adsorption energy between C–H and C–D bonds influence the process.

One final point should be considered based on this proposed mechanism. During the course of the batch process the gas composition transitions from an atmosphere of pure deuterium to a mixture of D_2, H_2, and HD. Hence, as the exchange reaction proceeds, the rate of swapping deuterium for hydrogen may slow due to a continual drop in the concentration of dissociated D_2. Presumably this will have no impact on the kinetics of adsorption/desorption, but will reduce the amount of exchange that occurs during each cycle. Thus, chains that attach to the catalyst at the early stages of the process will acquire more deuterium than those visiting the metal surface later.

Segment scale heterogeneity. From the NMR results, increasing the ethyl branch content beyond about 20-30% leads to a significant reduction in the amount of deuterium exchanged onto the hPBD polymers (Figure 3.5). Moreover, NMR analysis shows conclusively that the exchange occurs preferentially on the terminal methyl group. While the overall amount of deuterium drops from 69% (hPBD23-3) to 34% (hPBD32-50) it is important to recognize that even with an ethyl branch located on every other backbone carbon atom there is still considerable isotope exchange. We believe that the driving force for adsorption on the surface is thermodynamic, involving both the interaction of the segments with the metal catalyst and the solvent quality as discussed above. Intuitively, the linear PE chains afford access to the backbone C–H bonds in a more facile manner than those in highly branched hPBD. What is most striking is that isotactic polypropylene (*i*PP) exchanges no deuterium when reacted under the same conditions. The argument advanced previously was that the local chiral structure of the *i*PP repeat units may interfere with a planar local configuration required for efficient absorption. Our finding with atactic hPBD32-50 leads us to question this explanation. Clearly, this polymer is more crowded at a segment scale than *i*PP, e.g., PEE has a smaller statistical segment length than *i*PP at the same defined segment volume.[108] Another possibility is that isooctane is not an adequate solvent for *i*PP, as we have surmised with high molecular weight PE.

Chapter 5

Application: characterization of single molecule alignment in polyethylene during cold-drawing

* Reproduced in part from López-Barrón, C. R.; Zeng, Y.; Schaefer, J. J.; Eberle, A. P. R.; Lodge, T. P.; Bates, F. S. *Macromolecules* 2017, 50, 3627-3636. Copyright 2017 American Chemical Society.

5.1 Introduction

The technique of isotope labelling of polyolefins with deuterium, especially through direct isotope exchange, holds a special industry interest, as commercially polyolefin production is a very high volume business. In the scope of this thesis, we explore the first example of applying the isotope exchange reaction discussed in the previous chapters to analysis of a commercial polyethylene, providing a unique single molecular level of material characterization. The focus of this example, aside from the actual scientific facts revealed through the research, is also on proving the general idea of single molecular

characterization of commercial polyolefins. Contrast is introduced by isotope labelling and blending, then SANS can be applied to provide information about individual chains, with potential of combination with other characterization techniques to generate a comprehensive understanding of the relationship between single molecule behavior and the bulk material properties.

We characterize the single molecular alignment of polymer chains during cold-drawing. The material deformation under uniaxial tension consists of three representative behaviors as discussed in Chapter 1 (Figure 1.4). At small strain (less than 10%) the material appears as an elastic solid where the stress quickly accumulates with deformation in a nearly linear manner. At intermediate deformation, the material yields and undergoes plastic deformation. At very high level of deformation the material strain hardens before it eventually breaks, represented by a sharp increase of the total stress with strain. The above material response has a profound dependence on the semi-crystalline nature of the material. Hypotheses exist in regard to the structural change of polyethylene during cold-drawing. Sun, et al. proposed that two interpenetrating and continuous networks, the crystalline and amorphous part, co-exist in the bulk of an ethylene-octene copolymer material. The amorphous fraction of the material can be tuned with the comonomer content, and affects the critical strain required for crystal fragmentation.[109] Seguela, et al. on the other hand proposed that rather than breaking of crystallites,[110–113] the crystal blocks instead slips across each other and deform only in a homogeneously sheared manner. Other literature adopted a model which suggests a partial melting – recrystallization process is responsible for the microstructural development,[114–118] and is supported by molecular dynamics simulations.[119–121]

Previously researchers utilized in situ small angle and wide angle X-ray scattering (SAXS and WAXS) to analyze the structural change during polymer deformation.[32–34] For a semi-crystalline material, X-ray contrast comes from differences in electron density

between crystalline and non-crystalline regions, so these measurements are well suited for detecting crystalline structure from angstroms to microns in length scale. However, X-ray scattering cannot provide information about the single chain conformation around the length scale of R_g, which is the radius of gyration of the polymer chain. Molecular conformation is crucial to fully understand the mechanism of deformation that will support the evolution of morphology during elongation. Ideally, SANS is best suited for such measurements due to the single chain level contrast from isotope labelling. However, few reports on the molecular conformation during bulk material deformation have been reported due to the challenging nature of the measurements, mainly due to low neutron flux achievable (and long measurement time required as a consequence). Several ex-situ efforts were reported, and they do not directly correlate the conformational evolution and bulk stress.[77,122–128] To address these issues, we report the first alignment measurement for a semi-crystalline polyethylene subject to cold drawing, utilizing in situ SANS. These measurements provide a new perspective on the structural evolution of PE during cold drawing. The measurement is performed with the partially labelled polyethylene discussed in the previous chapters. Through selective fractionation and blending with a hydrogenous matrix, we are able to investigate the single chain alignment at a length scale of the entire chain. We hope to provide insight about chains of different lengths and their role in connecting the semi-crystalline network.

5.2 Experiment

5.2.1 Materials

Blends prepared from a hydrogenous polyethylene and several partially labelled polyethylene samples were prepared for this research. The polyethylene is the same commercial LLDPE discussed in Chapter 4, and is denoted as HPE in the following discussion. Isotope labelling was used to partially label the HPE, generating a DPE material with 63% H/D substitution, as determined by density measurements. HPE was fractionated by ExxonMobil Chemical Company to generate five fractions with different molecular weight, and relatively lower dispersity than the parent material, using a preparative fractionation instrument (PREP mc2, Polymer Char). The fractions are named F1, F2, F3, F4 and F5 with increasing molecular weight. Similarly, the labelled counterpart (DPE) was fractionated following the same method to generate fractions D(F1) through D(F5). The molecular weight distribution of the parent polymer and the fractions were determined by ExxonMobil Chemical Company with a high temperature SEC unit operated with a mobile phase of 1,2,4-trichlorobenzene at 140 °C, and calibrated with PE standards. The molecular weight distribution is illustrated in Figure 5.1. The molecular weight of the HPE, DPE and fractions are listed in Table 5.1. Average radii of gyration of these polymers are calculated assuming Gaussian coils and identical statistical segment length, a = 7.6 Å, as determined in Chapter 4, following Equation 5.1:

$$R_g = \sqrt{\frac{M_w a^2}{6M_o}} \qquad (5.1)$$

where M_o = 56 g/mol is the molar mass of each C4 repeat unit. Three blends were prepared by solution blending the partially labelled polymer with a hydrogenous matrix in boiling xylenes, followed by precipitation and vacuum drying. The blends are: (1) DPE/HPE, containing 10 wt% DPE and 90 wt% HPE, (2) D(F1)/H(F2-5), containing

fraction D(F1) and fractions F2 through F5, and (3) D(F5)/H(F1-4), containing fraction D(F5) and hydrogenous fractions F1 through F4. By such a strategy all blends have a molecular weight distribution unaltered from the parent HPE.

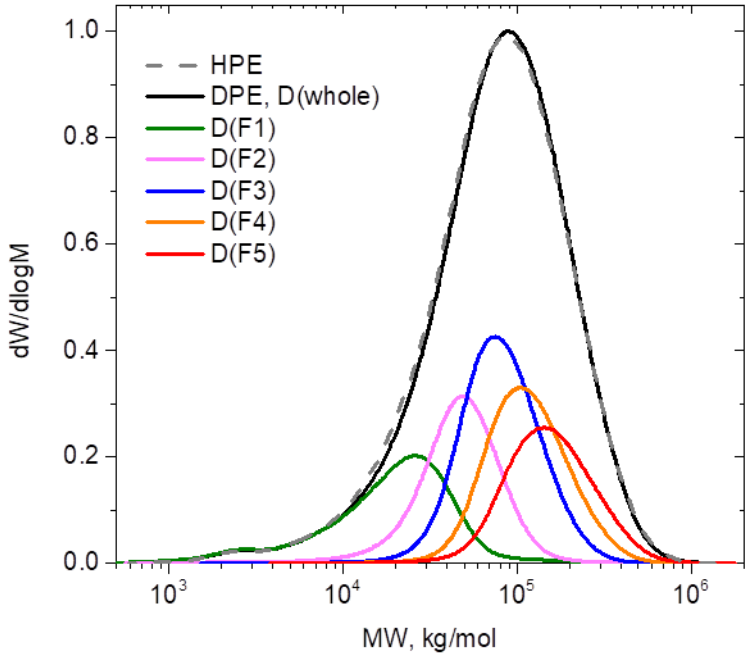

Figure 5. 1 Molecular weight distribution (MWD) of HPE, DPE and the fractions D(F1) to D(F5).

Table 5. 1 Molecular weights and radii of gyration of polyethylene and fractions

Sample	M_n, kg/mol	M_w, kg/mol	R_g^*, Å
HPE	46	113	139
DPE	41	110	138
D(F1)	11	27	68
D(F5)	127	190	181

* Calculated with a = 7.6 Å, the value from melt scattering at 150 °C.

5.2.2 In-situ tensile SANS measurement

As shown in Figure 5.2, a Linkam tensile stage (Linkam TST350) was directly mounted to the open sample environment of the SANS beam line for in-situ tensile SANS measurement. A 200 N load cell was installed to record the force response. Dogbone samples with gauge dimensions of 15 mm length, 2.5 mm width and 0.5 mm thickness were stretched at a constant rate of 0.1 mm/s for 780 s, resulting in 620% elongation ultimately. The symmetrical displacement of the two clamps allows the same area of the sample to be detected during the test (Figure 2a). Engineering Hencky strain is defined as

$$\varepsilon_H = \ln \frac{l}{l_0} \qquad (5.2)$$

where l and l_0 are the sample strand length and initial gauge length respectively. Deformation of sample is performed with two different schemes: (1) step-by-step mode, where the sample is stretched to a specific length and the stretching is paused for 10 min, while two-dimensional SANS patterns were collected, and (2) continuous mode, where the

sample is stretched at the constant 0.1 mm/s rate and SANS pattern is recorded simultaneously, but with an extra dimension of information, which is the time of each neutron hitting the detector. SANS measurements were performed on the NG7 30 m SANS instrument at the NIST Center for Neutronics Research (NCNR, Gaithersburg, MD) using a wavelength of λ = 6 Å and wavelength spread of $\Delta\lambda/\lambda$ = 0.11. The sample-to-detector distance is 1.55 m to cover the q range of 0.02 - 0.3 $Å^{-1}$. Using the IGOR macro provided by NCNR,[129] raw SANS data were corrected for background radiation and detector sensitivity. The step-by-step mode data is interpreted as is, while for the continuous mode, each experiment was repeated at least three times, and the data was combined into one single data file to generate more meaningful statistics. Time binning can be subsequently performed to pin down the chain deformation at different time periods across the experiment, essentially generating information comparable to that obtained from the step-by-step mode, with no need to worry about specimen relaxation during the 10 min counting intervals associated with the step-by-step experiment scheme.[43] Time binning was conducted with an increasing bin width so that each bin contains at least 40,000 total neutron counts. An example of time binning for D(F1)/H(F2-5) is tabulated in Table 5.2. The total neutron counts collected by the detector for a single experiment and for a combination of three repeats are illustrated in the bar graph in Figure 5.3, with the width of each bar corresponding to the bin width, and the height of each bar corresponding to the neutron counts recorded by the detector.

5.2.3 Scanning electron microscopy (SEM) investigation for the stretched samples

SEM is used for imaging of the structural alignment of the material, with contrast from the surface roughness, especially induced by crystallization. Three dogbone HPE samples were stretched at the same rate as that used for the in-situ SANS experiments (0.1 mm/s). The three samples were prepared as follows: (1) The sample was stretched to ε_H = 0.2

(120% deformation) and paused. The center of the strip was glued to a 1 cm by 1 cm silicon wafer pre-layered with a conductive tape, and cut off from the clamp, retaining the deformed strip shape. (2) The sample was stretched to $\varepsilon_H = 1.8$ (600% deformation) and paused. The center of the strip was glued to a 1 cm by 1 cm silicon wafer pre-layered with a conductive tape, and cut off from the clamp. (3) The sample was stretched to $\varepsilon_H = 1.8$ (600% deformation) and removed from the clamp. After five days, the relaxed strip center was cut off and glued to a 1 cm by 1 cm silicon wafer pre-layered with conductive tape. The three samples were subsequently coated with a thin layer of platinum and investigated with a JEOL 6500 SEM at 10 KV voltage, and working distance of 10 mm. The machine direction (MD), or the stretching direction, is determined under the microscope from the edge of the sample strips.

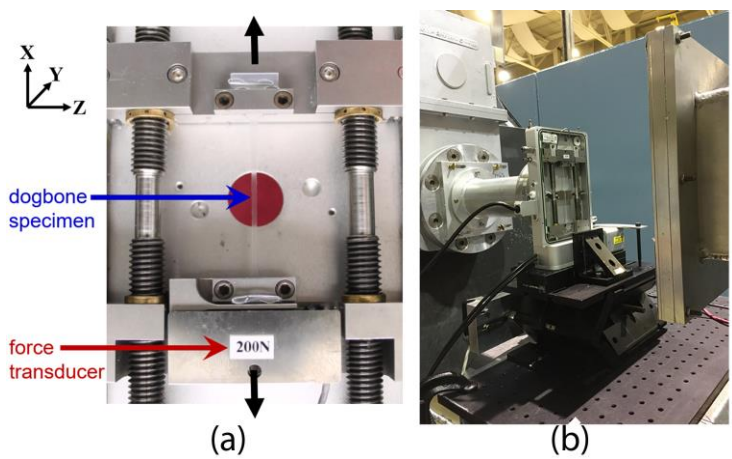

Figure 5. 2 (a) Detail of Linkam tensile stage showing a dogbone specimen being stretched. (b) Linkam tensile stage mounted in the SANS beam line.

5.2.4 SANS and SAXS for the PE at room temperature

SANS profiles of the partially labelled polymer, DPE, was obtained with the NG-7 30 m SANS instrument at NIST. The sample was prepared by thermal annealing at 150 °C in a vacuum oven for 1 h, and subsequently pressed into a stainless spacer with 1 inch outer diameter (OD) and 0.8 mm thickness. The pressure was applied by placing a 2 kg brass weight on top of two Teflon layered glass plates, between which the spacer and the polymer were located. The pressed sample was allowed to cool to ambient temperature inside the oven. The pressed sample, with the spacer attached, was sandwiched between two quartz windows provided by NIST and loaded into the sample holder. A sample-to-detector distance (SDD) of 13 m and a wavelength λ = 6 Å were used. Measurement was performed at room temperature.

SAXS measurements using the same partially labelled polymer were performed at Argonne National Laboratory using a SDD of 6 m and radiation wavelength λ = 0.886 Å. The sample was prepared by cutting off small pieces from the edges of the pressed SANS sample, and taping them onto a sample holder. These measurements were also performed at room temperature.

Table 5. 2 Time binning for D(F1)/H(F2-5)

Index	Bin center (s)	Bin width (s)	Hencky strain*	Total neutron counts (3 repeats combined)
1	7.5	15	0.05	118669
2	23.5	17	0.15	121590
3	41.5	19	0.24	123964
4	61.5	21	0.34	126609
5	83.5	23	0.44	130455
6	108	26	0.54	133272
7	135	28	0.64	136794
8	165	32	0.74	138425
9	198.5	35	0.84	135938
10	235.5	39	0.94	134264
11	276.5	43	1.04	139504
12	321.5	47	1.15	149508
13	371	52	1.25	161632
14	426	58	1.35	170809
15	487	64	1.45	180070
16	554.5	71	1.55	186085
17	629	78	1.65	194009
18	711.5	87	1.75	199630

* Value at the center of the bin

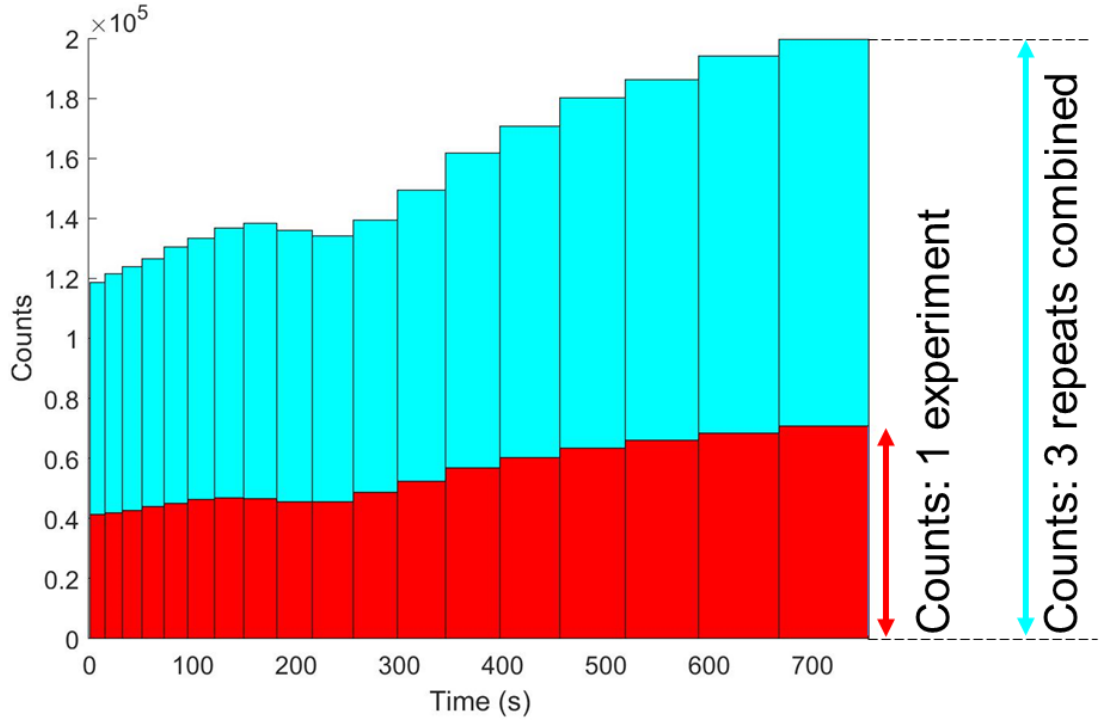

Figure 5. 3 Time binning for continuous stretch of D(F1)/H(F2-5). Bin width represents the time period of each bin. Bin height represents the total neutron counts detected by the detector, either for a single experiment (red), or for the combination of three repeats (blue).

5.3 Results and discussion

The 2D scattering patterns recorded for the blends at different Hencky strain by binning the continuously collected data at corresponding time periods are illustrated in Figures 5.4(b) and 5.5. Anisotropic patterns with horizontal streaks indicate vertically deformed and aligned scatterers, as expected for the vertically stretched polymer sample. Among these blends, D(F5)/H(F1-4) showed the highest level of anisotropy development, while D(F1)/H(F2-5) had relative lower extent of anisotropy. The 2D scattering patterns were annularly averaged as in Figure 5.4(b) and 5.4(c), within a ring corresponding to a q range of 0.03 $Å^{-1}$ to 0.09 $Å^{-1}$, effectively covering the radii of gyration measured from the three unstretched blends (Table 5.1). The 1D patterns, which are the averaged scattering intensity as a function of the azimuthal angle, ϕ, are illustrated in Figure 5.4(c). An alignment factor is defined as

$$A_f(\Delta q,\phi) = -\frac{\int_0^{2\pi} I(\Delta q,\phi)\cos(2\phi)\,d\phi}{\int_0^{2\pi} I(\Delta q)\,d\phi} \qquad (5.3)$$

which describes the degree of alignment, with $A_f = 0$ indicating the isotropic state and $A_f = 1$ representing fully aligned scatterers.[130] It has been shown by Wagner et al. that the alignment factor corresponds to an order tensor, **S** = <QQ>/tr<QQ> - **I**/3, where <QQ> stands for the second moment of the connector vector Q for the single chain segments. Therefore, by selectively analyzing the date centered around the q corresponding to the radius of gyration of chains, we are essentially evaluating the degree of chain alignments with respect to the stretching direction.

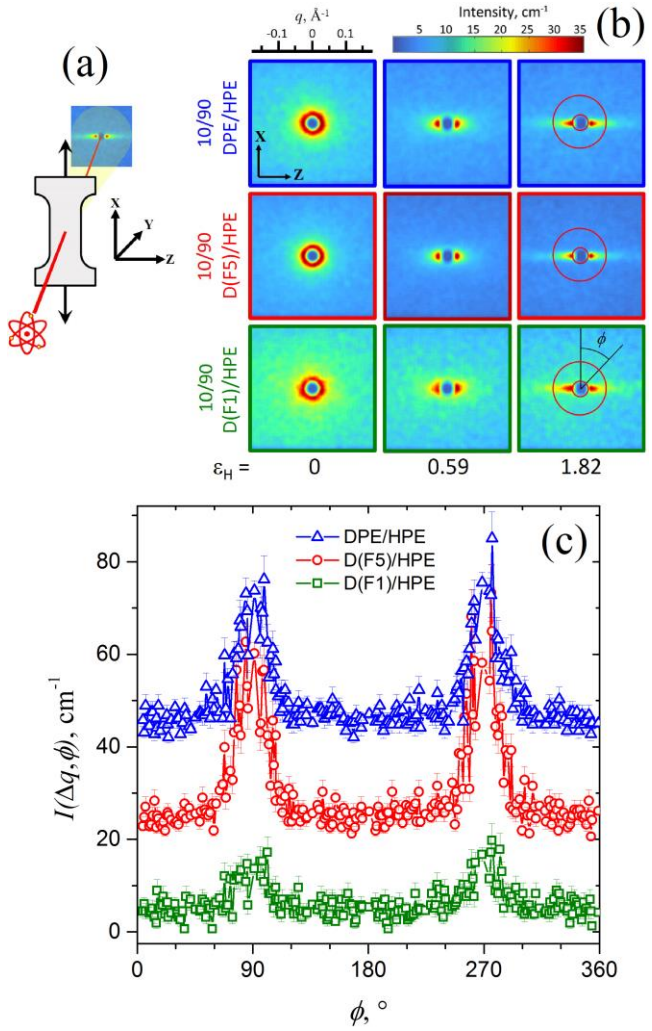

Figure 5. 4 (a) Schematic of the beam incident on the dogbone specimen. Arrows indicate the stretching direction. (b) 2D scattering patterns for DPE/HPE blends measured at three selected Hencky strain values (the rest of the 2D SANS profiles are given in Figure 5.4). (c) Annular averaged intensity versus azimuthal angle, measured for the three blends corresponding to the ring depicted in (b), which spans the q-range from 0.03 to 0.09 $Å^{-1}$.

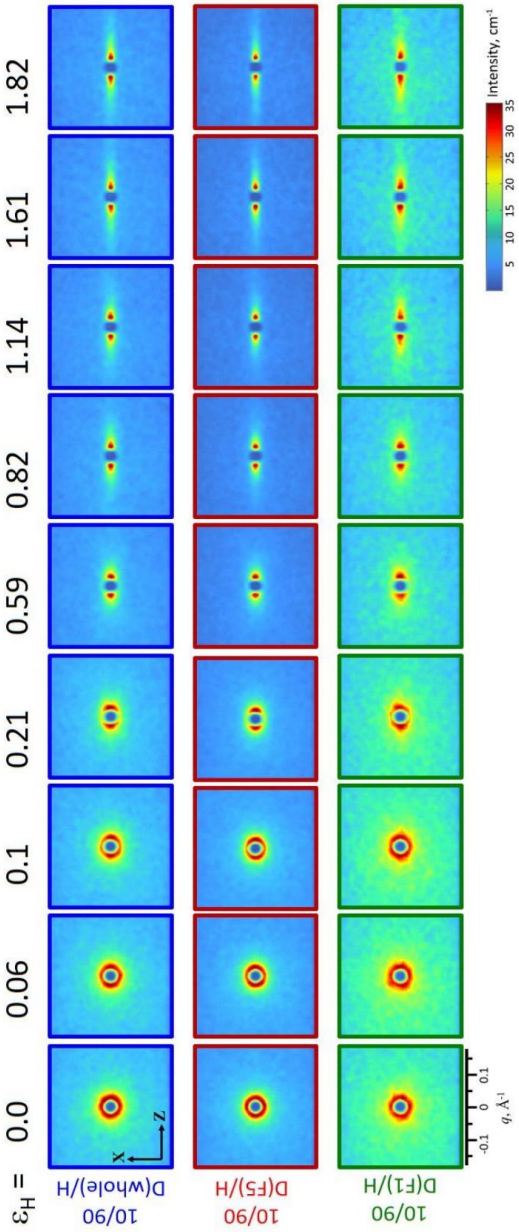

Figure 5. 5 SANS patterns at different Hencky strain values, measured in the continuous mode.

The engineering stress – Hencky strain response measured from the PE polymer in both the stepwise mode and the continuous mode is illustrated in Figure 5.6(a). The samples were stretched to 620% of the original length during a time period of 780 s without breaking. A typical mechanical behavior was seen, including an elastic deformation region at Hencky strains less than 0.1, a plastic region with yielding at a Hencky strain between 0.1 and 1.2, and a strain hardening regime observed at Hencky strains beyond 1.2. Note that during the step-by-step mode where stretching pauses for accumulation of neutrons on the detector, there exists non-negligible stress decay shown as "spikes down" in the stress – strain curve. This is more likely a result of relaxation from the non-bridging portion of chains floating in the amorphous volume of the material that were stretched due to entanglements, considering the force decay is fast and limited in magnitude. Such relaxation should not involve translational movements of chains, and will not have a significant impact on the overall orientation and alignment of the longer chains, as the molecular backbone is pinned by the crystallites. Consequently, the lost stress recovered promptly to the value prior to the decay upon further stretching. This is also supported by the consistence of stress – strain curves between the ones from the step-by-step mode and the continuous mode. Note, however, that the step-by-step mode may not be applicable for amorphous materials, such as non-crystalline polymers or semi-crystalline polymers in the melt, as the relaxation in these materials will be on the whole chain level and could result in rearrangement of centers of mass of the chains.

The alignment factor results were also investigated to support the above discussion. The alignment factors (A_f) of three blends calculated following Equation 5.3 during stretching experiments are illustrated in Figure 5.6(b). The results are from the step-by-step mode experiments. After stretching to the maximum length, the samples were removed from the tensile stage and re-attached to the beamline after at least five days to check the chain alignment retained from relaxation. The alignment developed during stretching was

largely retained even after the prolonged period of relaxation, indicating that polymer chains in the sample have a high degree of bonding to the crystallites, which have limited mobility at room temperature. We also analyzed the alignment factor from the data generated from the continuous measurements. Through time binning, the alignment factor of the sample DPE/HPE at different stage of stretching is calculated, and compared to the values measured from the step-by-step experiment. The results are illustrated in Figure 5.7. Degree of chain alignment from these two modes closely reside beside each other within experiment error, indicating that despite the relaxation during the paused periods through the experiment, the chain orientation is not disrupted. Curiously, Men, et al. performed experiments where cold-drawn PE was annealed at a temperature close to the melting point (thus speeding up the chain movements) and managed to observe significant stress relaxation, yet the global chain anisotropy survived such annealing as evidenced by SANS measurements.[127] This indicates that the relaxation of chains below the melting point is limited to a local scale, which explains the observed residual alignment that we observed even after the prolonged relaxation. Further clarification of these observations shall involve characterization from in-situ SAXS, WAXS and SALS.

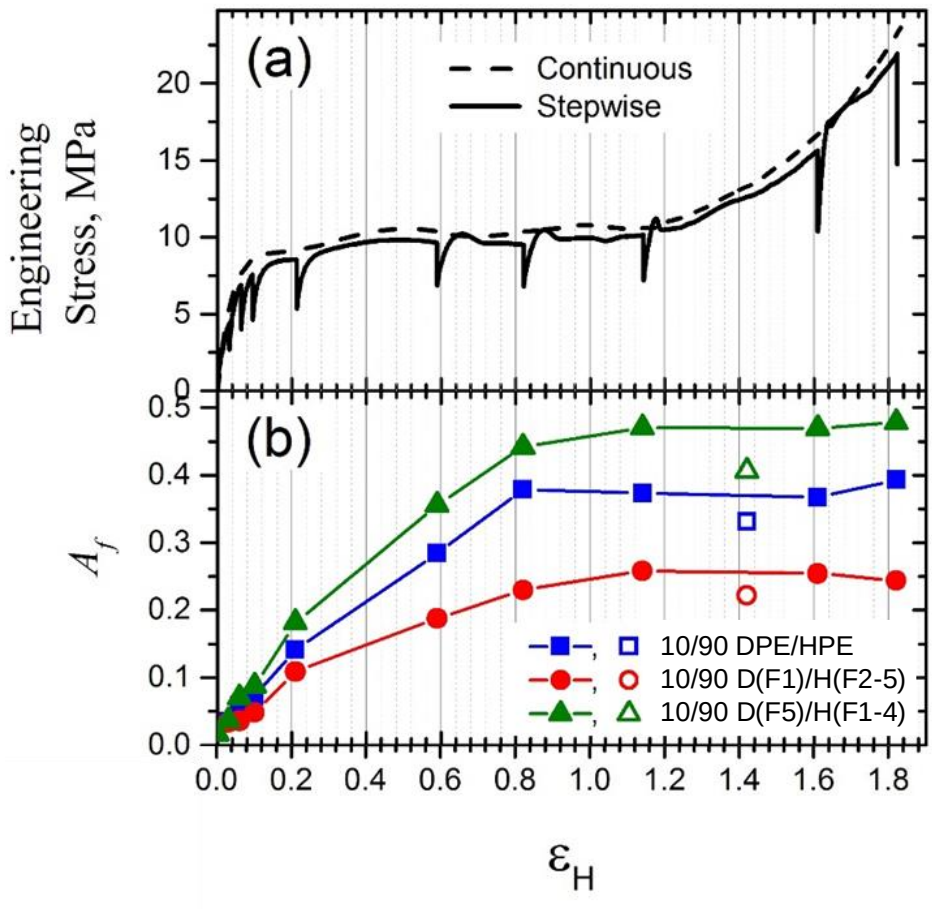

Figure 5. 6 PE force response curves. (a) Engineering stress as a function of Hencky strain in both step-by-step mode and continuous mode. (b) Alignment factor (A_f) as a function of Hencky strain for the three blends. The open symbols represent the A_f of each stretched sample after allowing these samples to relax at room temperature without constraints for at least five days.

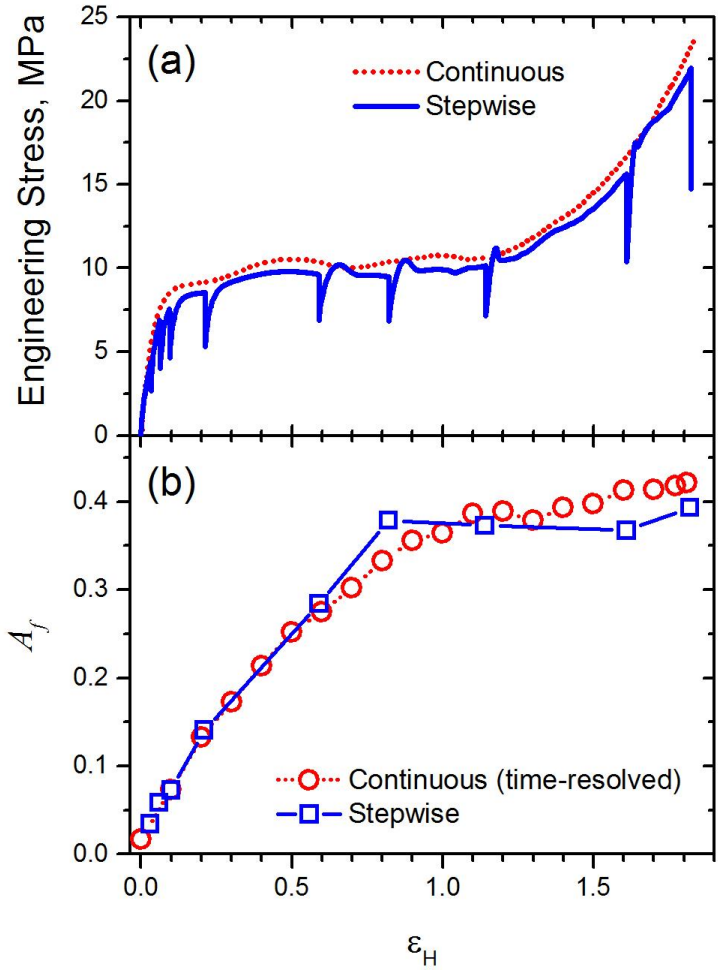

Figure 5. 7 (a) Engineering stress and (b) alignment factor versus Hencky strain, measured stepwise and continuously for DPE/HPE blend. A_f continuous data were obtained using time-resolved SANS measurements.

The alignment factor evolution during the sample stretching in tension provides a general picture of molecular deformation. The chains deform and orient rapidly as the sample passes through the elastic and plastic deformation regions. A plateau appears towards the end of deformation, indicating an equilibrium state of chain orientation is reached. The early formation of the plateau as indicated in Figure 5.6 coincides with the onset of the strain hardening. The observation provides a clue of the distinct molecular mechanism of elastic/plastic deformation and the strain hardening phenomenon. The

former deformation, with molecules deforming and orienting, is a process where the amorphous volume of the material is deformed, where chain strands tying crystallites together extend to account for the axial elongation of the sample strip. For such deformation the crystallites must rearrange to allow the c-axes of the crystallites to align with the tensile direction, yet fragmentation of crystallites is not required. Such rearrangement is supported by the SEM images of the stretched sample with $\varepsilon_H = 0.2$ (120% deformation, see section 5.2.3), just into the plastic deforming regime, as illustrated in Figures 5.8(a) and 5.8(b). The crystalline lamellae showed a collective orientation perpendicular to the machine direction (MD) or the stretching direction, while maintaining well defined shapes. Strain hardening, on the other hand, is more of an energy demanding process, evidenced by the rapidly increasing stress required for continuingthe deformation. Imaging of the most stretched sample with $\varepsilon_H = 1.8$ in Figures 5.8(c) and 5.8(d) revealed that the crystallites have reduced sizes and ill-defined shapes, which is a consequence of fragmentation. Other possible energy dissipation sources such as chains pulling out from the crystallites and slippage of crystalline stacks past each other are, however, not identified through the static imaging, but could also be present during material deformation. Chain alignment will not further develop during these processes, hence the plateau in the A_f – strain curves. The relaxation at room temperature is only allowed to take place in the amorphous volume of the sample, thereby the developed alignment is maintained, which can be observed in the SEM images of the relaxed samples in Figures 5.8(e) and 5.8(f). We attribute the droplet like structure (red arrows) to the recoil of the stretched amorphous materials.

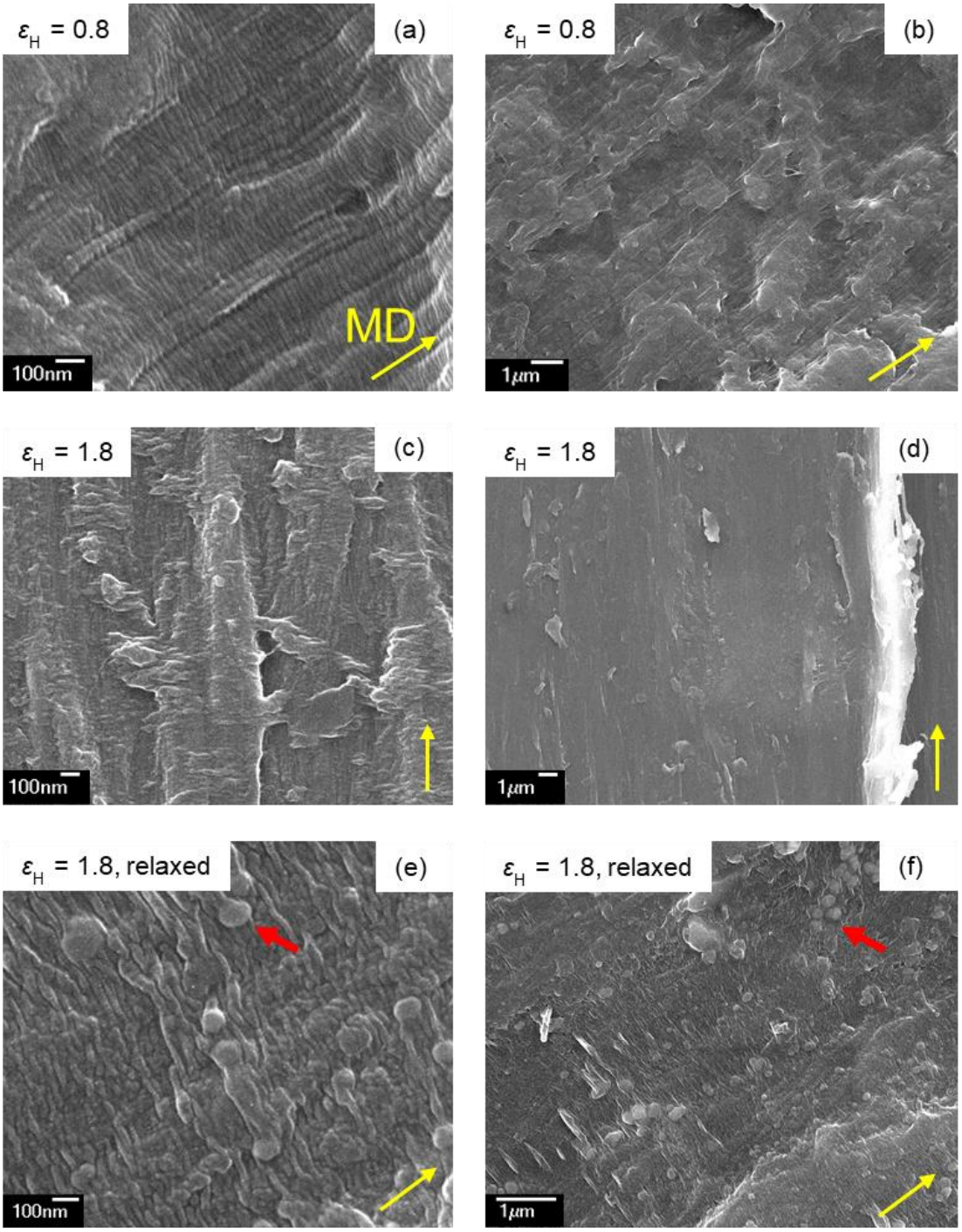

Figure 5. 8 SEM images of stretched PE. (a)(b) Stretched to ε_H = 0.8. (c)(d) Stretched to ε_H = 1.8. (e)(f) Stretched to ε_H = 1.8 and allowed to relax for 5 days. The yellow arrows indicate the machine direction (MD) of the tensile stage. The red arrows highlight the droplet like structure developed during the relaxation.

The alignment factor clearly revealed that among all the aligned samples, the blend D(F1)/H(F2-5) generate the lowest level of alignment factors, while D(F5)/H(F1-4) shows the highest. The blend DPE/HPE has an intermediate level of alignment factor development. The apparent explanation is that the longest chains, fraction F5, developed the highest level of orientation. This explanation is anticipated, as the longer chains have higher probability of bridging adjacent crystallites, effectively forming tie chains. The shorter chains, however, have a lower chance of forming such ties due to the low crystallinity of the polyethylene (usually around 30%), meaning a chain being able to connect two lamellae sheets should have a contour length at least long enough to span over the 70% amorphous volume. Chains failing to tie multiple crystallites essentially have a fluid like tail which always tend to recover to the equilibrium, coiled shape due to entropy constraints, thereby contributing less to the strand alignment. Longer chains tying rigid crystallites, on the other hand, will develop stretched inter-lamellae strands as the adjacent crystalline domains separate, and such deformation remains even after the external applied constraints are released. This scheme is illustrated in Figure 5.9

We support the above discussion by estimating the fraction of chains capable of bridging adjacent crystalline domains. First, the average inter-lamellae distance can be inferred from the SAXS and SANS patterns of the DPE sample, as illustrated in Figure 5.10. Both patterns show a broad peak well correlated with each other due to the contrast between the crystalline region and the amorphous region. The SANS pattern shows some impact from the wavelength spread of the neutrons, represented by slight broadening of the peak. For this reason, the maximum q position ($q^* = 0.03$ Å^{-1}, marked with the star) from the SAXS pattern is adopted to calculate the inter-lamellae distance, which is approximately

$$d = \frac{2\pi}{q^*} \approx 21 \text{ nm} \qquad (5.1)$$

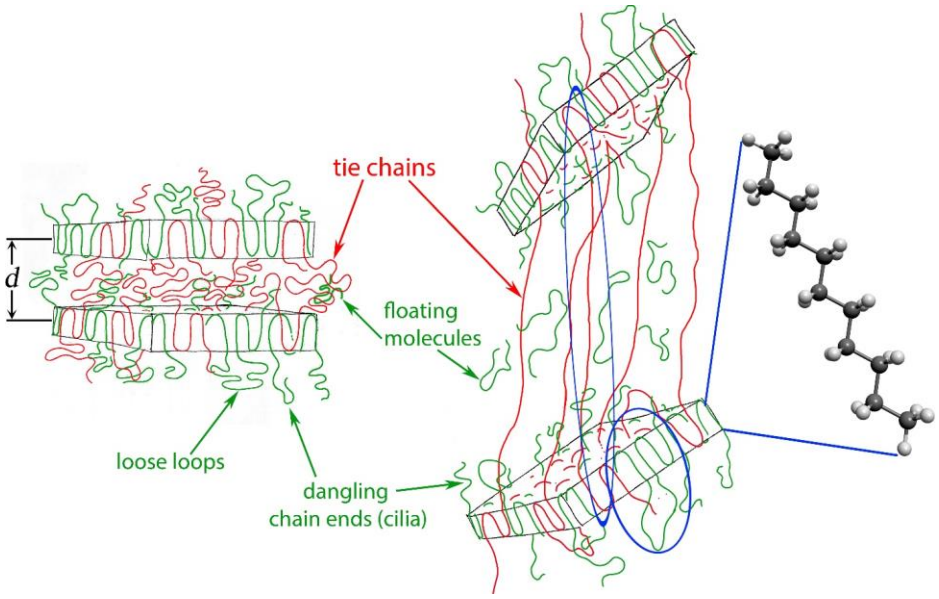

Figure 5.9 Schematic of the molecular alignment during cold drawing of a semicrystaline polymer. The strong alignment of the tie chains is highlighted. The (blue) ellipsoids illustrate the alignment measured by SANS. Illustrated at the right side are trans sequences consisting of 10 trans bonds.

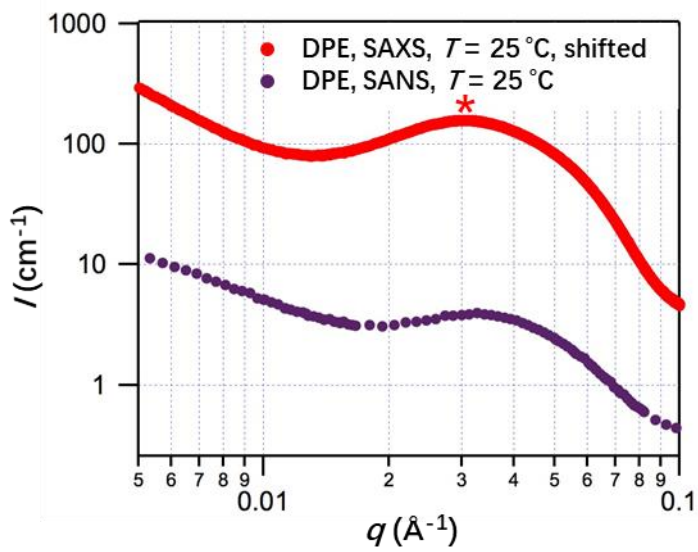

Figure 5. 10 SAXS and SANS patterns of DPE at room temperature. The star corresponds to the peak maximum, with $q^* = 0.03$ Å^{-1}. The SAXS pattern is vertically shifted for clarity.

We picture that only chains with equilibrium radii of gyration, R_g, higher than a critical value, $R_{g,c}$, have a significant chance of bridging adjacent crystallites. These chains should satisfy

$$2R_{g,c} > d \qquad (5.2)$$

or

$$2\sqrt{\frac{M_c a^2}{6M_o}} > d \qquad (5.3)$$

where M_o = 56 g/mol is the C4 repeat unit molar mass, and M_c is the critical molecular weight necessary to form tie chains. Adopting a = 7.6 Å, M_c is estimated to be 64 kDa. From the molecular weight distribution as illustrated in Figure 5.11, the total fraction of

chains in DPE, DF1 and DF5 whose molecular weights are higher than M_c are 61%, 5%, and 92% respectively. The hatched area represents the portion of chains with molecular weights beyond M_c. Qualitatively this explains the higher A_f values for the blend with higher molecular weight portion labelled, or D(F5)/H(F1-4). However, even this blend has more than 90% of labelled chains with high potential of forming tie chains, the ultimate alignment value observed from the plateau region of the A_f – strain curve is only around 0.48, instead of approaching ~0.9. A few factors should be taking into account when interpreting this result. First, for a chain bridging adjacent crystallites, only the strand between the two crystalline domain will be effectively stretched when subject to deformation. This suggests only part of a chain will be aligned. For example, Marqusee and Dill predicted that 73% of the chain strands emerging from a crystal fold back and re-enter the same crystal,[131] essentially forming loops which will not be significantly deformed (unless they intertwine with other loops from nearby crystals, forming a two chain bridge). Chains also lose volume available to form ties when the chain ends are dangling in the amorphous region. Furthermore, the lamellae spacing, *d*, is an averaged value. The broad peaks from the SANS and SAXS indicate that this spacing has a wide distribution, meaning that exceeding M_c does not guarantee that the chain will meet another crystal before it reaches all the way out with its arms: the local inter lamellae spacing must be at the right value within the distribution.

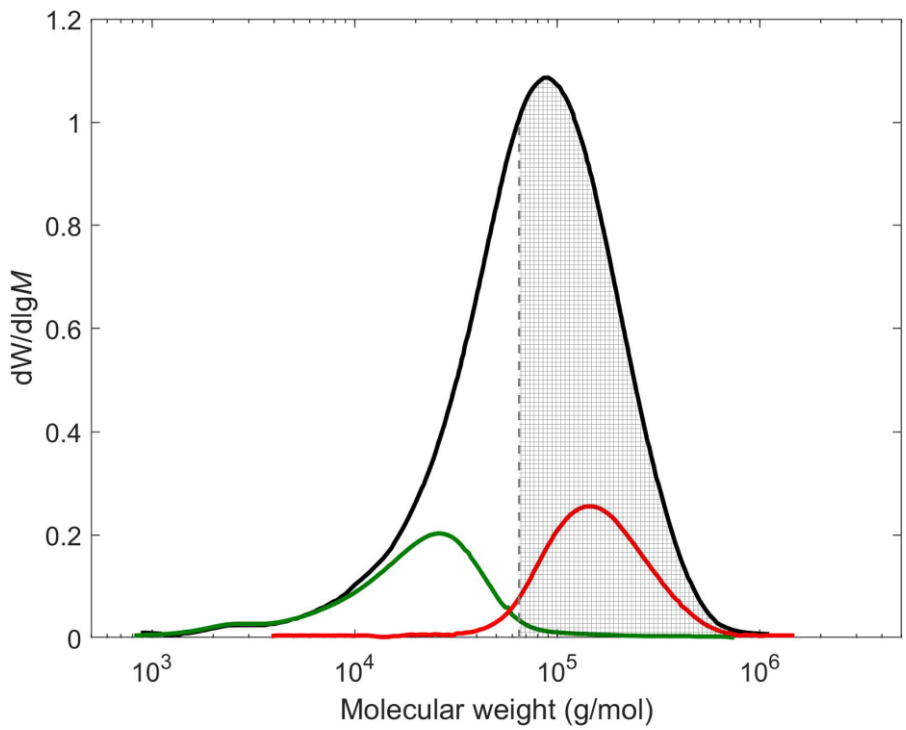

Figure 5. 11 Molecular weight distribution of DPE, DF1 and DF5. The hatched area represents the portion of chains whose molecular weights are beyond the critical value for forming tie chains, M_c = 64 kg/mol.

López-Barrón et al. also monitored the cold-drawing process via Raman spectroscopy.[132] They found a similar trend of how A_f varies with strain, which aligns well with that measured with SANS, i.e., rapid increase during the elastic and plastic deforming regime, with an eventual plateau into strain hardening. However, the alignment factor calculated from the Raman spectroscopy is much higher, with a plateau value of ~0.83, compared to the value from SANS, which eventually reaches ~0.47 for the blend with high molecular weight fraction labelled (D(F5)/H(F1-4)). The difference may be explained by the different length scales probed by the two techniques. For SANS, we are monitoring a

length scale that corresponds roughly to the entire chain by selecting only the signal from the q range that covers that length scale. As mentioned above, the loops and dangling ends will not contribute to the alignment at such a length scale. On the other hand, Raman is sensitive to aligned structure more locally, down to sequences with as short as ~10 bonds, which exists widely in crystalline domains, therefore these local segments are pre-aligned even before stretching (though not yet along the stretching direction). Considering that there still exists more than 40% of Gauche backbone units even in the most stretched samples as observed by López-Barrón et al., we see the aligned chain as like a river running in general towards a direction, but curving, and sometimes even folding back, and back towards the flowing direction again, along the path at the "Gauche sites". Though it is not unusual to find short river channels locally that perfectly align towards east (thus higher Raman A_f), the entire river is not a straight aligned structure (thus lower SANS A_f).

We now return to the different deformation models discussed at the beginning of this chapter. Seguela, et al. proposed that the main energy dissipation process is the slipping and shearing of crystalline stacks in semi-crystalline ethylene based polymers. They argue that "the chain folds that bridge the slip planes operating in the block boundaries gradually hampers the relative displacement of the crystal blocks and activates the plastic deformation within the core of the crystal blocks".[111] This correlates with our finding of the developing A_f during the elastic and plastic regime, as the tie chains bound the crystals together, and extends as the crystalline blocks separate. The hindering of crystal block displacement becomes obvious when the tie chains reach their maximum elongation, when the plateau in A_f – strain curve starts to develop. Our results also agree the mechanism proposed by Sun, et al., where the sample initially holds as a rigid crystalline structure (at small deformation), and eventually develops into a collection of disaggregated crystalline blocks.[109] They observed with in-situ SAXS that the long spacing between crystalline stacks initially increases at small strains, which correlates to the global stretching of the tie

chains, thereby increasing A_f. Curiously, they also observed a decrease in the long spacing upon plastic deformation. We did not observe such a decrease in our A_f – strain (Figure 5.6), therefore the decrease of measured long spacing must not be a result of the relaxation of the stretched amorphous layers, but more likely has to do with fragmentation of crystallites, during which a lot of closely placed crystal fragments will be generated. They observed that the long spacing eventually reached a plateau value, which potentially correlates with the plateau in A_f that we observed (Figure 5.7). Our results also agree with the mechanism proposed by Tang et al.,[133] that fibrillation will occur as PE is stretched beyond the natural draw ratio and reaches the strain hardening state. During this stage, fibrils slip past each other to accommodate further deformation, which will not affect the global alignment of chains. The plateau in A_f that we observed during the strain hardening regime aligns well with this assumption. The in situ rheo-SANS technique provides direct proof that helps to clarify the hypotheses discussed above, and is now ready to be extended to other complex systems.

5.4 Conclusions

We present the first in-situ measurements of the single chain alignment of a cold-drawn semi-crystalline polymer and relate the results to the mechanical response. We identified three regime of deformations: (1) an initial, low strain elastic regime, where the stress increases linearly with the strain, and chains align rapidly; (2) an intermediate plastic deforming regime, where the material yields and deforms, and continuously accumulates chain alignment; (3) an eventual strain hardening regime, where the stress accumulates as the strain develops, but the chains reach a saturated level of alignment. The low molecular weight portion and the high molecular weight portion exhibit significantly different levels of alignment, with the high molecular weight chains developing more alignment. This is due to the higher level of chains capable of forming tie chains in the high molecular weight

fraction. We also observed loss of chain alignment upon removal of external constraints followed by prolonged relaxation periods, but the loss is only partial, proving the relaxed samples are still in an aligned state on the molecular level. We also proved the viability of a data collection scheme where experiments are repeated and the data are combined and time binned, providing a method for addressing the low flux correlated to SANS technique. Our experiments provide new insights into the structural evolution of ethylene based semi-crystalline polymers during deformation. We believe this method can be readily expanded to other commercially important polyolefins.

Chapter 6

Summary and future work

6.1 Research summary

In this thesis, research aimed at resolving single chain alignment during polyethylene deformation has been described in detail. To achieve this goal, time resolved small angle neutron scattering (TR-SANS) in combination with rheological tools was applied. Research was conducted to explore the possibility of incorporating deuterium into polyolefins in a convenient and low cost manner, which is an indispensable step for creating SANS contrast. Two series of uniform ethylene-ethylethylene copolymers with molecular characteristics differing in molecular weight and short chain branching were synthesized, by first preparing polydiene precursors through anionic polymerization, followed by addition of hydrogen through heterogeneous catalytic hydrogenation. Deuterium labelling of these polyolefins was conducted with a heterogeneous catalytic hydrogen-deuterium exchange reaction. Molecular weight distribution and chain integrity were checked with size exclusion chromatography (SEC). The amount of deuterium incorporation was determined by density measurements, nuclear magnetic resonance spectroscopy (^{1}H-NMR), and infrared (IR) spectroscopy. Blends were prepared by solution blending of hydrogenous and deuterium labelled polymers. SANS was performed for both the pure labelled polymer and the blend. Modeling was applied to extract chain statistics from the labelled materials. For comparison, a commercially generated polyethylene was

deuterium labelled, again with the isotope exchange reaction. The distribution of deuterium as a function of molecular weight was determined with a newly developed method, an SEC-IR technique.[95] Numerical modeling was applied to obtain the chain statistics. The commercial polyethylene was then adopted as a probe material, fractionated to less disperse fractions and blended with the hydrogenous bulk polymer. The samples were stretched on a uniaxial tensile stage and monitored with SANS while being stretched. Time binning and data combination were utilized to enhance the signal to noise ratio and optimize the time resolution. An alignment factor was used to quantify the single chain alignment at different stages of sample deformation. The time resolved rheo-SANS was conducted at the National Institute of Standards and Technology (NIST). Scanning electron microscopy (SEM) was used to visualize the structural change of the stretched samples.

This thesis work prototypes and delivers a rheo-SANS platform capable of providing real time single chain evolution as the bulk material is deformed in a transient manner. Chapters 3 through 5 discuss a collection of efforts. First Chapter 3 describes the contrast acquisition step, where the polyolefins are deuterium labelled, where no prior control over the synthetic route is required. We found that by taking the benefit of not having to start with synthetic efforts, we have to sacrifice fine control over the deuteron placement among chains. Molecular weight and branching are found to shape the deuterium distribution within the labelled materials, with higher molecular weight and less branched portion taking off the largest chunk from the deuterium inventory. This supports that the isotope exchange is a kinetically controlled process. A few new techniques were developed during this part of work, including a quantification method for determination of deuterium content of hydrocarbons with FTIR.

Chapter 4 used the deuterium labelled material for further investigation. The inhomogeneity of deuterium distribution showed considerable impact on the SANS of the labelled materials. Modeling of the SANS intensity while simultaneously considering the

inhomogeneous deuterium distribution results in two findings, (1) that we are able to extract chain statistics that closely aligns with previously reported values, and (2) this in turn proves that the inhomogeneity of deuterium labelling does not eliminate the possibility of measuring chain statistics with the isotope exchanged material, as long as appropriate mathematical accommodation is accounted for. We were able to establish and justify a new protocol of quantifying the deuterium amount in an isotope exchanged commercial polyolefin as a function of molecular weight, utilizing a SEC-IR instrument, through collaboration with ExxonMobil Chemical Company.[95]

Chapter 5 demonstrated that the labelled polyolefin can assist in understanding how polyethylene molecules align during tensile deformation. We adopted a time resolved SANS method in combination with a rheological technique. Early in the experiment design phase we faced the challenge that neutron flux is too low for the transient process that we were trying to resolve. Enhancement of neutron counting statistics is achieved by repeating the experiments and employing a data combination algorithm. Once this is accomplished instrumentally the quantification becomes statistically meaningful. We started by selecting a simple system, probing the chain alignment in a polyethylene as the molecular weight is varied. We found using the rheo-SANS that chains aligns as the material is progressively stretched, and eventually plateaus as the material strain hardens. Longer chains align significantly more than the shorter chains, which is interpreted as the longer chains having the capability of bridging different crystal lamellae. Our findings provided new insights in interpreting the results from other techniques, including those obtained with SAXS, Raman, and infrared spectroscopy.

6.2 Future work

There are several aspects that are worth further investigation. First, we remain interested in understanding the impact of chain microstructure on the exchange behavior. Chain architecture variation, such as branch type, concentration and length should be connected to the exchange results. The deuterium distribution when there exists chain microstructure distribution should be understood. For example, it will be worthwhile to analyze the deuterium distribution in an isotope exchanged olefin block copolymer.

Second, it will be beneficial to obtain a direct quantification of chain adsorption characteristics on the heterogeneous catalyst surface. This will be challenging, as the reaction is conducted at a state beyond ambient conditions, with elevated temperature and pressure. A direct probing of the reaction system will need sealed sample containment capable of holding high temperature and high pressure conditions. Currently, pressure cells are available for optical and spectroscopy investigation.

Third, the impact of catalyst type should be analyzed. In this thesis work a porous catalyst is used. While for lower molecular weight polymers the porosity provides extra surface area to accommodate the exchange reaction, at high molecular weight it becomes problematic, as long chains at concentration beyond the overlapping concentration could form large interconnected structure and fail to enter the pores. Investigation of other types of catalysts with different metals, without pores, and with varying sizes remains an interest.

Next, it will be interesting to see whether the isotope exchange reaction can be extended to other types of polymers, such as polyethylene oxide (PEO) and polylactide (PLA) which are commonly used in our research group. In theory the bond activation from the transition metal does not prohibit incorporation of other type of functionalities. Actually, one early example of transition metal catalyst application is producing methanol from activated methane and water. The solvent system and reaction condition has to be extensively analyzed.

Last, the rheo-SANS platform has full potential for being expanded to other types of polyolefins, with various commercially interesting microstructure, such as short chain branching, long chain branching, comb and bottlebrushes, and blockiness of comonomers. We remain interested in understanding their contribution to the material property on a molecular level, which is difficult without the isotope exchange reaction and rheo-SANS platform. The rheo-SANS platform has the potential of being further developed to generate the full chain dimension, rather than providing merely the degree of chain alignment. To successfully achieve this target, instrument design should be modified to provide higher flux, for example by enlarging the sample aperture that defines the volume of the sample being investigated. In-situ measurement of the sample transmission and the sample thickness also have to be implanted. The current method can only cover a limited q range for each configuration, therefore it will be worthwhile to explore the possibility of switching the SANS scheme to a time-of-flight manner, where the q range can be expanded. Extending the current protocol to melt characterization will also be interesting.

Bibliography

(1) Brandsch, J.; Piringer, O. *Plast. Packag. Interact. with Food Pharm. Second Ed.* **2008**, 15.

(2) Crossland, B.; Bett, K. E.; Ford, H.; Gardner, A. K. *Proc. Inst. Mech. Eng. Part A Power Process Eng.* **1986**, 200, 237.

(3) Ziegler, K.; Breil, H.; Holzkamp, E.; Martin, H. Verfahren zur Herstellung von hochmolekularen Polyäthylenen, DBP 973626, 1960.

(4) Natta, G.; Pino, P.; Corradini, P.; Danusso, F.; Moraglio, G.; Mantica, E.; Mazzanti, G. *J. Am. Chem. Soc.* **1955**, 77, 1708.

(5) Grubbs, R. H.; Coates, G. W. *Acc. Chem. Res.* **1996**, 29, 85.

(6) D'Agnillo, L.; Soares, J. B. P.; Penlidis, A. *J. Polym. Sci. Part A Polym. Chem.* **1998**, 36, 831.

(7) Yan, D.; Wang, W. J.; Zhu, S. *Polymer (Guildf).* **1999**, 40, 1737.

(8) Desurmont, G.; Tokimitsu, T.; Yasuda, H. *Macromolecules* **2000**, 33, 7679.

(9) Ramachandran, R.; Beaucage, G.; Kulkarni, A. S.; McFaddin, D.; Merrick-Mack, J.; Galiatsatos, V. *Macromolecules* **2009**, 42, 4746.

(10) López-Barrón, C. R.; Brant, P.; Eberle, A. P. R.; Crowther, D. J. *J. Rheol. (N. Y. N. Y).* **2015**, 59, 865.

(11) Ramachandran, R.; Beaucage, G.; Rai, D. K.; Lohse, D. J.; Sun, T.; Tsou, A. H.; Norman, A.; Hadjichristidis, N. *Macromolecules* **2012**, 45, 1056.

(12) Bunn, C. W. *Trans. Faraday Soc.* **1939**, 35, 482.

(13) Spells, S. J.; Keller, A.; Sadler, D. M. *Polymer (Guildf).* **1984**, 25, 749.

(14) Spells, S. J.; Sadler, D. M. *Polymer (Guildf).* **1984**, 25, 739.

(15) Schelten, J.; Wignall, G. D.; Ballard, D. G. H.; Longman, G. W. *Polymer (Guildf).* **1974**, 15, 682.

(16) Schelten, J.; Ballard, D. G. H.; Wignall, G. D.; Longman, G.; Schmatz, W. *Polymer (Guildf).* **1976**, 17, 751.

(17) Callister, W.; Rethwisch, D. *Materials science and engineering: an introduction*; 2007; Vol. 94.

(18) Peterlin, A. *Kolloid-Zeitschrift Zeitschrift fur Polym.* **1967**, 216–217, 129.

(19) Hess, K.; Mahl, H.; Gütter, E. *Kolloid-Zeitschrift* **1957**, 155, 1.

(20) Peterlin, A. *J. Mater. Sci.* **1971**, 6, 490.

(21) Keith, H. D.; Padden, F. J.; Vadiminsky, R. G. *J. Polym. Sci. Part A-2* **1966**, 4, 267.

(22) Lustiger, A.; Ishikawa, N. *J. Polym. Sci. Part B Polym. Phys.* **1991**, 29, 1047.

(23) Brown, N.; Lu, X.; Huang, Y.-L.; Qian, R. *Makromol. Chemie. Macromol. Symp.* **1991**, 41, 55.

(24) Prasad, K.; Grubb, D. T. *J. Polym. Sci. Part B Polym. Phys.* **1989**, 27, 381.

(25) Crawford, S. M.; Kolsky, H. *Proc. Phys. Soc. Sect. B* **1951**, 64, 119.

(26) Raumann, G.; Saunders, D. W. *Proc. Phys. Soc.* **1961**, 77, 1028.

(27) Ward, I. M. *Proc. Phys. Soc.* **1962**, 80, 1176.

(28) Stein, R. S.; Norris, F. H. *J. Polym. Sci.* **1956**, 21, 381.

(29) Coutry, S. *Molecular deformation mechanisms in polyethylene.*; 2001.

(30) Onogi, S.; Asada, T. *J. Polym. Sci. Part C Polym. Symp.* **2007**, 16, 1445.

(31) Luap, C.; Müller, C.; Schweizer, T.; Venerus, D. C. *Rheol. Acta* **2005**, 45, 83.

(32) Butler, M.; Donald, A. *J. Appl. Polym. Sci.* **1998**, No. Md, 321.

(33) Butler, M. F.; Donald, A. M. *Macromolecules* **1998**, 31, 6234.

(34) Butler, M. F.; Donald, A. M.; Bras, W.; Mant, G. R.; Derbyshire, G. E.; Ryan, A. J. *Macromolecules* **1995**, 28, 6383.

(35) Graham, R. S.; Bent, J.; Clarke, N.; Hutchings, L. R.; Richards, R. W.; Gough, T.; Hoyle, D. M.; Harlen, O. G.; Grillo, I.; Auhl, D.; McLeish, T. C. B. *Soft Matter* **2009**, 5, 2383.

(36) McLeish, T. C. B.; Clarke, N.; de Luca, E.; Hutchings, L. R.; Graham, R. S.; Gough, T.; Grillo, I.; Fernyhough, C. M.; Chambon, P. *Soft Matter* **2009**, 5, 4426.

(37) Noirez, L.; Mendil-Jakani, H.; Baroni, P. *Macromol. Rapid Commun.* **2009**, 30, 1709.

(38) Sharma, J.; King, S. M.; Bohlin, L.; Clarke, N. *Nucl. Instruments Methods Phys. Res. Sect. A Accel. Spectrometers, Detect. Assoc. Equip.* **2010**, 620, 437.

(39) Boué, F. *Polym. Phys.* 47.

(40) Boué, F.; Nierlich, M.; Jannink, G.; Ball, R. *J. Phys.* **1982**, 43, 137.

(41) Blanchard, A.; Graham, R. S.; Heinrich, M.; Pyckhout-Hintzen, W.; Richter, D.; Likhtman, A. E.; McLeish, T. C. B.; Read, D. J.; Straube, E.; Kohlbrecher, J. *Phys. Rev. Lett.* **2005**, 95.

(42) Mortensen, K.; Kramer, O.; Batsberg, W.; Fetters, L. J. *Mat. Res. Soc. Symp. Proc.* **1987**, 79, 259.

(43) Calabrese, M. A.; Wagner, N. J.; Rogers, S. A. *Soft Matter* **2016**, 12, 2301.

(44) Ballard, D. G. H.; Wignall, G. D.; Schelten, J. *Eur. Polym. J.* **1973**, 9, 965.

(45) Gehlsen, M. D.; Rosedale, J. H.; Bates, F. S.; Wignall, G. D.; Hansen, L.; Almdal, K. *Phys. Rev. Lett.* **1992**, 68, 2452.

(46) Balsara, N. P.; Fetters, L. J.; Hadjichristidis, N.; Lohse, D. J.; Han, C. C.; Graessley, W. W.; Krishnamoorti, R. *Macromolecules* **1992**, 25, 6137.

(47) Hillmyer, M. A.; Maurer, W. W.; Lodge, T. P.; Bates, F. S.; Almdal, K. *J. Phys. Chem. B* **1999**, 103, 4814.

(48) Bates, F. S.; Cohen, R. E.; Berney, C. V. *Macromolecules* **1982**, 15, 589.

(49) Förster, S.; Khandpur, A. K.; Zhao, J.; Bates, F. S.; Hamley, I. W.; Ryan, A. J.; Bras, W. *Macromolecules* **1994**, 27, 6922.

(50) Lodge, T. P.; Bang, J.; Li, Z.; Hillmyer, M. A.; Talmon, Y. *Faraday Discuss.* **2005**, 128, 1.

(51) Bang, J.; Viswanathan, K.; Lodge, T. P.; Park, M. J.; Char, K. *J. Chem. Phys.* **2004**, 121, 11489.

(52) Lodge, T. P.; Bang, J.; Park, M. J.; Char, K. *Phys. Rev. Lett.* **2004**, 92, 145501.

(53) Lund, R.; Willner, L.; Richter, D.; Dormidontova, E. E. *Macromolecules* **2006**, 39, 4566.

(54) Choi, S. H.; Bates, F. S.; Lodge, T. P. *Macromolecules* **2011**, 44, 3594.

(55) Bai, L.; Sharma, R.; Cheng, X.; Macosko, C. W. *Langmuir* **2018**, 34, 1073.

(56) Bai, L.; He, S.; Fruehwirth, J. W.; Stein, A.; Macosko, C. W.; Cheng, X. *J. Rheol.* **2017**, 61, 575.

(57) Zhang, J.; Huo, M.; Li, M.; Li, T.; Li, N.; Zhou, J.; Jiang, J. *Polym.* **2018**, 134, 35.

(58) Li, T.; He, S.; Stein, A.; Francis, L. F.; Bates, F. S. *Macromolecules* **2016**, 49, 9507.

(59) Pleštil, J.; Pospíšil, H.; Kadlec, P.; Tuzar, Z.; Kříž, J.; Gordeliy, V. I. *Polymer (Guildf).* **2001**, 42, 2941.

(60) Chevigny, C.; Gigmes, D.; Bertin, D.; Jestin, J.; Boué, F. *Soft Matter* **2009**, 5, 3741.

(61) Case, L. C.; Atlas, J. D. *J. Polym. Sci.* **1960**, 45, 435.

(62) Habersberger, B. M.; Lodge, T. P.; Bates, F. S. *Macromolecules* **2012**, 45, 7778.

(63) Balsara, N. P.; Lohse, D. J.; Graessley, W. W.; Krishnamoorti, R. *J. Chem. Phys.* **1994**, 100, 3905.

(64) Gotro, J. T.; Graessley, W. W. *Macromolecules* **1984**, 17, 2767.

(65) Hucul, D. A.; Hahn, S. F. *Adv. Mater.* **2000**, 12, 1855.

(66) Sauter, D. W.; Taoufik, M.; Boisson, C. *Polymers (Basel).* **2017**, 9.

(67) Garnett, J. L.; Hodges, R. J. *J. Am. Chem. Soc.* **1967**, 89, 4546.

(68) Fujiwara, Y.; Moritani, I.; Danno, S.; Asano, R.; Teranishi, S. *J. Am. Chem. Soc.* **1969**, 91, 7166.

(69) Chatt, J.; Davidson, J. M. *J. Chem. Soc.* **1965**, 843.

(70) Jones, W. D.; Maguire, J. A. *Organometallics* **1986**, 5, 590.

(71) Hodges, R. J.; Garnett, J. L. *J. Phys. Chem.* **1969**, 73, 1525.

(72) Hodges, R. J.; Webster, D. E.; Wells, P. B. *J. Chem. Soc. D* **1971**, 0, 462.

(73) Hodges, R. J.; Webster, D. E.; Wells, P. B. *J. Chem. Soc. A* **1971**, 0, 3230.

(74) Garnett, J. L.; Long, M. A.; Peterson, K. B. *Aust. J. Chem.* **1974**, 27, 1823.

(75) Derdau, V.; Atzrodt, J.; Zimmermann, J.; Kroll, C.; Brückner, F. *Chem. - A Eur. J.* **2009**, 15, 10397.

(76) Eisen, M. S.; Marks, T. J. *Organometallics* **1992**, 11, 3939.

(77) Crist, B.; Tanzer, J. D.; Finerman, T. M. *J. Polym. Sci. Part B Polym. Phys.* **1989**, 27, 875.

(78) Willenberg, B. *Die Makromol. Chemie* **1976**, 177, 3625.

(79) Bates, F. S.; Dierker, S. B.; Wignall, G. D. *Macromolecules* **1986**, 19, 1938.

(80) Bates, F. S.; Wignall, G. D.; Koehler, W. C. *Phys. Rev. Lett.* **1985**, 55, 2425.

(81) Tanzer, J. D.; Crist, B. *Macromolecules* **1985**, 18, 1291.

(82) Nicholson, J. C.; Crist, B. *Macromolecules* **1989**, 22, 1704.

(83) Habersberger, B. M.; Baugh, D. W. *Macromolecules* **2018**, acs. macromol.7b02633.

(84) Bates, F. S.; Fredrickson, G. H.; Hucul, D.; Hahn, S. F. *AIChE J.* **2001**, 47, 762.

(85) Jenkins, A. D.; Kratochvíl, P.; Stepto, R. F. T.; Suter, U. W. *Pure Appl. Chem.* **1996**, 68.

(86) Ziegler, K. *Angew. Chemie* **1936**, 49, 499.

(87) SZWARC, M. *Nature* **1956**, 178, 1168.

(88) Flory, P. J. *J. Am. Chem. Soc.* **1940**, 62, 1561.

(89) Young, R. N.; Quirk, R. P.; Fetters, L. J. *Anionic Polym.* 1.

(90) Grubisic, Z.; Rempp, P.; Benoit, H. *J. Polym. Sci. Part B-Polymer Phys.* **1996**, 34, 1707.

(91) Hiemenz, P. C.; Lodge, T. *Polymer chemistry*; CRC Press, 2007.

(92) Kraus, G.; Stacy, C. J. *J. Polym. Sci. Part A-2 Polym. Phys.* **1972**, 10, 657.

(93) Chen, Y. Y.; Lodge, T. P.; Bates, F. S. *J. Polym. Sci. Part B Polym. Phys.* **2002**, 40, 466.

(94) Pangborn, A. B.; Giardello, M. A.; Grubbs, R. H.; Rosen, R. K.; Timmers, F. J. *Organometallics* **1996**, 15, 1518.

(95) Kang, S.; Zeng, Y.; Lodge, T. P.; Bates, F. S.; Brant, P.; López-Barrón, C. R. *Polym. (United Kingdom)* **2016**, 102, 99.

(96) Charlet, G.; Delmas, G. *Polymer (Guildf).* **1981**, 22, 1181.

(97) Hamada, F.; Fujisawa, K.; Nakajima, A. *Polym. J.* **1973**, 4, 316.

(98) Kiran, E.; Zhuang, W. *Polymer (Guildf).* **1992**, 33, 5259.

(99) Habersberger, B. M.; Hart, K. E.; Gillespie, D.; Huang, T. *Macromolecules* **2015**, 48, 5951.

(100) Londono, J. D.; Narten, A. H.; Wignall, G. D.; Honnell, K. G.; Hsieh, E. T.; Johnson, T. W.; Bates, F. S. *Macromolecules* **1994**, 27, 2864.

(101) Benoit, H.; Benmouna, M.; Wu, W. L. *Macromolecules* **1990**, 23, 1511.

(102) Akcasu, A. Z.; Klein, R.; Hammouda, B. *Macromolecules* **1993**, 26, 4136.

(103) Hammouda, B. In *Polymer Characteristics*; pp 87–133.

(104) Graessley, W. W.; Krishnamoorti, R.; Reichart, G. C.; Balsara, N. P.; Fetters, L. J.; Lohse, D. J. *Macromolecules* **1995**, 28, 1260.

(105) Fetters, L. J.; Graessley, W. W.; Krishnamoorti, R.; Lohse, D. J. *Macromolecules* **1997**, 30, 4973.

(106) Leibler, L. *Macromolecules* **1980**, 13, 1602.

(107) Rosedale, J. H.; Bates, F. S. *J. Am. Chem. Soc.* **1988**, 110, 3542.

(108) Fetters, L. J.; Lohse, D. J.; Richter, D.; Witten, T. A.; Zirkel, A. *Macromolecules* **1994**, 27, 4639.

(109) Sun, Y.; Fu, L.; Wu, Z.; Men, Y. *Macromolecules* **2013**, 46, 971.

(110) Romo-Uribe, A.; Manzur, A.; Olayo, R. *J. Mater. Res.* **2012**, 27, 1351.

(111) Seguela, R.; Rietsch, F. *J. Mater. Sci. Lett.* **1990**, 9, 46.

(112) Séguéla, R.; Darras, O. *J. Mater. Sci.* **1994**, 29, 5342.

(113) Gaucher-Miri, V.; Séguéla, R. *Macromolecules* **1997**, 30, 1158.

(114) Flory, P. J.; Yoon, D. Y. *Nature* **1978**, 272, 226.

(115) Popli, R.; Mandelkern, L. *J. Polym. Sci. Part B Polym. Phys.* **1987**, 25, 441.

(116) Lucas, J. C.; Failla, M. D.; Smith, F. L.; Mandelkern, L.; Peacock, A. J. *Polym. Eng. Sci.* **1995**, 35, 1117.

(117) Manzur, A. *J. Appl. Polym. Sci.* **2008**, 108, 1574.

(118) Wang, Y.; Jiang, Z.; Wu, Z.; Men, Y. *Macromolecules* **2013**, 46, 518.

(119) Lee, S.; Rutledge, G. C. *Macromolecules* **2011**, 44, 3096.

(120) Kim, J. M.; Locker, R.; Rutledge, G. C. *Macromolecules* **2014**, 47, 2515.

(121) Yeh, I.-C.; Andzelm, J. W.; Rutledge, G. C. *Macromolecules* **2015**, 48, 4228.

(122) Sadler, D. M.; Barham, P. J. **1983**.

(123) Sadler, D. M.; Barham, P. J. *Polymer (Guildf).* **1990**, 31, 36.

(124) Sadler, D. M.; Barham, P. J. *Polymer (Guildf).* **1990**, 31, 43.

(125) Sadler, D. M.; Barham, P. J. *Polymer (Guildf).* **1990**, 31, 46.

(126) Tanzer, J. D.; Crist, B.; Graessley, W. W. *J. Polym. Sci. Part B Polym. Phys.* **1989**, 27, 859.

(127) Men, Y.; Rieger, J.; Lindner, P.; Enderle, H. F.; Lilge, D.; Kristen, M. O.; Mihan, S.; Jiang, S. *J. Phys. Chem. B* **2005**, 109, 16650.

(128) Men, Y.; Rieger, J.; Lindner, P.; Enderle, H. F.; Lilge, D.; Kristen, M. O.; Mihan, S.; Jiang, S. *Polymer (Guildf).* **2007**, 48, 2464.

(129) Kline, S. R. *J. Appl. Crystallogr.* **2006**, 39, 895.

(130) Walker, L. M.; Wagner, N. J. *Society* **1996**, 2298.

(131) Marqusee, J. A.; Dill, K. A. *Macromolecules* **1986**, 19, 2420.

(132) López-Barrón, C. R.; Zeng, Y.; Schaefer, J. J.; Eberle, A. P. R.; Lodge, T. P.; Bates, F. S. *Macromolecules* **2017**, 50, 3627.

(133) Tang, Y.; Jiang, Z.; Men, Y.; An, L.; Enderle, H. F.; Lilge, D.; Roth, S. V.; Gehrke, R.; Rieger, J. *Polymer (Guildf).* **2007**, 48, 5125.

Appendices

A.1 Permission of reuse for Figure 1.1

ROYAL SOCIETY OF CHEMISTRY LICENSE
TERMS AND CONDITIONS

Dec 15, 2017

This Agreement between Mr. Yiming Zeng ("You") and Royal Society of Chemistry ("Royal Society of Chemistry") consists of your license details and the terms and conditions provided by Royal Society of Chemistry and Copyright Clearance Center.

License Number	4250251144960
License date	Dec 15, 2017
Licensed Content Publisher	Royal Society of Chemistry
Licensed Content Publication	Transactions of the Faraday Society
Licensed Content Title	The crystal structure of long-chain normal paraffin hydrocarbons. The "shape" of the <CH2 group
Licensed Content Author	C. W. Bunn
Licensed Content Date	Dec 31, 1969
Licensed Content Volume	35
Licensed Content Issue	0
Type of Use	Thesis/Dissertation
Requestor type	academic/educational
Portion	figures/tables/images
Number of figures/tables/images	1
Format	print and electronic
Distribution quantity	5
Will you be translating?	no
Order reference number	
Title of the thesis/dissertation	Mechanism and application of a heterogeneous hydrogen-deuterium exchange reaction
Expected completion date	Dec 2017
Estimated size	140
Requestor Location	Mr. Yiming Zeng 407 7th St SE Apt 312 DINKYTOWN, MN 55414 United States Attn: Mr. Yiming Zeng
Billing Type	Invoice
Billing Address	Mr. Yiming Zeng 407 7th St SE Apt 312 DINKYTOWN, MN 55414 United States Attn: Mr. Yiming Zeng
Total	0.00 USD

A.2 Permission of reuse for Figure 1.5

JOHN WILEY AND SONS LICENSE
TERMS AND CONDITIONS

Dec 15, 2017

This Agreement between Mr. Yiming Zeng ("You") and John Wiley and Sons ("John Wiley and Sons") consists of your license details and the terms and conditions provided by John Wiley and Sons and Copyright Clearance Center.

License Number	4250320155765
License date	Dec 15, 2017
Licensed Content Publisher	John Wiley and Sons
Licensed Content Publication	Journal of Polymer Science Part A: Polymer Chemistry
Licensed Content Title	Intercrystalline links in polyethylene crystallized from the melt
Licensed Content Author	H. D. Keith,F. J. Padden,R. G. Vadimsky
Licensed Content Date	Apr 1, 1966
Licensed Content Pages	15
Type of use	Dissertation/Thesis
Requestor type	University/Academic
Format	Print and electronic
Portion	Figure/table
Number of figures/tables	2
Original Wiley figure/table number(s)	Figure 7 Figure 8
Will you be translating?	No
Title of your thesis / dissertation	Mechanism and application of a heterogeneous hydrogen-deuterium exchange reaction
Expected completion date	Dec 2017
Expected size (number of pages)	140
Requestor Location	Mr. Yiming Zeng 407 7th St SE Apt 312 DINKYTOWN, MN 55414 United States Attn: Mr. Yiming Zeng
Publisher Tax ID	EU826007151
Billing Type	Invoice
Billing Address	Mr. Yiming Zeng 407 7th St SE Apt 312 DINKYTOWN, MN 55414 United States Attn: Mr. Yiming Zeng
Total	0.00 USD